KOMUNIKÁCIE
COMMUNICATIONS

Dear reader,

A characteristic feature of human beings is the ability to move. In the ancient time it was the environment that decisively determined not only the need of people for movement but also technical and technological aspects of the process.

The first means of movement – first means of transport were substantially influenced by the geographical environment. Only later, together with the development of technology, they were adjusted to social, economic, ecologic and ergononomic requirements. They are not, in fact, dependent on geographic and climatic conditions.

Recently there has been a significant change in the relation of transport and environment. While in the past it was the environment which determined when, where, and how to move, at present this relation acts in the opposite way. Transportation needs brought about by economic and social conditions and transportation technology influence the environment to a great extent. That is why quality and cleanness of the environment together with safety of transport have become a decisive criterion at designing not only means of transport but also transport networks, at organization of transport and territorial planning.

To meet all these demanding tasks it is necessary to behave in a rational way. One way to meet the objective is to cope with the topic also in a theoretical way.

Modern technical means, computer technology with software and hardware and extensive theoretical knowledge from basic scientific disciplines enable to complexly solve topics of means of transport theory.

The first issue of the year 2005 you are paying attention to, deals with some theoretical topics of means of transport from a broader point of view. It is not only a point of view of their design but also from the point of view of closely related factors, e.g. production, operation, ...

Being responsible for this issue I very much regret having to announce the death of Prof. Dr. Hab. Inž. Zygmunt Szlachta, who died late in December last year in Cracow, due to a serious car accident. Professor Szlachta was a member of our editorial board and visiting professor of the Faculty of Mechanical Engineering of the University of Žilina.

Professor Szlachta was the author of many books and scientific publications. You can find his article also in this issue. In the deceased we lose a recognized specialist in the area of diesel engines. We will remember him as a hardworking colleague and great friend.

Vladimír Hlavňa

https://doi.org/10.26552/com.C.2005.1.5-10

Juraj Gerlici – Tomáš Lack *

WHEELSET/RAIL GEOMETRIC CHARACTERISTICS ASSESSMENT WITH REGARD TO WHEELSET ROLLING

The geometric relation between a wheelset and a rail is assessed with the help of geometric characteristics. Geometric characteristics are: equivalent conicity function, delta r function placement of contact points of a wheelset and a rail, tangent gamma function and effective conicity.

It turned out that these characteristics are at present the most important not only for the judgment of ride characteristics of a vehicle on the rail but also for the wearing of wheel treads and rail heads, e. i., for the assessment of the track and vehicles in order to find out the current state and for the assessment of changes of the wheels and rails profile shapes in order to improve the current state too. The process of geometric characteristic assessment of a wheelset and rail with regard to wheelset rolling is analysed in the article.

1. Introduction

Wheelset rolling is determined by the geometric position of a wheelset with regard to a track.

The profiles geometry and the lateral movement of a wheelset have an influence on the contact points position and on the wheelset rolling, as well as on other geometric characteristics for which the contact points represent input data.

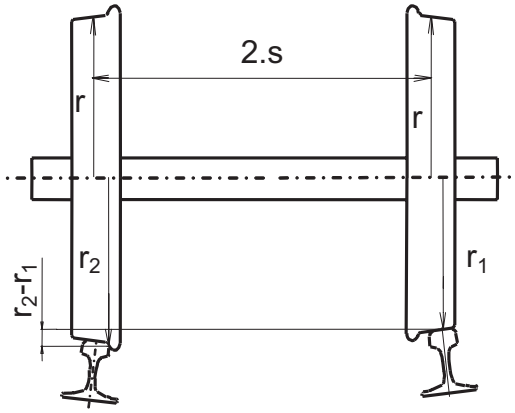

Fig. 1 Difference of wheels rolling immediate radii of one wheelset at its lateral movement.

For further analyses we arise from the assumption that the lateral movement of the profiles, not the point of gravity of the wheelset movement, is important.

It means, that we understand under the term of the lateral translation movement *y* the parallel translation of wheels profiles coordinate system, not the lateral translation of the wheelset coordinate system itself. The point of gravity of the wheelset can move in a lateral direction by values different from the lateral movement on the high level of contact points. This happens with regard to the geometry of points in contact. In extreme cases the movement of the point of gravity can move in an opposite direction as "the profiles".

Wheelset point of gravity in the y-direction

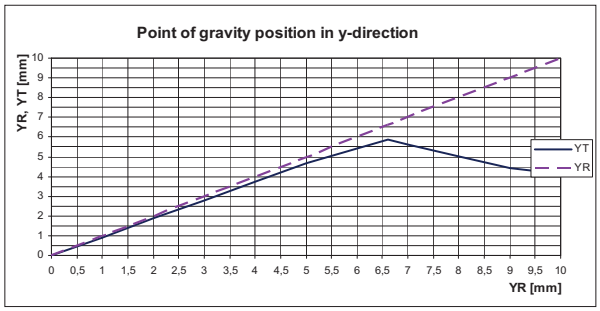

Fig. 2 Wheelset point of gravity position YT with regard to the profile movement in the y- direction, for the S1002/UIC60/1:40 profiles.

The wheel profiles move on the rail profiles in a lateral direction (*YR*). Contact points of the profile couples wheel/rail are found. The final rolling is determined on the base of a contact point on the wheel tread and of a wheel radius. In Fig. 2 is *YR*(*YR*) dependence curve and *YT*(*YR*) dependence curve difference.

2. The geometric characteristics analysis process

The wheelset profiles transformation via turning around contact points by the φ angle.

The wheelset rolling is calculated in the following way:

* **Juraj Gerlici, Tomáš Lack**
Faculty of Mechanical Engineering, University of Žilina, Univerzitná 8215/1, SK-010 26 Žilina, Slovakia,
E-mail: juraj.gerlici@fstroj.utc.sk, tomas.lack@fstroj.utc.sk

A wheelset is placed into a track at a certain y_R lateral movement.

The right and left profiles are in the wheelset coordinate system.

Contact points of the wheelset and the track at the rolling angle $\varphi = 0$ are found.

The minimum value of the function of difference d determines the contact point position between the wheel and the rail.

$$d(y, y_R) = z_S(y) - z_R(y - y_R) \quad (1)$$

The *y*- coordinate of a contact point on the rail at the wheelset profile movement is the *y*-coordinate of the function of difference *d* when the function of difference *d* reaches the extreme (minimum).

$$[Y_S(y_R) = y]_{d = \min\limits_{y \in (Wheel \cap Rail)}(d)} \quad (2)$$

The minimum value of the function of difference d at the wheel profile movement y_R equals the value of the function of difference *d* at the *y*-direction coordinate which equals at the same time the *y*-direction coordinate of the contact point on the rail profile.

$$d_{min}(y_R) = [d(y, y_R)]_{y = Y_S} \quad (3)$$

The whole wheelset preliminary tilts by the φ angle on the base of the difference assessment of the size of immediate radii of wheels rolling:

$$\varphi = \varphi_0 + arctg((d_{1\,min} - d_{2\,min}) / (2 \cdot s)),$$

$\varphi_0 = 0$ at the first cycle of computation,
$d_{1\,min}$ = *y*-direction coordinate of the right wheel contact point + right wheel radius,
$d_{2\,min}$ = *y*-direction coordinate of the left wheel contact point + left wheel radius.

The wheelset rolling by φ angle consists of summation of turning around the right wheel contact point by $\varphi/2$ angle and turning around the left wheel contact point by $\varphi/2$.

The right wheel profile turns by the φ angle in the coordinate system with the beginning in the contact point of the left wheel and the rail (Fig. 4). The transformed profile is furthermore the φ angle function. The contact point of the right wheel and the rail is found.

The left wheel profile turns by the φ angle in the coordinate system with the beginning in the contact point of the right wheel and the rail (Fig. 5). The transformed profile is the φ angle function. The contact point of the right wheel and the rail is found.

Parameters d_{1min} a d_{2min} are assessed again. If their difference is greater than the precision ratio ε (when computing 10^{-6}) the wheel profiles turn by the φ angle according to the equation (3), while the value φ_0 is substituted by the φ from the previous computation. The computation or the φ angle is repeated until the difference of parameters d_{1min} and d_{2min} is lower than ε.

The inverse transformation of the wheelset contact points position into the coordinate system of the wheelset is realised via the turning by the φ angle.

The geometric characteristics are evaluated.

The difference of geometric characteristics courses is determined with regard to the wheelset rolling from the geometric characteristics without rolling.

3. Contact point searching

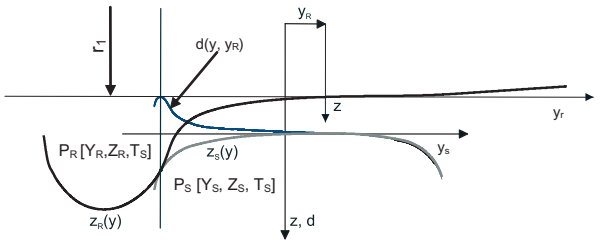

Fig. 3 Contact point of the right wheel and rail

$d\ (y, y_R)$	function of difference of the z-direction coordinate of profiles,
$P_S[Y_S, Z_S, T_S]$	contact point of a rail,
$P_R[Y_R, Z_R, T_R]$	contact point of a wheel,
$Z(P_R)$	z- direction coordinate of a contact point of a wheel,
z_R	profile of a wheel,
z_S	profile of a rail,
y_R	movement of a wheel profile.

4. Profiles transformations

4.1 Profile transformation by turning around the left wheel contact point

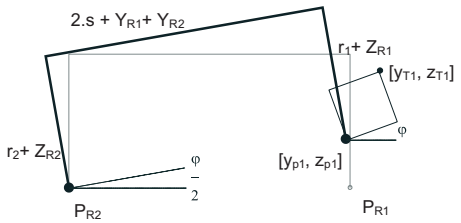

Fig. 4 Left contact point - wheels profiles transformations.

$$\begin{Bmatrix} y_{p1} \\ z_{p1} \end{Bmatrix} = \begin{bmatrix} \cos\left(\frac{\varphi}{2}\right) - 1 & \sin\left(\frac{\varphi}{2}\right) \\ \sin\left(\frac{\varphi}{2}\right) & 1 - \cos\left(\frac{\varphi}{2}\right) \end{bmatrix} \cdot$$

$$\cdot \begin{Bmatrix} 2 \cdot s + Y_{R1} + Y_{R2} \\ r_2 + Z_{R2} - (r_1 + Z_{R1}) \end{Bmatrix} \quad (5)$$

$$\begin{Bmatrix} y_{T1} \\ z_{T1} \\ 1 \end{Bmatrix} = \begin{bmatrix} \cos(\varphi) & -\sin(\varphi) & y_{p1} + Y_{R1} \\ \sin(\varphi) & \cos(\varphi) & z_{p1} + Z_{R1} \\ 0 & 0 & 1 \end{bmatrix} \cdot \begin{Bmatrix} y_1 + Y_{R1} \\ z_1 - Z_{R1} \\ 1 \end{Bmatrix} \quad (6)$$

s	half taping line distance,
r_1	right wheel radius,
r_2	left wheel radius,
$z_{R1}(y)$	right wheel profile function,
$z_{R2}(y)$	left wheel profile function,
φ	turning angle,
$P_{R1}[Y_{R1}, Z_{R1}, T_{R1}]$	right wheel contact point,
$P_{R2}[Y_{R2}, Z_{R2}, T_{R2}]$	left wheel contact point,
$z_{R1T}(y)$	right wheel profile transformed function,
$z_{R2T}(y)$	left wheel profile transformed function.

4.2 Profile transformation by turning around the right wheel contact point

$$\begin{Bmatrix} y_{p2} \\ z_{p2} \end{Bmatrix} = \begin{bmatrix} \cos\left(\frac{\varphi}{2}\right) - 1 & \sin\left(\frac{\varphi}{2}\right) \\ -\sin\left(\frac{\varphi}{2}\right) & \cos\left(\frac{\varphi}{2}\right) - 1 \end{bmatrix} \cdot$$

$$\cdot \begin{Bmatrix} 2 \cdot s + Y_{R1} + Y_{R2} \\ r_2 + Z_{R2} - (r_1 + Z_{R1}) \end{Bmatrix} \quad (7)$$

$$\begin{Bmatrix} y_{T2} \\ z_{T2} \\ 1 \end{Bmatrix} = \begin{bmatrix} \cos(\varphi) & \sin(\varphi) & y_{p2} + Y_{R2} \\ -\sin(\varphi) & \cos(\varphi) & z_{p2} + Z_{R2} \\ 0 & 0 & 1 \end{bmatrix} \cdot \begin{Bmatrix} y_2 - Y_{R2} \\ z_2 - Z_{R2} \\ 1 \end{Bmatrix} \quad (8)$$

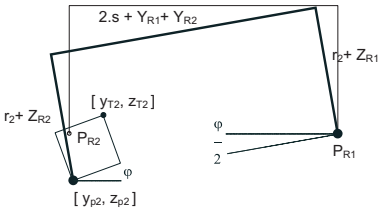

Fig. 5 Right contact point – wheels profiles transformations.

5. Wheelset contact points inverse transformation into the rail coordinate system via the turning by the φ angle

In point 1, contact points were found in the wheelset coordinate system. Now it is necessary to transform them into the rail coordinate system.

5.1 Right wheel contact point inverse transformation

$$\begin{Bmatrix} y_{p1} \\ z_{p1} \end{Bmatrix} = \begin{bmatrix} \cos\left(\frac{\varphi}{2}\right) - 1 & \sin\left(\frac{\varphi}{2}\right) \\ \sin\left(\frac{\varphi}{2}\right) & 1 - \cos\left(\frac{\varphi}{2}\right) \end{bmatrix} \cdot$$

$$\cdot \begin{Bmatrix} 2 \cdot s + Y_{R1O} \\ r_2 + Z_{R2O} - (r_1 + Z_{R1O}) \end{Bmatrix} \quad (9)$$

$$\begin{Bmatrix} y_{R1} \\ z_{R1} \\ 1 \end{Bmatrix} = \begin{bmatrix} \cos(\varphi) & \sin(\varphi) & Y_{R1O} \\ -\sin(\varphi) & \cos(\varphi) & Z_{R1O} \\ 0 & 0 & 1 \end{bmatrix} \cdot$$

$$\cdot \begin{Bmatrix} Y_{R1} - y_{p1} - Y_{R1O} \\ Z_{R1} - z_{p1} - Z_{R1O} \\ 1 \end{Bmatrix} \quad (10)$$

5.2 Left wheel contact point inverse transformation

$$\begin{Bmatrix} y_{p2} \\ z_{p2} \end{Bmatrix} = \begin{bmatrix} \cos\left(\frac{\varphi}{2}\right) - 1 & \sin\left(\frac{\varphi}{2}\right) \\ -\sin\left(\frac{\varphi}{2}\right) & \cos\left(\frac{\varphi}{2}\right) - 1 \end{bmatrix} \cdot$$

$$\cdot \begin{Bmatrix} 2 \cdot s + Y_{R1O} + Y_{R2O} \\ r_2 + Z_{R2O} - (r_1 + Z_{R1O}) \end{Bmatrix} \quad (11)$$

$$\begin{Bmatrix} y_{R2} \\ z_{R2} \\ 1 \end{Bmatrix} = \begin{bmatrix} \cos(\varphi) & -\sin(\varphi) & Y_{R2O} \\ \sin(\varphi) & \cos(\varphi) & Z_{R2O} \\ 0 & 0 & 1 \end{bmatrix} \cdot$$

$$\cdot \begin{Bmatrix} Y_{R2} - y_{p2} - Y_{R2O} \\ Z_{R2} - z_{p2} - Z_{R2O} \\ 1 \end{Bmatrix} \quad (12)$$

$P_{R1O}[Y_{R1O}, Z_{R1O}, T_{R1O}]$ – right wheel contact point from the previous iteration step,
$P_{R2O}[Y_{R2O}, Z_{R2O}, T_{R2O}]$ – left wheel contact point from the previous iteration step,
$P_{R1}[Y_{R1}, Z_{R1}, T_{R1}]$ – right wheel contact point turned by the φ angle,
$P_{R2}[Y_{R2}, Z_{R2}, T_{R2}]$ – left wheel contact point turned by the φ angle.

6. Computation of the geometric characteristics at the wheelset rolling

The separate points of the characteristics are determined step by step for $y = y_{Rmin}$ to y_{Rmax} with the step Δy_R. The procedure suitable for computer processing is determined by the equations 13–30.

1. $\varphi = 0$ (13)
2. $d_{1\,\min} = Contact\ point(y, z_{S1}, z_{R1}, P_{S1}, P_{R1}) + r_1$ (14)
3. $d_{2\,\min} = Contact\ point(y, z_{S2}, z_{R2}, P_{S2}, P_{R2}) + r_2$ (15)
4. $\varphi = \varphi + arctg((d_{1\,\min} - d_{2\,\min}) / (2\,.\,s))$ (16)
5. Saving of previous wheelset contact points
   - $P_{R1O} = P_{R1}$ (17)
   - $P_{R2O} = P_{R2}$ (18)
6. Transformation of wheelset profiles via their turning around the contact points by the φ angle. $(s, r_1, r_2, z_{R1}, z_{R2}, P_{R1}, P_{R2}, \varphi, z_{R1T}, z_{R2T})$
7. $d_{1\,\min} = Contact\ point(y, z_{S1}, z_{R1T}, P_{S1}, P_{R1}) + r_1$ (19)
8. $d_{2\,\min} = Contact\ point(y, z_{S2}, z_{R2T}, P_{S2}, P_{R2}) + r_2$ (20)
9. If $Abs(d_{1\,\min} - d_{2\,\min}) > 1.10^{-6}$ go to point 4
10. Wheelset contact points inverse transformation $(s, r_1, r_2, P_{R1O}, P_{R2O}, P_{R1}, P_{R2}, \varphi)$
    - $P_{S1}[y] = P_{S1}$ (21)
    - $P_{R1}[y] = P_{R1}$ (22)
    - $P_{S2}[y] = P_{S2}$ (23)
    - $P_{R2}[y] = P_{R2}$ (24)
11. $\Delta r[y] = r_1 + Z_{R1} - (r_2 + Z_{R2})$ (25)
12. $Tg_1[y] = T_{R1}$ (26)
13. $Tg_2[y] = -T_{R2}$ (27)
14. $Tg[y] = Tg_1[y] + Tg_2[y]$ (28)
15. $Ek[y] = \dfrac{\Delta r[y]}{2 \cdot y}$ for $y <> 0$, $Ek[y] = 0$ for $y = 0$ (29)
16. $\varphi[y] = \varphi$ (30)

$z_{S1}(y)$ right rail profile function,
$z_{S2}(y)$ left rail profile function,
P_{R1} right wheel contact point vector,
P_{R2} left wheel contact point vector,
y_{Rmin} minimum wheelset movement (−10mm),
y_{Rmax} maximum wheelset movement (10mm),
Δr Δr function vector,
Δy_R wheelset movement step,
P_{S1} right rail contact point vector,
P_{S2} left rail contact point vector,
Tg_1 tangent gamma function vector for the right wheel,
Tg_2 tangent gamma function vector for the left wheel,
Ek effective conicity vector,
Tg tangent gamma function vector.
φ wheelset rolling vector,

6.1 Rolling angle course at lateral wheelset movement

The development of the wheelset rolling angle size with regard to the lateral movement of the wheelset profile on the rail head profile has been obtained on the base of computations. The inclination of the wheelset axes is changed in the frame of the movement interval <−10, 10> by the values according to Fig. 6. This is valid for the couple of profiles of the wheel theoretic shapes S1002 and the rail head profile of UIC 60.

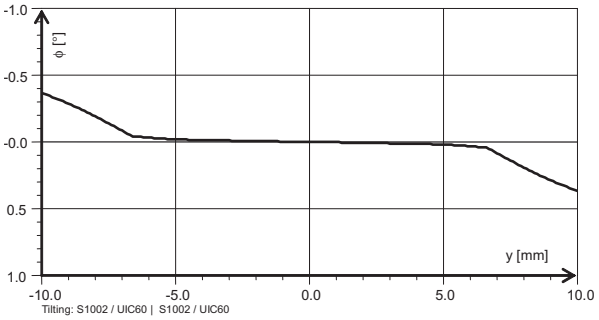

Fig. 6 Course of wheelset rolling angle.

7. The influence of the wheelset rolling on the shape of geometric characteristics

7.1 Contact points

The position of contact points between a wheelset and a rail influences the characteristics. The decisive factor which influences difference in the shape of characteristics is the difference of the contact point position in the case when the rolling is not taken into consideration and in the case when the wheelset rolling is taken into consideration.

In Fig. 7 the contact points distribution is shown (in this case standard combination of profiles S1002/UIC60/1:40/460) without regard to the rolling and in the Fig. 8 with regard to the rolling. In this case the difference is visible at the lateral wheelset movement greater than approximately 7 mm.

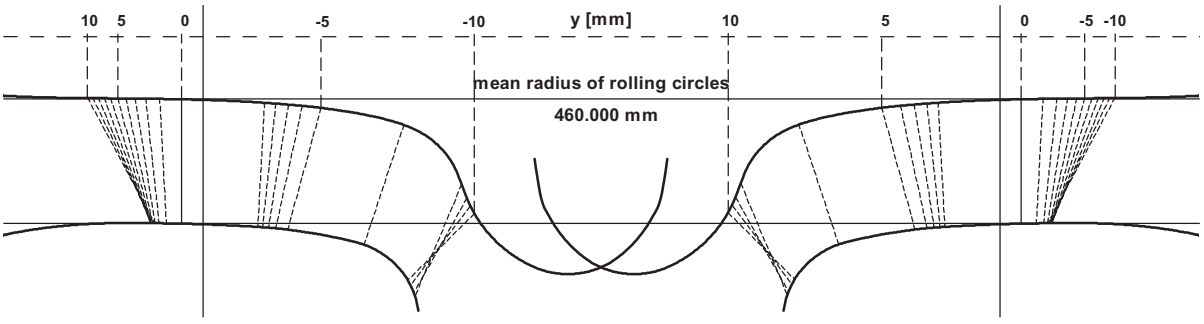

Fig. 7 Contact points distribution of non-rolled wheelset.

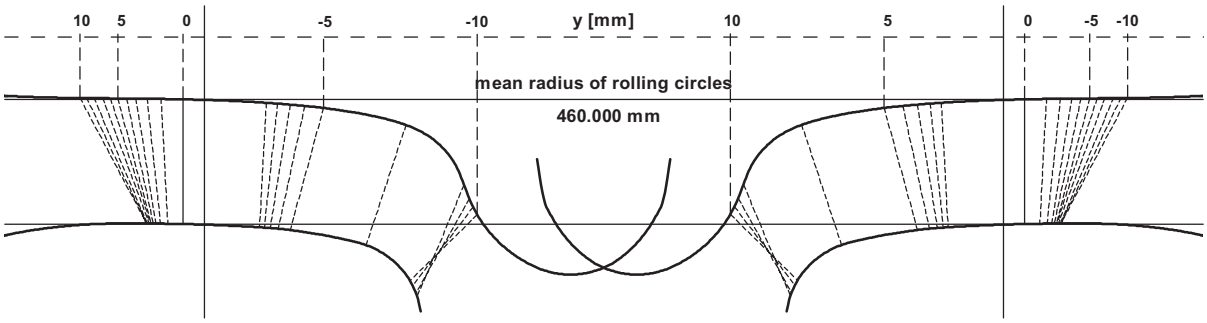

Fig. 8 Contact points distribution of rolled wheelset.

7.2 delta r function, tangent gamma function

The development of the Δr function values when taking into consideration the wheelset rolling under the influence of different contact circles radii.

tion with the rolling angle development and with the contact points distribution development. The differences are negligible for the amplitude range of a wheelset approximately $<-6, 6>$.

In this case, the other characteristics, effective and equivalent conicity, similar to the Δr function and tangent gamma function

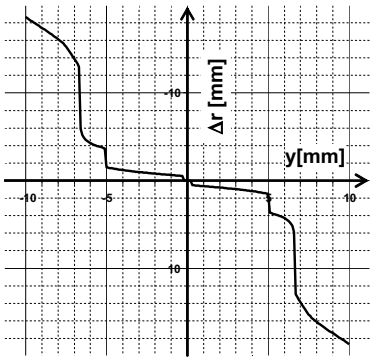

Fig. 9 Δr function.

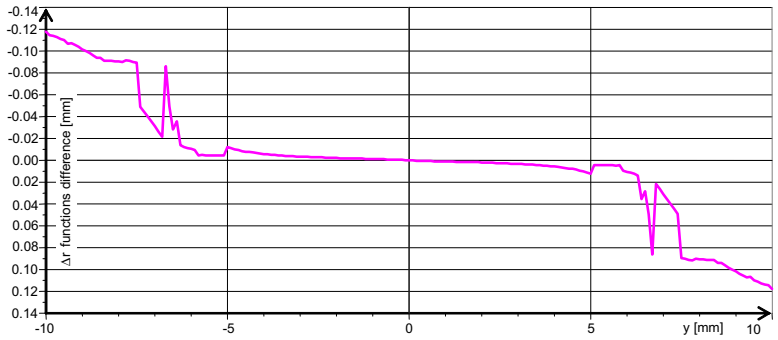

Fig.10 Δr functions difference with regard to the wheelset rolling and without regard to wheelset rolling.

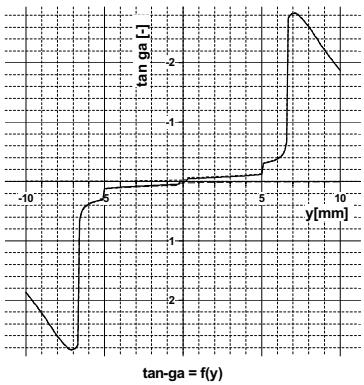

Fig.11 Tangent gamma (tan-ga) function.

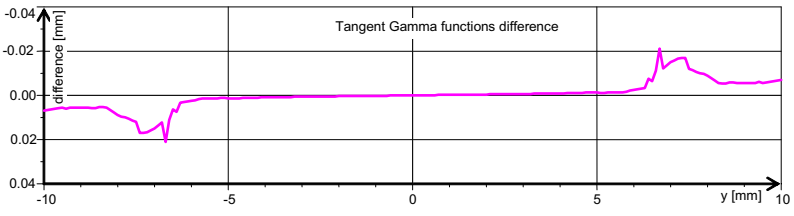

Fig. 12 Tangent gamma functions difference with regard to the wheelset rolling and without regard to wheelset rolling.

The differences in the Δr function and tangent gamma function values are visible in the Fig. 10 and 12. They are in coordina-

differ only slightly from characteristics computed without taking into consideration the wheelset rolling.

8. Conclusions

The wheelset rolling at the lateral wheelset movement on the track expresses on the shape and size of geometric characteristics.

The significance of the change depends on the profiles shape of the wheel tread and on the rail head profile. When evaluating a standard couple of profiles: wheel S1002, rail UIC60, rail slope of 1:40 and the wheel radius 460 mm, the influence of rolling expresses in the amplitude range $<-6, 6>$ to a minimum extension. The influence is negligible in the range $<-7, -6>$ and $<6, 7>$, when the wheelset is rolled to the value approximately 0.1°.

References

[1] GERLICI, J., LACK, T.: *Contact of a railway wheelset and a rail* (in Slovak). Scientific monograph, ISBN 80-8070-317-5, EDIS – publishing house of University of Žilina, 2004.
[2] GERLICI, J., LACK, T.: *Rail geometry analysis - from the point of view of wearing in the operation.* Komunikácie - ved. listy Žilinskej univerzity, EDIS – publishing house of University of Žilina, 2003.
[3] GERLICI, J., LACK, T.: *Railway wheel and rail geometry influence on ride properties of the vehicle* (In Slovak). In: 16. International Conference PRORAIL 2003, Žilinská univerzita, EDIS – publishing house of University of Žilina, 2003.
[4] GERLICI, J., LACK, T., KADOROVÁ, M.: *Calculation of the Equivalent Conicity Function with a Negative Slope.* Komunikácie - ved. listy Žilinskej univerzity, EDIS – publishing house of University of Žilina, 2004.
[5] UIC Code 519: *Method for determining the equivalent conicity.* Draft of January 2003 Original version, 2003.

https://doi.org/10.26552/com.C.2005.1.11-15

Vladimír Hlavňa – Dušan Sojčák *

AN ANALYSIS OF HEAT FLOWS IN THE COMBUSTION ENGINE OF A SHIP NON-CONVENTIONAL ENERGETIC SYSTEM

The paper describes a possibility of implementation of a non-conventional energetic system for ships. The described system is a source of heat at three levels, cool, refined electric energy and mechanical energy. Individual secondary energies are acquired by means of transformation of primary chemically bound energy in fuel. Primary energy is transformed by means of a combustion engine used as a driving unit of ships designed for transportation of passengers and goods. Mechanical energy can be used to drive a ship and its equipment. Exergy as a source of heat and cool for technological equipment of a ship. The implementation of a non-conventional system of a ship offers more possibilities for effective usage and increases energetic evaluation of the combustion engine in this means of transport. The paper analyses heat flows in the non-conventional cooling circuit of the combustion engine of a ship energetic system.

1. Introduction

Referring to [2] the non-conventional energetic system (NES) can be considered a source of electric energy, mechanical energy as well as heat energy. Heat energy can be obtained at three levels as:

- Highly potential heat in the form of water heated up to 100 °C, which can be used by the ship for heating and technological operations,
- Medium potential heat, such as water heated up to 40/55 °C to heat household water,
- Low potential heat of 7/16 °C suitable for air conditioning.

To achieve optimal use of the energies it is necessary to define a convenient cooperation between the primary – main source of energy and equipment working with it. A suitable cooperation can lead to a more effective energetic assessment of the primary source, i.e. less consumption of primary energy needed to provide the required output energetic flows.

The non-conventional energetic system is based on flows of energy from the main or auxiliary ship combustion engine. It can ensure the supply of the energies for the ship energetic system. At present attention is focused on the investigation of cooperation of the combustion engine with the absorptive cooling equipment, Figure 1. This cooperation is required by the need for application of technological and air conditioning operations aboard by means of the ship energetic center.

2. An analysis of cooperation between the combustion engine and cooling equipment

The absorptive cooling equipment can provide cooling for technological and air conditioning purposes in the energetic system of the ship. This can be provided by means of a suitable cooler.

To ensure the operation of such cooling equipment thermal energy featuring certain thermal states is needed. The suitable thermal states are provided by the cooling system of the combustion engine. We refer to the use of after-expansion energy accumulated in the engine coolant. This energy can be transported from the cooling system in two ways:

- To interconnect the combustion engine cooling system with the cooling equipment by means of hydraulic pipe and exchanger,
- To let the working medium from the absorptive cooling equipment flow directly to the engine block and in this way make full use of the temperature gradient of the cooling system at the defined flow. Losses in the hydraulic pipe and exchanger can thus be avoided. Alternative coolant must be used as a working medium in the engine cooling system.

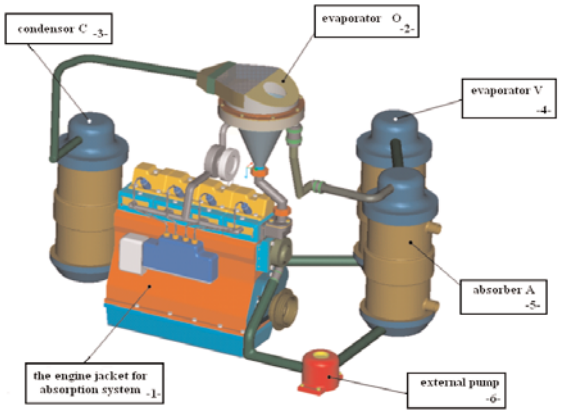

Fig. 1. Cooperation of the combustion engine and absorptive cooling equipment.

As the alternative coolant features other physical properties and the process of exergy usage in the cooling system is carried

* **Hlavňa Vladimír, Sojčák Dušan**
Faculty of Mechanical Engineering, University of Žilina, Univerzitná 1, 010 26 Žilina, Slovakia,
E-mail: Vladimir.Hlavna@fstroj.utc.sk, Dusan.Sojcak@fstroj.utc.sk

out under certain pressure and thermal conditions, it is expected that some changes in specific heat flows due to wet inserted cylinders will occur. Specific heat flows depend on mass flow of the coolant along individual cylinders, on velocity profile of flow in the engine block and on temperature gradient in the cooling system. The temperature profile on the cylinder liner corresponds to each heat flow.

To investigate heat flows and corresponding temperature profiles on the cylinder liner which result from the exchange of the coolant and from the change of pressure conditions in the engine cooling jacket it is necessary do design a model and define assumptions. For the purpose of the analysis we chose a diesel four cylinder engine having revolutions of 1500 min^{-1}. Figure 2. shows a real cooling space which was transformed to a calculation model - Figs. 3. and 4.

A mathematical model for flow analysis

We start from the mathematical model for turbulent flow of the type "renormalized groups – RNG $k-\varepsilon$ – turbulent model". The renormalization procedure applied into turbulence lies in a gradual elimination of little whirls, while equations of motion are transformed (Navier - Stokes equations) so that turbulent viscosity, forces and nonlinear members are transformed. If we suppose that these whirls are related to dissipation ε, then the turbulent viscosity μ_t is dependent on the size of turbulent whirls and the RNG method constructs this viscosity by means of iterative elimination of narrow bands of wave numbers. The following equation is used for iterative process,

$$\frac{d\,\mu_{eff}}{dl} = \frac{A_i\,\varepsilon l^3}{\mu(l)^2}\,. \tag{1}$$

The RNG model derived by a statistical method, averaged, is formally of the same form as the classical $k-\varepsilon$ model. The equation for transfer of motion is in the form:

$$\frac{\partial}{\partial t}(\rho\bar{u}_i) + \frac{\partial}{\partial x_j}(\rho\bar{u}_i\,\bar{u}_j) = \frac{\partial}{\partial x_j}\left[\mu_{eff}\left(\frac{\partial\bar{u}_i}{\partial x_j}+\frac{\partial\bar{u}_j}{\partial x_i}\right)-\right.$$

$$\left.-\left(\frac{2}{3}\,\mu_{eff}\frac{\partial\bar{u}_i}{\partial x_i}\right)\right] - \frac{\partial\bar{p}}{\partial x_i} + \rho g_i + F_i\,, \tag{2}$$

and, subsequently, transport equations are used:

$$\frac{\partial}{\partial t}(\rho_k) + \frac{\partial}{\partial x_j}(\rho\pi_j k) = \frac{\partial}{\partial x_j}\left(\alpha_k\,\mu_{eff}\frac{\partial k}{\partial x_j}\right) + \mu_t S^2 - \rho\varepsilon \tag{3}$$

$$\frac{\partial}{\partial t}(\rho\varepsilon) + \frac{\partial}{\partial x_j}(\rho\mu_j\varepsilon) = \frac{\partial}{\partial x_j}\left(\alpha_\varepsilon\,\mu_{eff}\frac{\partial\varepsilon}{\partial x_j}\right) +$$

$$+ C_{1\varepsilon}\frac{\varepsilon}{k}\,\mu_t S^2 - C_{2\varepsilon}\,\rho\frac{\varepsilon^2}{k} - R$$

For more details see [4].

Accepted assumptions.

The solution of heat spreading by means of conduction, convection, radiation in the combustion engine and in the cooling system is a highly complicated issue. The mathematical model including a complex state of heat spreading and other phenomena at passing from part of the combustion chamber to the space of the cooling system through all the elements is very complicated. This complication characterizes the defining of equation and geometric model and, consequently, calculation network. It is, therefore, necessary to accept more assumptions, which bring to the calculation itself simplifications and, thus, inaccuracy.

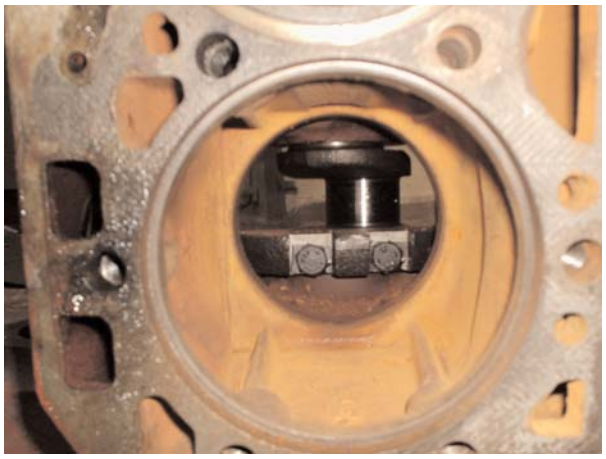

Fig. 2. Shape of the cooling space.

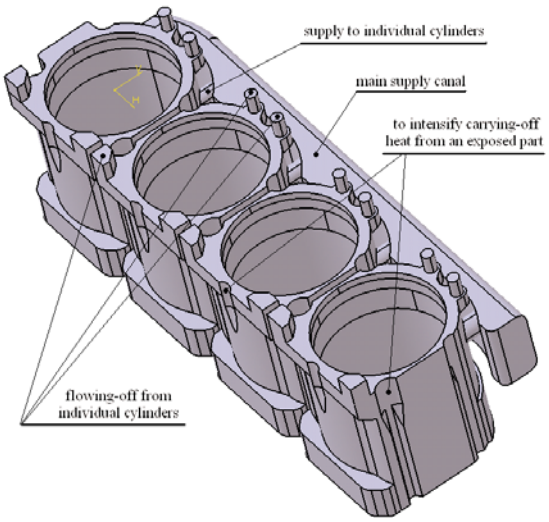

Fig. 3. Model of the cooling space.

Assumptions:

- Volume of liquid is considered only in the engine block, i. e. without the cylinder head,
- Influent field caused by the pump is not considered,
- The most serious assumption relates to combustion process. The model does not include the influence of combustion process. This influence can be observed only in the change of heat flows

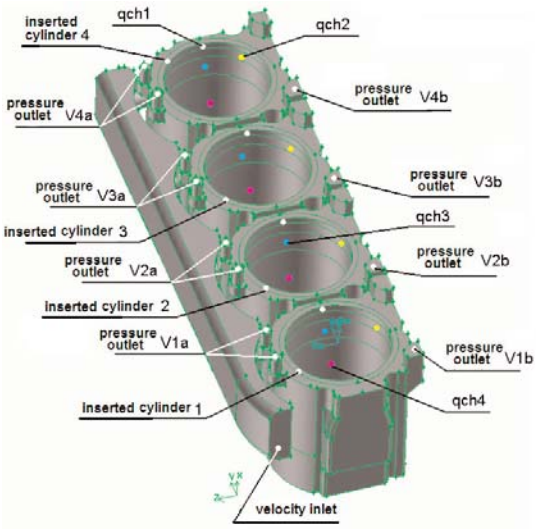

Fig. 4. Model of cooling space with defined places for calculation

through the cylinder liner at the calibration of the model for outside heat balance. Heat flows are caused by temperatures pertaining to the surfaces qch_1, qch_2, qch_3, qch_4. Here the assumption is accepted that the equal quantity of fuel from which equal quantity of heat is released be supplied into each cylinder. In this way heat flow through the cylinder liners occurs.

- An equally defined temperature profile on each cylinder liner from the side of combustion space is assumed.

Physical properties of alternative coolant:

Heat flows and temperature profiles acquired by calculation for water are considered referential. They serve for consequent comparison with heat flows and temperature profiles of an alternative coolant. The physical properties of the alternative coolant are shown in the graphs in Figs. 5 and 6. They are necessary for calculation.

Defined values of boundary conditions:

The value of boundary condition for pressure output is measured in the pump discharge, Fig. 7. The values of pressure for

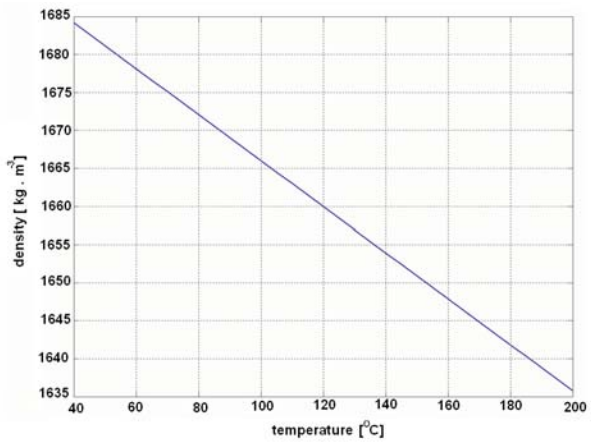

Fig. 6. Influence of change in temperature on density of alternative coolant

both (water and alternative coolant) liquids were measured in the input channel of the SM block and then applied to the boundary conditions of the pressure outlet type.

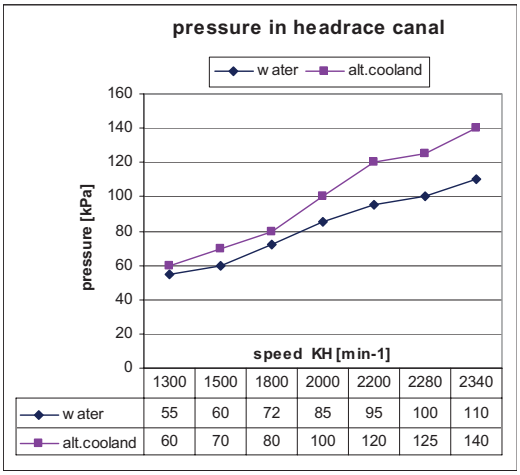

	1300	1500	1800	2000	2200	2280	2340
w ater	55	60	72	85	95	100	110
alt.cooland	60	70	80	100	120	125	140

Fig. 7. Characteristic of the coolant pump

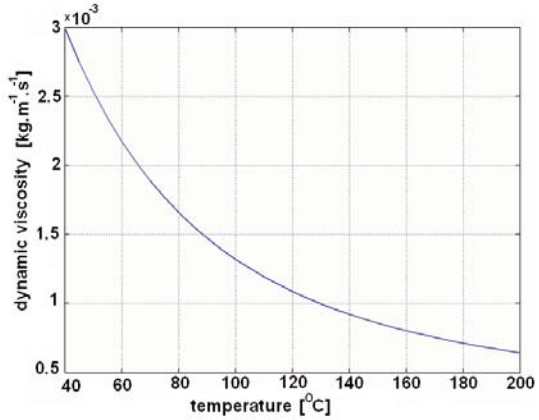

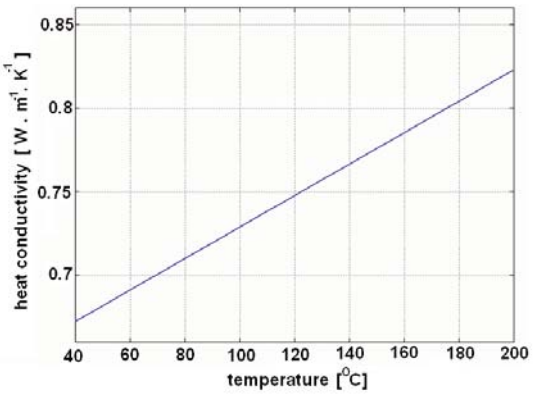

Fig.5. Influence of change in temperature on heat conductivity and dynamic viscosity of alternative coolant

For velocity input - mass flow of fluid through the block is defined and consequently the following values are calculated:

- water = 1.01 kg.s^{-1}
  at temperature of 357.44 K, v = 0.567 m.s^{-1},
- alternative coolant = 1.88 kg. s^{-1}
  at temperature of 352.24 K, v = 0.611 m.s^{-1}.

To bring about heat flows - temperatures on qch1, qch2, qch3, qch4 are applied so that the average temperature leaving the block will be equal to the one experimentally measured.

3. The results achieved

Suitability of the alternative coolant under heat, thermal, flow and pressure conditions is defined by means of velocity profile in the engine block, mass flow along individual cylinders, heat flows from the wet liners and by means of thermal profiles o the wet side of the inserted cylinders – see Figs. 8. – 13.

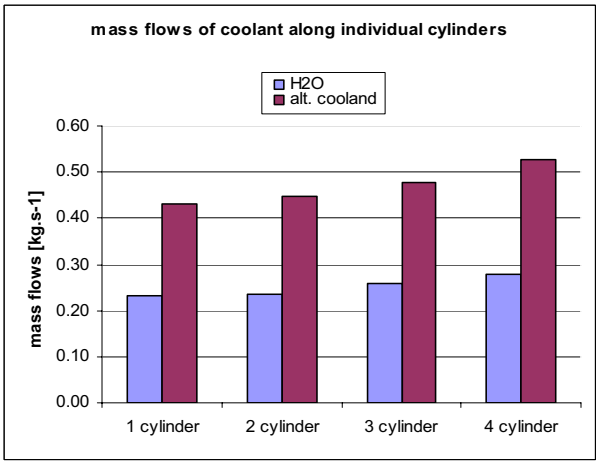

Fig. 8. Mass flows of coolant along individual cylinders

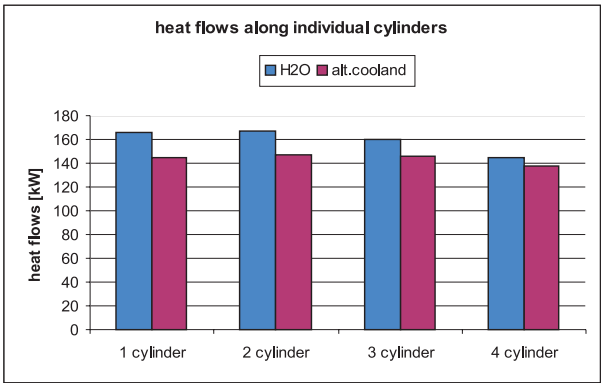

Fig. 9. Heat flows along individual cylinders

The above defined heat flows from the inserted cylinders correspond to the defined mass flows and velocity profiles. Though, temperature profiles on the wet wall of the inserted cylinder correspond to the heat flows. They characterize the cooling influence of individual coolants.

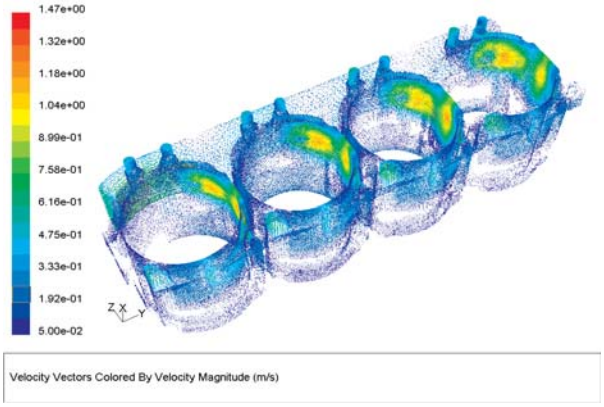

Fig. 10. Velocity field of coolant H_2O in the ICE block.

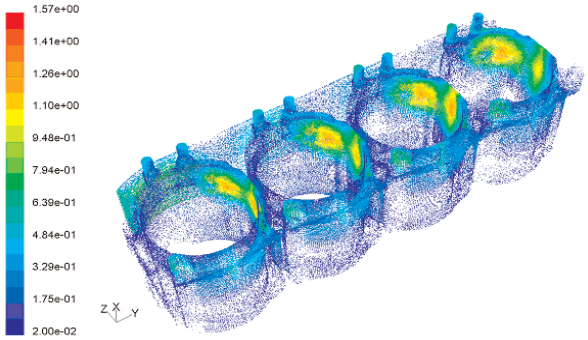

Fig. 11. Velocity field of alternative coolant in the ICE block.

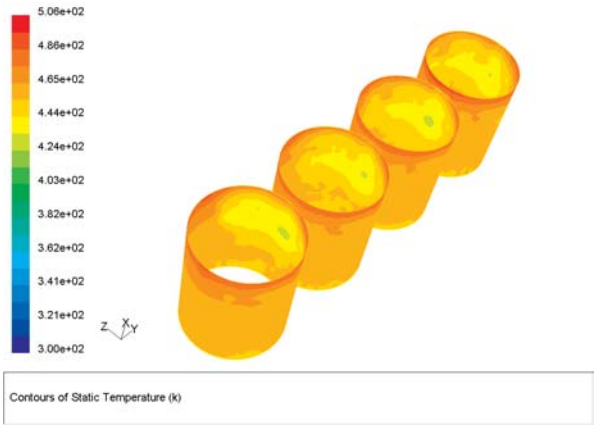

Fig. 12. Temperature profile on the wet wall of the inserted cylinder for alternative coolant – thermal state at 1500 min^{-1}.

4. Conclusion

From the measured and calculated parameters we can assume that the alternative coolant brings about favorable values.

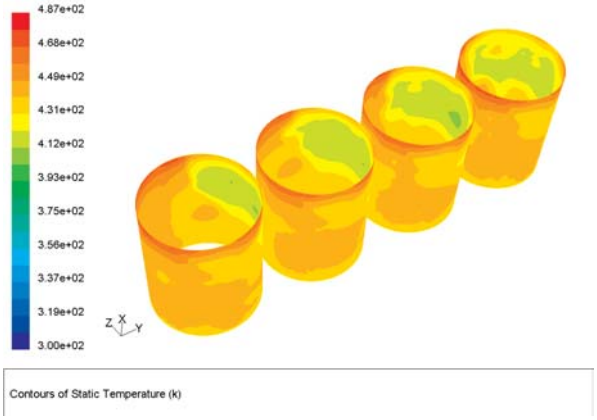

Fig. 13. Temperature profile on the wet wall of the inserted cylinder for H_2O – thermal state at 1500 min^{-1}.

The values of the velocity field for both liquids do not exceed the recommended interval of maximum values of velocities defined by the interval 1–2 $m.s^{-1}$. After the change of the cooling medium, the maximum velocities increased.

With regard to the higher density of the alternative coolant there is an increase in mass flows along individual cylinders.

Due to the change of the cooling medium (other physical properties) there was a decrease in the heat flows from individual liners. Though, their values remain within the interval of the recommended values, which is defined by the range of 110 to 190 $kW.m^{-2}$ for a category of engines of which one engine was used for the experiment.

From the acquired temperature profiles we can assume that after the change of the coolant there is a more uniform distribution of temperatures along the circumference and also alongside the cylinders.

The model defined in this way is able to model pressure and thermal states of the combustion engine block in dependence on flow conditions. These states result directly from the conditions of cooperation of the combustion engine with the absorptive cooling equipment.

References

[1] HLAVŇA, V., HUDÁK, A.: *Some problems of ICE cooling systems,* Konstrukcja, badania, eksploatacja, technologia pojazdow samochodowych i silnikow spalinowych, PAN Krakow, Zeszyt Nr. 26–27, 2003
[2] HLAVŇA, V, SOJČÁK, D.: *Non-conventional energetic system for ships,* Czasopismo techniczne z. 6 – M/2004, ISSN 0011-4561
[3] PIROCH, P.: *Efektívnejšie využitie energie paliva v nekonvenčnom spaľovacom motore,* (in Slovak) Písomná práca k dizertačnej skúške, ŽU v Žiline, 2002
[4] SOJČÁK, D.: *Spaľovací motor s nekonvenčným chladiacim okruhom,* (in Slovak), Písomná práca k dizertačnej skúške, ŽU v Žiline, 2003
[5] KONDEPUD, D.: *Modern thermodynamics,* John Wiley and Sons, 1998
[6] ŞENCAN, A., YAKUT, A., DİKMEN, E.: *New model for determining the thermodynamic properties of libr-h2o solution,* G.U. Journal of Science 17(1):101-110 – 2004, ISSN 1303-9709

The contribution was created within the framework of the project Nr. APVT – 20 – 010302, which is supported by the Agency for Support of Science and Technology of the Slovak Republic.

https://doi.org/10.26552/com.C.2005.1.16-21

komunikácie
COMMUNICATIONS

Milan Sága – Milan Letrich – Roman Kocúr *

AN ANALYSIS OF VEHICLE VIBRATION WITH UNCERTAIN SYSTEM PARAMETERS

The study proposes an application of fuzzy arithmetic for analysis of randomly excited structures with uncertain or inexact system parameters. The purpose of the paper is to investigate possibilities of a fuzzy technique in a vehicle dynamic analysis. The solution of the problem will be realised in MATLAB using the program CAR_FUZ.M with a special module INTLAB.

1. Introduction

Engineering models of carrying structures are inevitably based on idealization of reality. Therefore, various degrees of idealization will provide different results. Generally, each engineering model has to consist of three fundamental components coherent to each other [1, 8]:

- loading (harmonic, periodic, stochastic etc.),
- structural model (geometry, material properties etc.),
- response (displacements, accelerations, stresses, cumulative damage etc.).

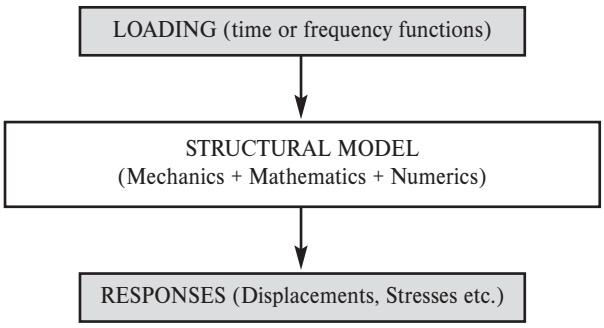

Fig. 1 Engineering models of structures

Uncertainty of each computational component (in loading or structural parameters) can be characterised by probability theory or fuzzy sets approach. Generally, uncertainties are often classified as imprecision, modelling and random [7]:

- *imprecision* is due to vagueness in a characterizing performance in terms such as "good" or "unacceptable"
- *modelling* uncertainty is due to reality idealization by the modeled structure and further simplifications in the computational models,
- *random* uncertainty reflects variations in the operating environment and lack of the designer control.

Several methods include safety factors, "worst-case scenario", probabilistic methods and fuzzy set based methods. This study focuses only on the treatment by fuzzy uncertainties, using fuzzy set theory and numerical analysis.

Fuzzy set based methods use possibility distributions to model uncertainties and assess safety. The possibility distributions are estimated using numerical data or expert opinion. In theory, probabilistic methods should be more effective for problems involving only random uncertainties, because they account for more information about these uncertainties than the other methods. However, to be applied, probabilistic methods may require more information than is available. On the other hand, fuzzy techniques require less data than probabilistic methods [1, 2].

The theory of fuzzy sets was formulated by Zadeh [9]. A fuzzy set x is the set with boundaries that are not sharply defined. A function, called membership function (MSF), signifies the degree to which each member of a domain X belongs to the fuzzy set x [11]. For a fuzzy variable $x \in <x1, x2>$, (or $x \in \boldsymbol{x}$), the membership function is defined as $\mu(x)$. If $\mu(x) = 1$, x is definitely a member of the $\boldsymbol{x}$ [5, 6, 11]. If $\mu(x) = 0$, x is definitely not a member of the $\boldsymbol{x}$. For every x with $0 < \mu(x) < 1$, the membership is not certain. Typical membership functions of fuzzy sets are shown in figures 1 and 2.

By fuzzy technique, the complete information about the uncertainties in the model can be included and one can demonstrate how these uncertainties are processed through the calculation procedure in MATLAB [1, 2].

$$\mu_A(x) = \begin{cases} 0, & x < a_1 \\ \dfrac{x - a_1}{a_2 + a_1}, & a_1 \le x \le a_2 \\ 1, & x = a_2 \\ \dfrac{a_3 - x}{a_3 - a_2}, & a_2 \le x \le a_3 \\ 0, & x > a_3 \end{cases}$$

* **Milan Sága, Milan Letrich, Roman Kocúr**
Faculty of Mechanical Engineering, Department of Applied Mechanics, University of Žilina, Univerzitná 1, 01026 Žilina, Slovakia,
E-mail: Milan.Saga@fstroj.utc.sk

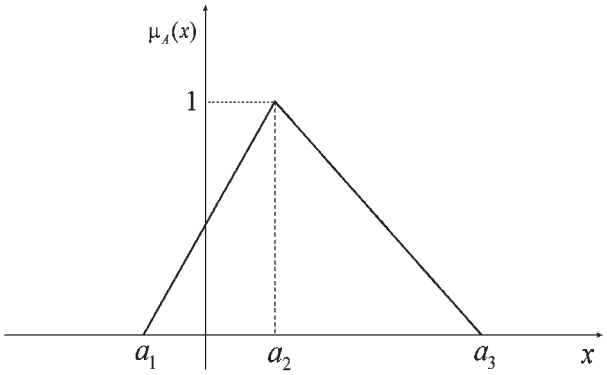

Fig. 2 MSF for a triangular fuzzy number

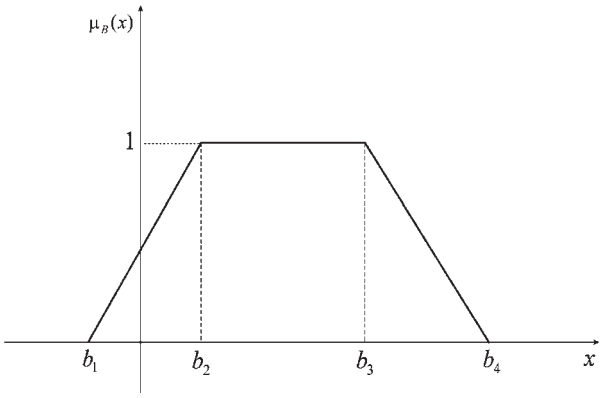

Fig. 3 MSF for a trapezoidal fuzzy number

$$\mu_A(x) = \begin{cases} 0, & x < b_1 \\ \dfrac{x - b_1}{b_2 + b_1}, & b_1 \le x \le b_2 \\ 1, & b_2 \le x \le b_3 \\ \dfrac{b_4 - x}{b_4 - b_3}, & b_3 \le x \le b_4 \\ 0, & x > b_4 \end{cases}$$

2. Numerical study of random vibration of a fuzzy vehicle computational model

Vehicle dynamic models are often characterized by uncertain system parameters. A main goal of this example will be to analyse the influence of "uncertain" mass, damping, stiffness parameters to structural response and the mark of ride quality in a chosen point. The input will be expressed by a fuzzy random function (fuzzy function of the behaviour power spectral density).

Let's consider a 7-DOFs railway vehicle model (Fig. 4). The geometry of the model is following: L = 24.5 m, a_1 = 12 m, a_2 = 12.5 m, $c_1 = c_2$ = 1 m, coordinates of the point A: x_A = 13.5 m, z_A = 1.1 m. The vehicle speed will be v = 80 km/h. Other vehicle parameters will be:

- mass of the body of coach m_1 = 16100 [kg],
- moment of inertia with respect to the axis z J_{z1} = 787570 [kg.m^2],
- moment of inertia with respect to the axis x J_{x1} = 13700 [kg.m^2],
- mass of the bogie m_2 = 3050 [kg],
- moment of inertia with respect to the axis x J_{x2} = 1230 [kg.m^2],
- stiffness of primary springing k_2 = 360000 [N/m],
- stiffness of secondary springing k_1 = 200000 [N/m],
- damping coefficient of primary springing b_2 = 20000 [N.s/m],
- damping coefficient of secondary springing b_1 = 10000 [N.s/m].

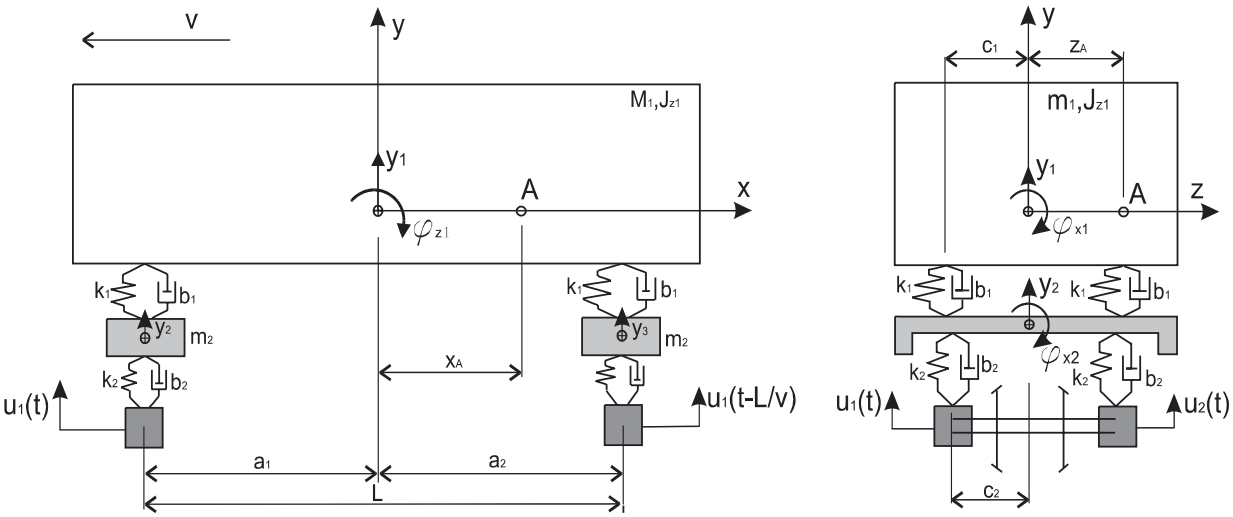

Fig. 4 Dynamic model of the railway vehicle

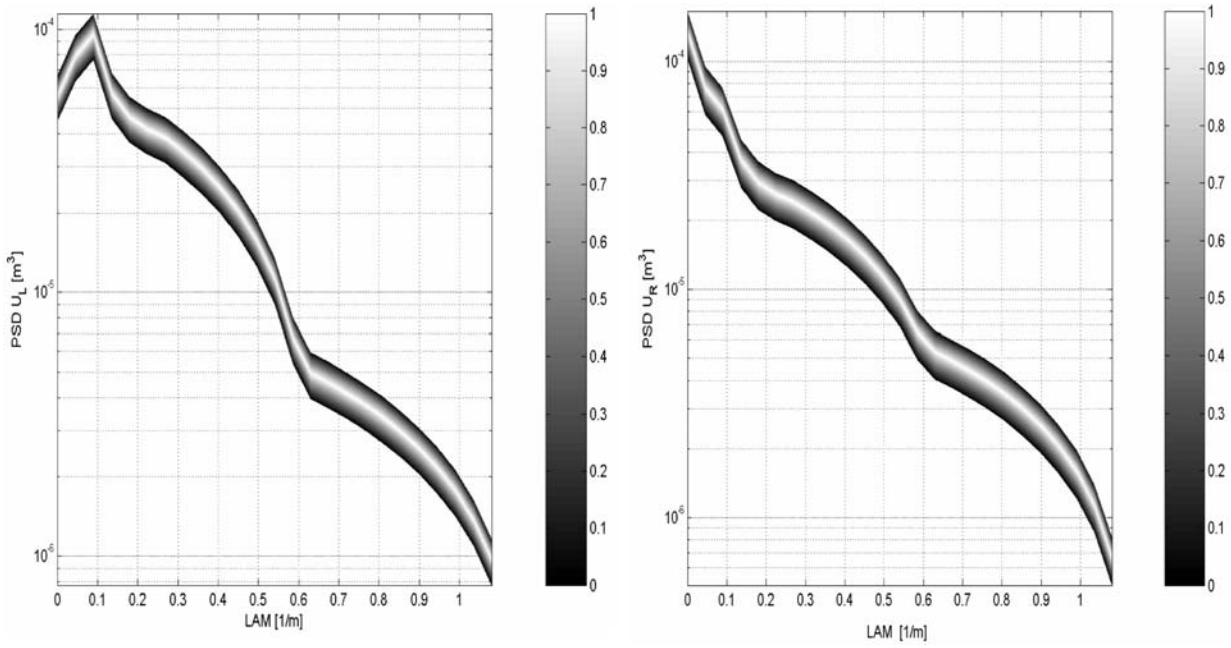

Fig. 5 Fuzzy PSD of the vertical track irregularities-left and right rail ($u_1 = u_L$, $u_2 = u_R$), LAM = spatial frequency [l/m]

The following assumptions were employed to derive this model:

- The inputs of the system are two track undulations in the vertical direction.
- The unevenness of the track at the left rail and at the right rail are presented in Fig. 5 by using the power spectral density [3]. The motion of the wheels is restricted to the vertical direction only.

It is assumed that the model is linearized around the operating state and that the coordinates

$$\boldsymbol{y} = [y_1, \varphi_{z1}, \varphi_{x1}, y_2, \varphi_{x2}, y_3, \varphi_{x3}]^T$$

are measured from the equilibrium state. The equations of motion will be interpreted as follows

$$\boldsymbol{M} \cdot \ddot{\boldsymbol{y}} + \boldsymbol{B} \cdot \dot{\boldsymbol{y}} + \boldsymbol{K} \cdot \boldsymbol{y} = \boldsymbol{T_b} \cdot \boldsymbol{u} + \boldsymbol{T_k} \cdot \boldsymbol{u}.$$

Matrices M, B, K, T_b, T_k are presented in Appendix. Fuzzification of the structural parameters has been realised by multiplication of matrices M, B, K by the fuzzy number x presented in Fig. 6.

Applying the fundamental principles of correlation theory we can solve the equations of motion in the frequency domain using the known input fuzzy power spectral density (Fig. 5) as follows [4]

$$\boldsymbol{S}_{yy}(\omega) = \boldsymbol{H}(i\omega) \cdot \boldsymbol{T}(i\omega) \cdot \begin{bmatrix} S_{u1u1}(\omega) & 0 \\ 0 & S_{u2u2}(\omega) \end{bmatrix} \cdot$$
$$\cdot \boldsymbol{T}^T(-i\omega) \cdot \boldsymbol{H}^T(-i\omega)$$

where $\boldsymbol{H}(i\omega) = (-\omega^2 \cdot \boldsymbol{x} \cdot \boldsymbol{M} + i \cdot \omega \cdot \boldsymbol{x} \cdot \boldsymbol{B} + \boldsymbol{x} \cdot \boldsymbol{K})^{-1}$ and

$$\boldsymbol{T}(i\omega) = (i \cdot \omega \cdot \boldsymbol{T}_b + \boldsymbol{T}_k) \cdot \begin{bmatrix} 1 & 0 \\ 0 & 1 \\ e^{(-i \cdot \omega \cdot L/v)} & 0 \\ 0 & e^{(-i \cdot \omega \cdot L/v)} \end{bmatrix}.$$

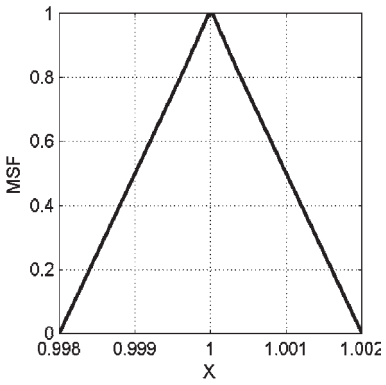

Fig. 6 Fuzzy number x

The fuzzy PSD function of the vertical motion of the point A is

$$\boldsymbol{S}_A(\omega) = [1 \quad -x_A \quad -z_A \quad 0 \quad 0 \quad 0 \quad 0] \cdot$$
$$\cdot \boldsymbol{S}_{yy}(\omega) \cdot [1 \quad -x_A \quad -z_A \quad 0 \quad 0 \quad 0 \quad 0]^T$$

and the mark of ride quality [4] will be

$$W_A = 3.33 \cdot \left(\frac{1}{2\pi} \cdot \int_0^{\omega_{\max}} \omega^4 \cdot S_A(\omega) \cdot d\omega \right)^{1/6}.$$

By using the results, it is possible to study the influence of the accumulation of uncertain vehicle parameters. For this purpose,

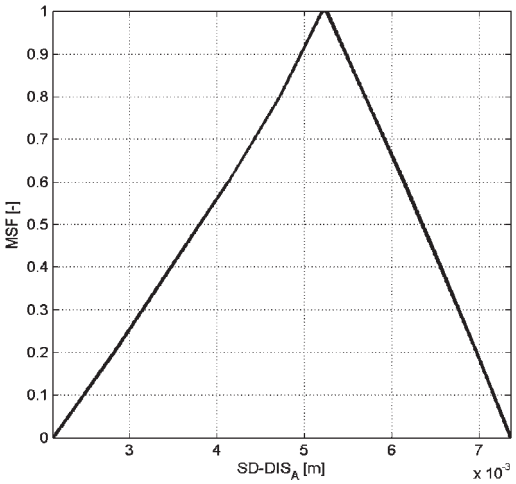

Fig. 7 Fuzzy standard deviation of the vertical displacement of

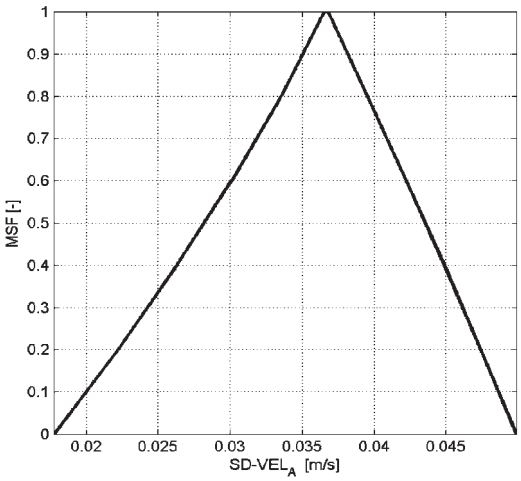

Fig. 8 Fuzzy standard deviation of the vertical velocity of point A

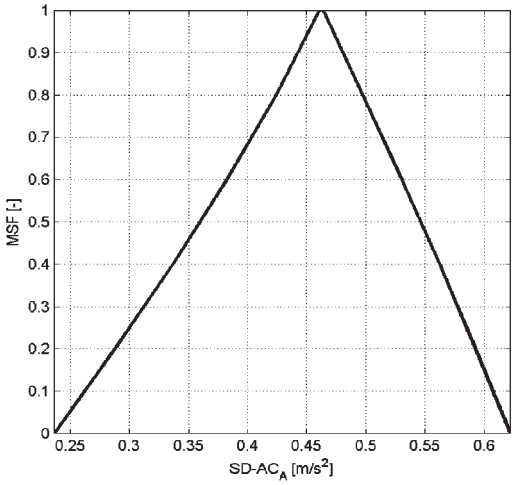

Fig. 9 Fuzzy standard deviation of the vertical acceleration of point

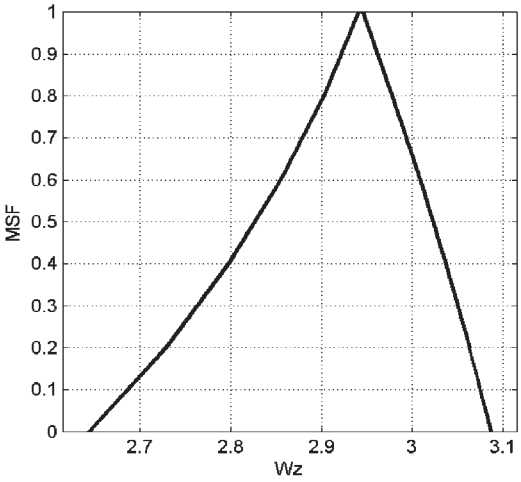

Fig. 10 Fuzzy mark of the ride quality of point A

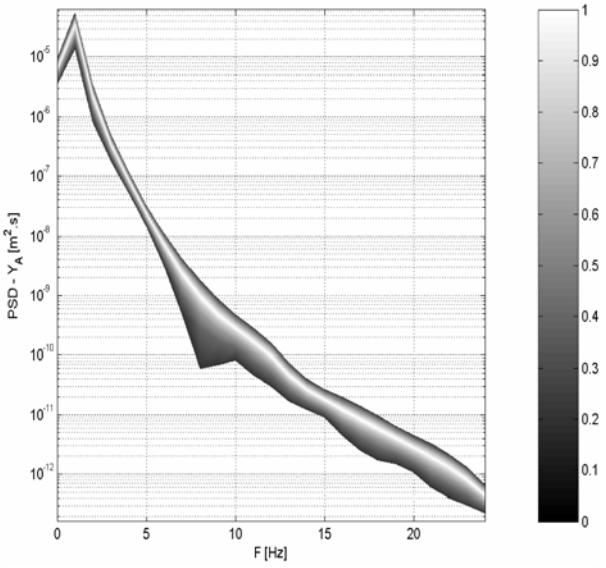

Fig. 11 Fuzzy PSD of the vertical dispavement of point A

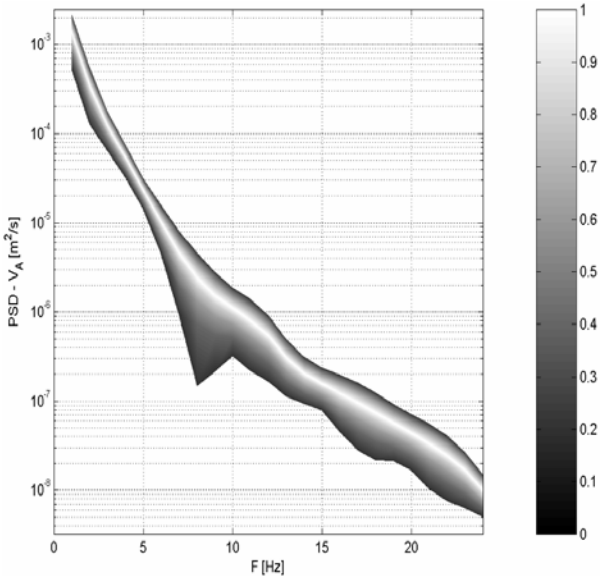

Fig. 12 Fuzzy PSD of the vertical velocity of point A

the program CAR_FUZ.M was developed. The aim of the solution was to analyse the fuzzy standard deviation of the vertical displacement, velocity, acceleration and the mark of ride quality WA in point A which are presented in Figs. 7, 8, 9 and 10. Figs. 11, 12, and 13 present the fuzzy power spectral density of the vertical vibration in point A.

3. Conclusion

The paper discusses the possibility of fuzzy arithmetic application in stochastic structural analysis. The use of fuzzy arithmetic provides a new possibility of the appraisal of machineries quality. Due to this numerical approach we can more authentically analyse mechanical, technological, service and economic properties of investigated structures.

In this paper, we have investigated the possibilities of stochastic solution for a simple vehicle computational model with fuzzy structural parameters. We have evaluated power spectral density and standard deviation of the vertical displacement, velocity and acceleration in selected point of the carriage (See Fig. 4). The fuzzy technique enables to appreciate the results in a broader context.

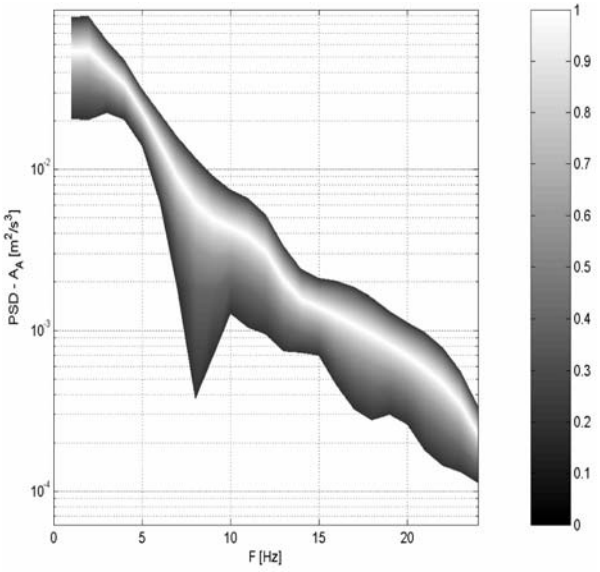

Fig. 13 Fuzzy PSD of the vertical acceleration of point A

This work has been supported by the VEGA grant No. 1/0280/03.

References

[1] MOENS D., VANDEPITTE D.: *Frequency response analysis of uncertain damped structures using the Fuzzy Finite Element Method*, WCCM V, 7.-12. 7. 2002, Vienna, Austria.
[2] KULPA, Z., POWNUK, A., SKALNA, I.: *Analysis of linear mechanical structures with uncertainties by means of interval methods*, Computer Assisted Mechanics and Engineering Sciences, 1998, Vol. 5, Poland, pp. 443–477.
[3] KALINČÁK, D.: *The power spectral densities of the measured track irregularities,* Intern. Scient. Conf. „The transport of the 21st century", Warszawa, Poland, pp. 111–118
[4] FREIBAUER L.: *Railway vehicles dynamics* (in Czech), NADAS, Praha, 1991.
[5] MOORE R.E.: *Methods and Applications of Interval Analysis*, SIAM, Philadelphia, 1979.
[6] NEUMAIER A.: *Interval Methods for Systems of Equations*. Cambridge University Press, Cambridge, 1990.
[7] MAGLARAS G., EFSTRATIOS N., HAFTKA R. T., CUDNEY H. H.: *Experimental comparison of probabilistic methods and fuzzy set based methods for designing under uncertainty, Uncertainty modelling in Vibration and Fuzzy Analysis of structural Systems, Series on Stability, Vibration and control of Systems, Series B: Vol. 10*, world Scientific Publishing Company, Singapore, 1997, pp. 253–318.
[8] HANSS, M.: *A nearly strict fuzzy arithmetic for solving problems with uncertainties,* 19th Int. Conf. of the North American Fuzzy Information Processing Society – NAFIPS '2000, pp. 439–443, Atlanta, USA, 2000.
[9] ZADEH, L. A.: *Fuzzy sets, Information and Control,* vol. 8, pp.338–353, 1965.
[10] ELISHAKOFF, I., DUAN, D.: *Application of Mathematical Theory of Interval Analysis to Uncertain Vibrations,* Proc. of NOISECON'94, Ft. Lauderdale, Florida, pp. 519–524, 1994.
[11] NOVÁK, V: *Fuzzy sets and their applications* (in Czech), SNTL Praha, 1990.

APPENDIX

The mass matrix $\boldsymbol{M}$ has seven non-zero entries along the main diagonal:

$$\boldsymbol{M} = \begin{bmatrix} n_1 & 0 & 0 & 0 & 0 & 0 & 0 \\ 0 & Jz_1 & 0 & 0 & 0 & 0 & 0 \\ 0 & 0 & Jx_1 & 0 & 0 & 0 & 0 \\ 0 & 0 & 0 & m_2 & 0 & 0 & 0 \\ 0 & 0 & 0 & 0 & Jx_2 & 0 & 0 \\ 0 & 0 & 0 & 0 & 0 & m_2 & 0 \\ 0 & 0 & 0 & 0 & 0 & 0 & Jx_2 \end{bmatrix}.$$

The stiffness matrix $\boldsymbol{K}$ is

$$\boldsymbol{K} = \begin{bmatrix} 4\cdot k_1 & 2\cdot(a_1-a_2)\cdot k_1 & 0 & -2\cdot k_1 & 0 & -2\cdot k_1 & 0 \\ 2\cdot(a_1-a_2)\cdot k_1 & 2\cdot k_1\cdot(a_1^2-a_2^2) & 0 & -2\cdot k_1\cdot a_1 & 0 & 2\cdot k_1\cdot a_1 & 0 \\ 0 & 0 & 4\cdot k_1\cdot c_1^2 & 0 & -2\cdot k_1\cdot c_1^2 & 0 & -2\cdot k_1\cdot c_1^2 \\ -2\cdot k_1 & -2\cdot k_1\cdot a_1 & 0 & 2\cdot k_1 + 2\cdot k_2 & 0 & 0 & 0 \\ 0 & 0 & -2\cdot k_1\cdot c_1^2 & 0 & 2\cdot k_1\cdot c_1^2 + 2\cdot k_2\cdot c_2^2 & 0 & 0 \\ -2\cdot k_1 & 2\cdot k_1\cdot a_1 & 0 & 0 & 0 & 2\cdot k_1 + 2\cdot k_2 & 0 \\ 0 & 0 & -2\cdot k_1\cdot c_1^2 & 0 & 0 & 0 & 2\cdot k_1\cdot c_1^2 + 2\cdot k_2\cdot c_2^2 \end{bmatrix}.$$

The damping matrix $\boldsymbol{B}$ is:

$$\boldsymbol{B} = \begin{bmatrix} 4\cdot b_1 & 2\cdot(a_1-a_2)\cdot b_1 & 0 & -2\cdot b_1 & 0 & -2\cdot b_1 & 0 \\ 2\cdot(a_1-a_2)\cdot b_1 & 2\cdot b_1\cdot(a_1^2-a_2^2) & 0 & -2\cdot b_1\cdot a_1 & 0 & 2\cdot b_1\cdot a_1 & 0 \\ 0 & 0 & 4\cdot b_1\cdot c_1^2 & 0 & -2\cdot b_1\cdot c_1^2 & 0 & -2\cdot b_1\cdot c_1^2 \\ -2\cdot b_1 & -2\cdot b_1\cdot a_1 & 0 & 2\cdot b_1 + 2\cdot b_2 & 0 & 0 & 0 \\ 0 & 0 & -2\cdot b_1\cdot c_1^2 & 0 & 2\cdot b_1\cdot c_1^2 + 2\cdot b_2\cdot c_2^2 & 0 & 0 \\ -2\cdot b_1 & 2\cdot b_1\cdot a_1 & 0 & 0 & 0 & 2\cdot b_1 + 2\cdot b_2 & 0 \\ 0 & 0 & -2\cdot b_1\cdot c_1^2 & 0 & 0 & 0 & 2\cdot b_1\cdot c_1^2 + 2\cdot b_2\cdot c_2^2 \end{bmatrix}.$$

and the left side matrices are as follows

$$\boldsymbol{T}_k = \begin{bmatrix} 0 & 0 & 0 & 0 \\ 0 & 0 & 0 & 0 \\ 0 & 0 & 0 & 0 \\ k_2 & k_2 & 0 & 0 \\ k_2\cdot c_2 & -k_2\cdot c_2 & 0 & 0 \\ 0 & 0 & k_2 & k_2 \\ 0 & 0 & k_2\cdot c_2 & -k_2\cdot c_2 \end{bmatrix} \qquad \boldsymbol{T}_b = \begin{bmatrix} 0 & 0 & 0 & 0 \\ 0 & 0 & 0 & 0 \\ 0 & 0 & 0 & 0 \\ b_2 & b_2 & 0 & 0 \\ b_2\cdot c_2 & -b_2\cdot c_2 & 0 & 0 \\ 0 & 0 & b_2 & b_2 \\ 0 & 0 & b_2\cdot c_2 & -b_2\cdot c_2 \end{bmatrix}.$$

https://doi.org/10.26552/com.C.2005.1.22-25

komunikácie
COMMUNICATIONS

Miroslav Tesař *

THE INFLUENCE OF LIQUID LOAD MOTION ON ROLLOVER STABILITY OF ROAD TANKERS

Rollover threshold is an essential factor in research into road tanker behavior since the accidents involving these vehicles frequently have fatal consequences, especially when their load is of a flammable or toxic nature.

The following article presents a method of identifying the influence of liquid motion in a partially filled road tanker. The method is based on simulation using a mathematical model developed with the help of MSA (Multi-body System Analysis) software. This software enables the user to evaluate all the factors that influence rollover stability. Mechanical pendulum methodology has been used to simulate the liquid motion.

The road tanker model was tested in compliance with the results obtained by measuring carried out on a SCANIA 124 L truck combined with a ZVVZ trailer. Simulation tests were carried out for the drive on a circular track and in a drive around a roundabout, which is considered the most dangerous manoeuvre in respect to vehicle rollover.

1. Introduction

Vehicle rollover has always resulted in a serious accident, especially for heavy trucks. Rapid development of road transport combined with significant growth in the number of road accidents has been recently recorded with heavy trucks representing a major share. Most accidents are caused by heavy road vehicle rollover. Heavy vehicle rollover appears to be a serious problem requiring careful evaluation especially for the vehicles transporting hazardous loads (i.e. road tankers), which can be classified as a subject of ADR regulations.

There are roughly 1,500 types of material transported on the roads that are classified as dangerous. This number is far from being finite, as the list of dangerous substances has been continuously growing. It is estimated that in the year 2010, dangerous substances will make 80 % of all the transported goods.

Regarding this aspect, heavy road truck rollover, especially road tankers, is clearly a serious and topical problem. This fact is supported by the fact that rollover accidents have recently been the focal point of numerous research works.

2. Problems of Vehicle Rollover

Heavy vehicle stability in cornering is primarily influenced by the following four factors: centre of gravity, wheel gauge, road turn diameter and speed of the vehicle. Besides these factors, there is also secondary rollover effect – suspended mass roll (vehicle body), which depends on suspension characteristics. Centrifugal force in cornering develops vehicle roll around its rollover centre line. This roll will generate the rollover of a vehicle equipped with soft suspension at lower speeds than that of a stiff suspension. Shift and lift of the center of gravity will cause an increase in the roll moment that adds to further reduction of the roll speed. This applies even in case that the load slips on the bearing length to the side. All the above-indicated effects can be represented by static forces, and these can be simulated on a tilting table.

The real situation is more complicated due to a variety of different dynamic effects; therefore a similar simple illustration is not sufficient. It is especially so in the case of road tankers that are difficult to describe because of the effects of free liquid motion in the tank.

Liquid – Vehicle Interaction

Numerous studies have been carried out examining the interaction of liquid sloshing and vehicle rollover. Most of the studies done in the 80s and 90s of the previous century are based on computer simulations using models with differing capabilities of processing. The most significant problem is the method utilized to simulate liquids in free motion. The most suitable seems to be the method published by Ranganathan et al.[1] in 1993. This method is based on substituting the liquid motion by a pendulum, whose parameters are derived from the amount of liquid in the tank. The structure, including the principal parameters of the pendulum, is given in Figure 1.

Description of the items in Figure 1:

A	pendulum centre
a_A, a_k, a_0	lateral acceleration
M	weight of moving liquid
m_0	weight of steady state liquid
l_k	pendulum length depending on the level of tank filling

* **Miroslav Tesař**
University of Pardubice, The Jan Perner Transport Faculty, Czech Republic, E-mail: Miroslav.Tesar@upce.cz

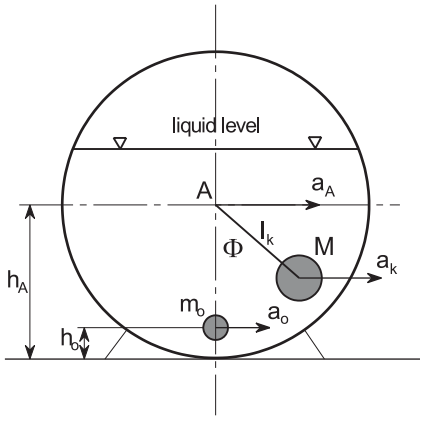

Fig. 1: Liquid motion demonstrated by means of mathematic pendulum

The method for calculation of motion of pendulum is the same as the method applied for mathematic model of vehicle.

This method makes use of markers. In accordance with ISO 2382 a marker is symbol for indication of location.

Every primary element is localized with a marker having a local coordinate system whose location in the global coordinate system a is defined by the origin location and orientation in the global coordinate system by means of transformation matrix T_{ab}

Transformation matrix T_{ab} of motion b:a is

$$T_{ab} = T_{1n} = \begin{bmatrix} a_{11} & a_{12} & a_{13} & a_1 \\ a_{21} & a_{22} & a_{23} & a_{22} \\ a_{31} & a_{32} & a_{33} & a_3 \\ 0 & 0 & 0 & 0 \end{bmatrix} = \begin{bmatrix} S_{ab} & u_{ab} \\ 0 & 1 \end{bmatrix} \quad (1)$$

$$S_{ab} = [a_{ik}] \quad (2)$$

$$u_{ab} = \lceil a_1, a_2, a_3 \rceil \quad (3)$$

where: S_{ab} – is matrix of heading angle cosines
u_{ab} – is column vector of origin O_n in space a.

Resulting transformation matrix T_{ab} or T_{1n} of finite location of the local coordinate system b is defined by a product of transformation matrices of basic motions according to:

$$T_{1n} = T_{12} \cdot T_{23} \cdot T_{34} \cdot T_{n-1,n} \quad (4)$$

For example, for fluid sloshing (pendulum motion) the point M location (Fig. 1.) is fixed with marker b defined by matrix equation (5). This equation describes the motion of point M of local coordinate system n (marker b.) in space 1 (tank, space a). This equation is matrix parametric equation of point:

$$r_{1M} = T_{12}T_{23}T_{34}T_{n+1,n} \cdot r_{nM} = T_{1n} \cdot r_{nM} \quad (5)$$

where: r_{1M} – is column vector of point M in coordinate system 1 (equation 6)

r_{nM} – is column vector of point M in coordinate system n (equation 7)

$$r_{1M} = \lceil x_{1M}, y_{1M}, z_{1M}, 1 \rceil \quad (6)$$

$$r_{nM} = \lceil x_{nM}, y_{nM}, z_{nM}, 1 \rceil \quad (7)$$

Vectors of speed v_{1M} and vectors of acceleration a_{1M} in coordinate system 1 (global coordinate system a) are the following:

$$v_{1M} = \dot{T}_{1n} \cdot r_{nM}$$

$$a_{1M} = \ddot{T}_{1n} \cdot r_{nM}$$

We have been involved in rollover stability for several years. The method presented above was used for evaluating the influence of liquid sloshing on road tanks stability. A pendulum substituting free liquid motion was integrated in the mathematical model of a road tank.

The overall layout of the model is demonstrated in Figure 2.

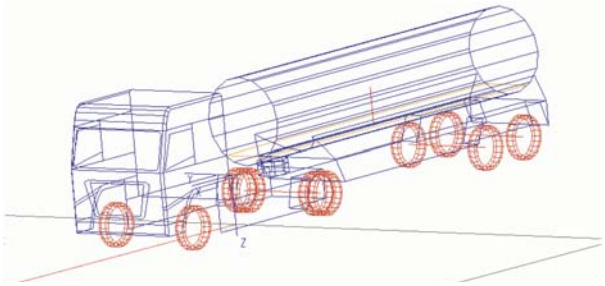

Fig.2: Overall layout of road tank model

The mathematical model of a road tanker was made with the help of MSA (Multi-body System Analysis) software. This software was developed for static, kinematic and dynamic analysis of complex mathematic systems. Other software modules enable users to model even such complex dynamic processes as a road vehicle run. The software contains a group of user variable modules: DRIVE/Transmission to select the vehicle transmission parameters, DRIVE/Driver to define the nominated road route combined with various driver characteristics and DRIVE/Tire – a tire defining module.

The mathematical model is assembled in a way that includes all the factors affecting rollover stability. Weights and inertia momentums of a truck and trailer suspension, inertia momentums of un-sprung mass reduced to wheels, weight and inertia momentum of free liquid in a road tank are the factors integrated in the mathematic model. The model structure enables one to define any suspension type involving the various characteristics of springing elements and shock absorbers including flexible backstops.

To verify the mathematical model, the following values were measured on a real vehicle on a circular track: speed, lateral accel-

eration, suspended mass rollover. The same values were computed using the mathematical simulation of the identical vehicle and drive. Comparison of the results is given in the charts in Figure 3. The results show a very high level of coincidence proving that a mathematic model can be used for testing the influence of liquid on rollover stability.

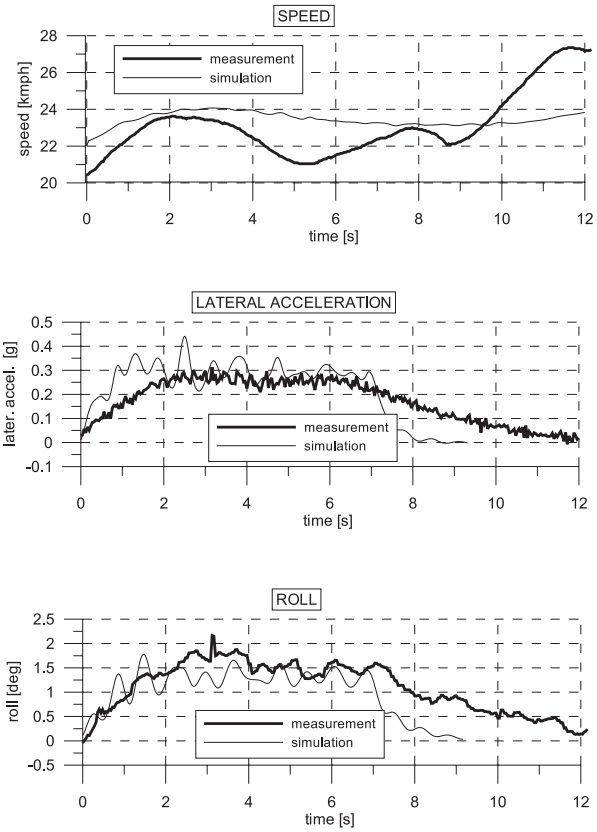

Fig. 3: Results of mathematic model verification

Numerous simulation tests were carried out with this model to verify the influence of liquid sloshing on rollover stability. The individual simulation tests were carried out with different levels of tank filling. Driving on a circular track and drive through a roundabout were selected for testing.

3. Results of Simulation Tests

The tests results showed that liquid sloshing depends on two major factors: firstly, on the level of tank filling and secondly, on the way in which the vehicle is actually driven. This assumption is based on the comparison of simulation tests results in individual ways of driving.

The drive on the circular track can be considered a steady state with its results approaching the static state. Comparing lateral acceleration and roll values in driving on circular track at constant speed proved this. The results are given in Figures 4 and 5.

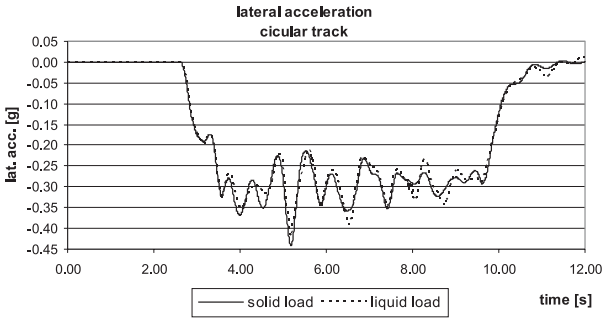

Fig. 4: Comparing lateral acceleration with solid and liquid load

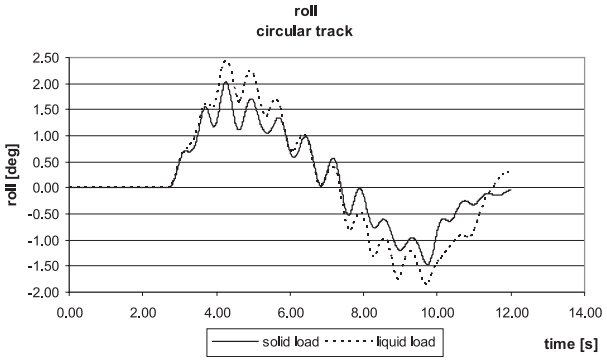

Fig. 5: Comparing the roll with solid and liquid load

The results show that the value of lateral acceleration stays almost unchanged. The roll angle is greater with a liquid load. This is caused by the shift in the center of gravity of liquid sloshing to the sides and upwards. The ratio between the roll and stabilizing moment changes and the vehicle rolls more extensively. Yet is this change not large enough to cause the vehicle rollover.

A different situation occurs when the vehicle drives through a roundabout. Roundabouts are considered the most dangerous manoeuvre from the rollover point of view. Figures 6 and 7 show the simulation of a drive through a roundabout.

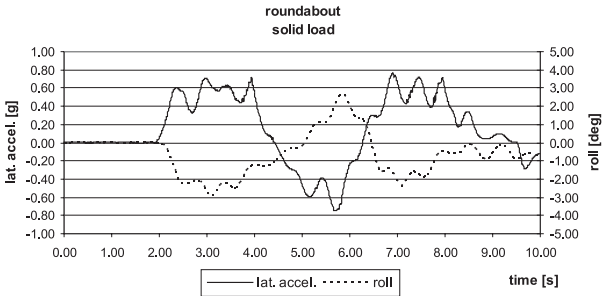

Fig. 6: Roll and acceleration course with solid load.

The record of a drive through a roundabout with solid load (Fig. 6) shows that the course of lateral acceleration and vehicle roll correspond to the changes in entering and exiting the roundabout. The vehicle negotiated the whole track without any problems.

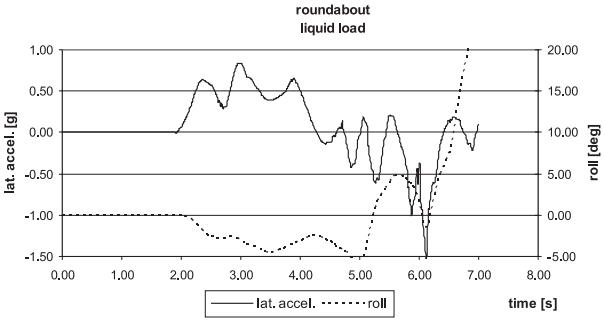

Fig. 7: Roll and acceleration course with liquid load

Figure 7 shows the influence of liquid on the vehicle behaviour in driving through a roundabout. When entering the roundabout, the vehicle drives through the right turn, then through a roundabout with a constant diameter. The change of direction is demonstrated in both the charts at the time of around the 5th second. The vehicle starts to roll in the opposite direction. Then it exits the roundabout, which leads to a rapid change of direction. Another roll appeared between the 6th and 7th second at the vehicle with solid load. The vehicle with liquid load also starts to roll but the back motion of sloshing liquid causes a sudden transfer of the gravity center and the vehicle starts to roll over. Even an experienced driver would not be probably able to prevent the rollover at this stage. At the 7th second the vehicle rolls over. This is the time when the vehicle with solid load drives through the right turn in exiting the roundabout. The vehicle behavior can be seen in the animation of the simulation outputs. Figure 8 shows the vehicle with solid load and Figure 9 shows the vehicle with liquid load at the same instant of time in driving through the roundabout. The liquid moves and the trailer wheels on one side lift. In the back motion the rolling energy reaches the values that cause the vehicle rollover.

4. Conclusion

The results of simulation tests demonstrate that this method can be used to assess the influence of liquid sloshing on rollover stability of road tanks. Significant factor is the level of tank filling. Another aspect to consider is the way of driving. It seems that a drive through a roundabout followed by a rapid change of direction towards the exit is the most dangerous manoeuvre. Numerous simulation tests will have to be carried out to find out the relations between tank filling, speed and the type of manoeuvre. The results will contribute to a deeper insight into complex dynamic processes that significantly influence rollover stability of partially filled road tanks. This will help to reduce the probability of road accidents of vehicles transporting dangerous load whose results are in most cases fatal.

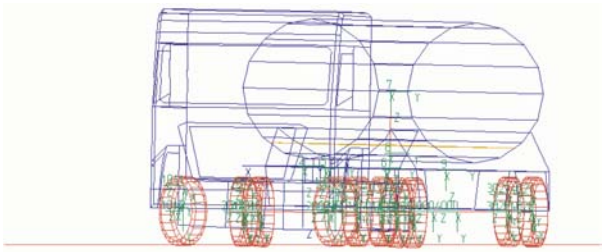

Fig. 8: Vehicle with solid load

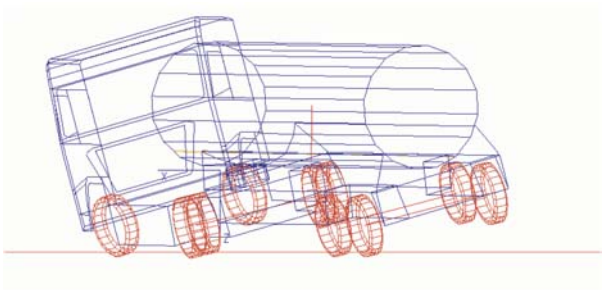

Fig. 9: Vehicle with liquid load. At the same instant of time, the vehicle with liquid load rolls over due to the effect of liquid sloshing.

References

[1] RANGANATHAN, R., YING, Y., MILES, J. B.: *Development of Mechanical Analogy Model to Predict the Dynamic Behavior of Liquids in Partially Filled Tank Vehicles.* SAE Paper 942307.

[2] TESAŘ, M., ET ALL.: *Research of evaluation of heavy vehicles rolls stability methods.* Final report. Project MoT. University of Pardubice, The Jan Perner Transport Faculty, 2004.

https://doi.org/10.26552/com.C.2005.1.26-30

komunikácie
COMMUNICATIONS

Andrzej Ambrozik *

THE METHOD OF DETERMINATION OF HEAT EMISSION CHARACTERISTICS IN PISTON SELF-IGNITION INTERNAL COMBUSTION ENGINE

The article presents the method of plotting real indicator diagrams for piston internal combustion engines. Owing to the analysis of the diagrams, it is possible to determine the self-ignition delay period and also the characteristics of the relative amount of heat emitted in combustion process. The methodology worked out by the author accounts for changes in the amount and thermodynamic properties of the working medium present in the cylinder.

1. Introduction

Thermodynamic and thermochemical processes taking place in the cylinder of a piston, internal combustion engine have been thoroughly investigated, among others, in the USA, Japan and EU countries. The research is stimulated by the development of electronic systems controlling the engine work, which are widely applied to automotive vehicles. Those systems make the engine attain the required power and the optimum work indicators due to the minimum fuel consumption, the minimum emission of harmful components of exhaust gases and noise. They also provide for high reliability and long service life.

The combustion process is responsible for satisfying the abovementioned requirements. Therefore, it is the combustion process and possible improvements on it that draw the most attention. A cylinder pressure indicator diagram is useful here. It can be either computed or taken experimentally. With it, it is possible to determine and analyse the engine indicators and evaluate the characteristics of combustion heat emission. Moreover, it allows us to determine balance composition of basic components of combustion products versus the crankshaft rotation angle and also engine work hardness, etc.

In the paper, the author presents the basic issues concerning the analysis and simulation of indicator diagrams on the basis of randomly set characteristics of the relative amount of heat emitted in combustion.

2. Experimental determination of an indicator diagram

In order to determine the characteristics of the relative amount of heat emitted in combustion it is necessary to have a precise diagram illustrating pressure changes in the cylinder, instantaneous cylinder volumes, a reliable model of heat transfer between the working medium and combustion chamber walls. We also need to know the composition, amount and properties of the gas mixture.

The above-mentioned factors [1, 4, 7, 8] are decisive for the accuracy of heat emission characteristics determination. The error in the determination of those quantities may result from:

1) flow of lines of reference (environment),
2) thermal surge (shock),
3) error in specifying the piston position in TDC on an experimentally taken indicator diagram,
4) no averaging of repeatedly taken diagrams (averaging according to approx. 33 ÷ 50 realisations) or smoothing of the averaged experimental indicator diagram,
5) quantification errors (sampling, resolution) in the real diagram.

The measurement system for investigations into piston internal combustion engines should also satisfy the following requirements:

- it must be equipped with accurate sensors,
- it should be possible to record a number of quantities simultaneously,
- measurements must be taken quickly and accurately, the values of measured quantities have to be recorded precisely,
- the quality control of measured quantities has to be kept while they are recorded and it must be possible to repeat a measurement if necessary.

The engine T359M investigations were carried out at the engine test stand equipped with eddy-current brake of WS-230 type manufactured by SCHENCK Company. The location of measurement points in engine indication is shown in Fig. 1.

Installed at the analyser input, replaceable insert NS-582 allows us to adjust the input signal voltage and to filter four simultaneously recorded and processed quantities presented in the digital form. The synchronous addressing system in the function of the crankshaft rotation angle makes it possible for the measured quan-

* **Andrzej Ambrozik**
Technical University of Kielce, Aleja Tysiąclecia Państwa Polskiego 7, PL-25314 Kielce, Poland, E-mail: silspal@eden.tu.kielce.pl

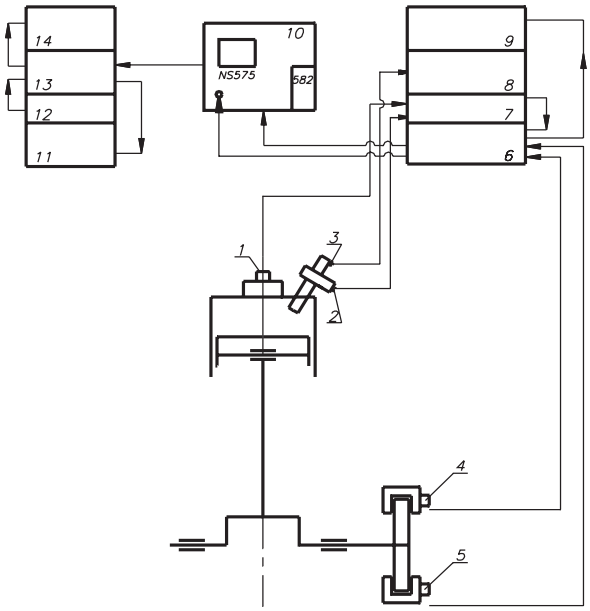

Fig. 1. Diagram of measurement points location in engine indication: 1 – piezoelectric sensor, type 642, of KISTLER company, for pressure measurements in the cylinder, 2 – piezoelectric sensor, type 1AE -123, manufactured by WRL, for fuel injection pressure measurements, 3 – capacitive needle lift sensor, 4 – photoelectric angular addressing sensor, 6 – angular addressing control system, 7 – charge amplifier, type MPU532, 8 – reactance transducer, type 51BO2, of DISA company, 9 - digital control voltmeter C-549A, 10 – digital recorder of measured runs, type NS-575, of NORTHERN company, with cartridge 582, 11 – printer DZM-180, 12 – disc memory UNIPOLBRIT, 13 – computer, 14 – monitor NEPTUN 156

tities to come as discrete 1024 data for 360° CA or 720° CA. If one or two runs are recorded, the resolution can be increased twice or four times, respectively.

With the analyser reading system it is possible to:
- continuously watch the display of runs recorded in separate memory groups and also overlay them onto one another so that they can be compared,
- screen manually the registered data with a potentiometer, where data is read on the digital value indicator,
- reproduce the registered runs on $X - Y$ or $Y - t$ recorders, oscilloscopes or loop oscillographs,
- the system series or digital input is compatible with teleprinter, printer, cassette memory or digital monitor,
- the system parallel or digital output is compatible with printer.

The correctness of TDC setting in the required channel is checked with reference to the zero value of the first derivative of compression pressure changes run.

Measurements must be preceded by static and dynamic sensor calibration with respect to the measurement current conditions.

3. The preparation of experimental an indicator diagrams for analysis

If we want to prepare an experimentally taken diagram for further analysis, first of all, it is necessary to correctly specify the piston position in TDC on the indicator diagram and also to smooth the values of pressures. It should be remembered that the diagram of pressure in the working medium compression – expansion in the cylinder is not symmetrical with TDC, even if the combustion process does not take place. That results from the fact that there are the previous cycle exhaust gases leftovers and there is heat transfer between the working medium and the cylinder. Nevertheless, it often happens that in order to determine the piston TDC in the indicator diagram, we make use of the point, at which the first derivative of the compression pressure diagram equals zero.

For the sake of correction of TDC point location in the indicator diagram, it is also possible to rely on the condition that the mean indicated pressure pi, computed on the basis of measured pressure values equals the mean indicated pressure determined as the sum of exactly measured effective pressure and accurately determined mean pressure of mechanical losses occurring in the cylinder.

The correction of TDC point location in the indicator diagram can be also made on the basis of the condition that a fuel portion is completely burnt as a whole until the instant at which the outlet valve opens. This condition is satisfied when the relative amount of the heat emitted $x \approx 1{,}0$. The condition, however, is not completely true as it does not take into account the dissociation heat of such exhaust gases components as H_2O and CO_2, which can be quite large if the exhaust gases temperature exceeds 2500 K.

Smoothing pressures in the indicator diagram is aimed at filtering out high frequency, often random diagram disturbances [8]. That involves connecting the measurement points with a smooth, interpolation curve. As a result, we obtain more regular characteristics of the relative amount of the heat emitted in a combustion process.

4. Combustion incipience, self-ignition delay period

Combustion process incipience in forced ignition engines is the time instant corresponding to the spark-over. Combustion incipience in self-ignition engines is connected with the fuel injection angle of advance and self-ignition delay period.

Self-ignition delay period is the time calculated from the beginning of the fuel injection into the combustion chamber to the chain-thermal explosion of the pre-flame reaction. It is registered in the indicator diagram as the start of very rapid increase in the working medium pressure and temperature caused by fuel combustion [3]. The length of this period significantly affects the initial stage of combustion: combustion rate, increase in pressure and temperature, engine starting properties, noise and others. N. N. Semenov, who investigated the kinetics of the pre-flame chain

reaction and experimental data [7], stated that for the delay period τ_i of gas mixtures self-ignition, the following condition is satisfied: $\varphi \cdot \tau_i = \text{const}$, where φ is the factor of the self-acceleration of pre-flame reactions.

$$\varphi = \varphi_o \, \mathrm{p}^n \exp\left(-\frac{E_a}{\overline{R}_T}\right) \tag{1}$$

It is assumed that the constant rate of branching of the chain reaction φ_o is proportional to the number of particle collisions, and the latter, in turn, depends on the fuel concentration in combustible mixture, that is on its pressure and temperature. This assumption and generalisation of the experimental data led A.I. Tolstov to the formula for the computation of self-ignition delay period:

$$\tau_i = 10^{-2} B \left(\frac{T_{pw}}{p_{pw}}\right)^{0.5} e^{\frac{E_i}{\overline{R}_T}} \tag{2}$$

where: $B = B_o(1 - K_n)$; $B_o \approx 3.8 \cdot 10^{-4}$; whereas $K = 1.6 \cdot 10^{-4}$ is a coefficient which accounts for the impact of the intensity of the working medium motion in the cylinder (proportional to the angular velocity n) on heat and mass transfer processes in the self-ignition focus and other working medium parameters at the start of fuel injection. Quantity E_i stands here for conventional energy of activation of pre-flame reactions and is a universal gas constant.

Formula (2) is widely applied to calculations of combustion in self-ignition engines. In order to enhance the accuracy and reliability of computation results, it is advisable to make the quantities B_o or E_i more precise in accordance with experimental data for a given engine.

Calculating quantity τ_i in accordance with the experimental indicator diagram, we take into account that a pressure changes rate at the end of compression is usually quite high and it is difficult to make up for errors while specifying the inflection point of a pressure p curve, connected with combustion incipience. This point can be quite clearly determined with reference to the intersection point of temperature curves [6].

In order to do that, in accordance with values set $\mathrm{p}(\alpha)$, in the vicinity to the predicted point of self-ignition occurrence, we compute the set of temperatures from the state equation. We plot graphs $T(\alpha)$ and on their basis we determine the instant of self-ignition occurrence as the point of intersection of different characteristics $T(\alpha)$, that is: characteristics $T(\alpha)$ determined for compression and combustion. When we compute heat emission characteristics with the use of experimental indicator diagrams, the instant of self-ignition is determined with reference to the rapid increase in heat emission.

The methods of determining the instant of self-ignition occurrence are presented in the graphic form in Fig. 2. The intersection of characteristic $T(\alpha)$ for compression, determined at the assumption that air is the working medium with characteristic $T(\alpha)$, determined for $\alpha \leq \alpha_{TDC}$ at the assumption that the working medium are the products of complete and total combustion of the fuel fed to the engine. Curve $T(\alpha)$ for compression is plotted for $\alpha \geq \alpha_{pw}$, whereas curve $T(\alpha)$ for combustion – when $\alpha \leq \alpha_{TDC}$.

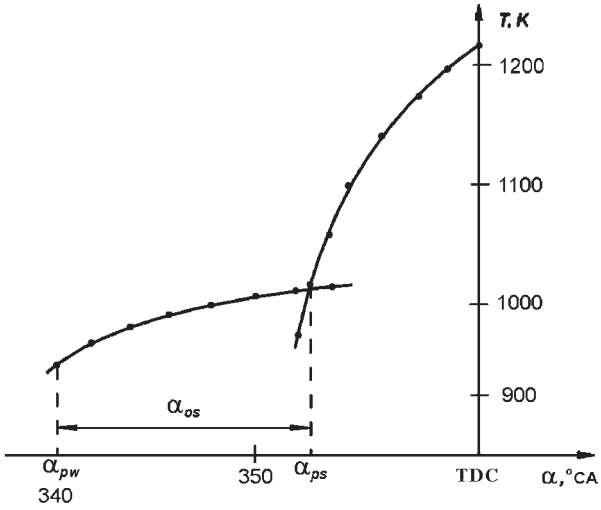

Fig. 2. The method of determination of the self-ignition delay period presented in the graphic form α_{pw} - fuel injection start, α_{ps} - combustion incipience

The self-ignition delay period is:

$$\alpha_i = \alpha_{ps} - \alpha_{pw}, \, ^\circ\mathrm{CA} \tag{3}$$

$$\tau_i = \frac{\alpha_i}{6n}, \, \mathrm{s} \tag{4}$$

The maximum rate of pressure increase in the self-ignition delay period is:

$$\left(\frac{\Delta P}{\Delta \alpha}\right)_{\max} = \frac{p_{\alpha_{ps}} - p_{\alpha_{pw}}}{\alpha_i}, \frac{pa}{^\circ CA} \tag{5}$$

The conventional energy of activation of pre-flame reactions is determined from the dependence obtained after the logarithmisation of Tolstov's formula (2):

$$E_i = \overline{R} T_{pw} \ln \frac{100\tau_i}{B\left(\frac{T_{pw}}{p_{pw}}\right)^{0.5}}; \tag{6}$$

If the computed value of quantity E_i is found in the interval $<23000, 24000 \frac{J}{mol}>$, for the fuel fed to the self-ignition engine, it means that the determined value of fuel activation energy is sufficiently reliable. The value of activation energy determined in this way can be used in calculations of self-ignition delay period in the same engine fed with the same fuel but working under different conditions.

5. The determination of characteristics of heat emission in combustion on the basis of an experimentally taken indicator diagram

Having prepared an experimentally taken indicator diagram for further analysis we should compute:

1. The amount of fuel charge burnt in a single working cycle of the engine:

$$g_c = \frac{Ge}{30 \cdot n \cdot z} \text{ or } g_c = \frac{p_\alpha V_s \eta_v}{R T_d M_o \lambda}, \ \frac{kg}{working\ cycle} \tag{7}$$

2. The value of the theoretical number of air kilo-moles necessary for complete and entire combustion of 1kg of fuel of known elementary composition.

$$M_o = \frac{1}{0{,}21}\left(\frac{C}{12} + \frac{H}{4} - \frac{O}{32}\right), \ \frac{kmol}{kg \cdot fuel} \tag{8}$$

where: C, H, O – carbon, hydrogen and oxygen mass participation in the fuel: $C + H + O = 1$.

3. Number of kilo-moles of working medium performing a single working cycle of the engine:

$$M_{cz} = \eta_v \frac{P_d V_s}{R T_d} \quad \text{lub} \quad M_{cz} = \lambda g_c M_o \tag{9}$$

where: η_v – degree of cylinder filling; λ – coefficient of excess air.

4. Kilomolar specific heats of the working medium.
The value of kilomolar specific heat is assumed to be linearly dependent on temperature [5], i.e.:

$$c_v = a + bT_{śr}; \quad \kappa - 1 = \frac{\overline{R}}{\overline{c}_v} \tag{10}$$

where: κ – adiabate exponent; a and b – temperature coefficients of specific heats.

In the paper the following notation is assumed: coefficients for air – a_λ and b_λ, those for exhaust gases – a_γ and b_γ, and those for compression – a_{spr} and b_{spr}.

5. Kilomolar specific heats of the working medium which changes its composition in combustion.
The values of these specific heats are computed from the dependence:

$$\overline{c}_{vspl} = a_i + b_i T_i; \ \overline{c}_{pspal} = R + a_i + b_i T_i \tag{11}$$

where:

$$\left.\begin{aligned} a_i &= a_{spr}(1 - x) + x \cdot a_\gamma \\ b_i &= b_{spr}(1 - x) + x \cdot b_\gamma \end{aligned}\right\} \tag{12}$$

Quantity x stands for the relative amount of the fuel that has come into reaction until considered time instant, it is calculated from the dependence:

$$x = \frac{Q_s(\alpha)}{\xi g_c W_u} \tag{13}$$

6. The changing number of kilo-moles of working medium in combustion can be accounted for by the introduction of instantaneous value of molar changes coefficient [6]. The values of theoretical and current coefficient of molar changes in the theory of internal combustion engines are calculated from the dependence:

$$\beta_o = 1 + \frac{\frac{H}{4} + \frac{0}{32}}{\lambda M_o} \quad \text{and} \quad \beta = \frac{\beta_o + \gamma}{1 + \gamma} \tag{14}$$

The instantaneous value of the coefficient of kilomolar changes in combustion can be calculated from the formula:

$$\beta_x = 1 + \frac{\beta_o - 1}{1 + \gamma} \cdot x \tag{15}$$

The instantaneous number of kilomoles of the working medium in the cylinder can be computed from the dependence:

$$M_x = \lambda g_c M_o \beta_x \tag{16}$$

6. The determination of characteristics of the relative amount of heat emitted in combustion

The relative amount of heat emitted in combustion is determined on the basis of the equation of the first law of thermodynamics and the state equation of the working medium in the cylinder:

$$\left.\begin{aligned} dQx &= dU + pdV + dQ_{sc} + dQ_{dys} \\ pV &= M\overline{R}T \end{aligned}\right\} \tag{17}$$

The instantaneous and total amount of heat released in combustion is calculated from the dependence:

$$dQ_x = \xi g_c W_u d_x; \ Q = \xi g_c W_u \tag{18}$$

where: ξ – coefficient of heat emission in combustion.

The amount of heat transferred to the walls of the combustion chamber is calculated in accordance with Newton's formula [2]:

$$dQ_{sc} = \alpha_g F dt \tag{19}$$

Quantity α_g is calculated on the basis of empirical dependences provided in the literature on the subject [2]. Quantity F stands for the surface transferring the heat, whereas dt can be substituted with a finite quantity:

$$\Delta t = \frac{\alpha_1 - \alpha_{i-1}}{6 \cdot n} \tag{20}$$

where: α – crankshaft rotation angle kąt, computed in °CA.

In the computation methodology put forward by the author, it is assumed that dissociation phenomenon does not occur in combustion, i.e. $Q_{dys} = 0$.

Inserting dependences (18), (19) and (20) into (17) and applying transformations, we obtain the formula which accounts for the calculation of the relative amount of heat released in combustion:

$$X_i = \frac{1}{\xi g_c W_o}\left\{\frac{1}{\kappa - 1}\left[\kappa p_i + \frac{p_{i-1}}{2}(V_i - V_{i-1}) + \right.\right.$$

$$\left.\left. + \frac{V_i + V_{i-1}}{2}(p_i - p_{i-1})\right] + \alpha g_i F_i \frac{\alpha_i - \alpha_{i-1}}{6 \cdot n}\right\} \qquad (21)$$

The rate at which the relative amount of heat is emitted in combustion is calculated from the dependence:

$$\dot{x}_i = \frac{x_i - x_{i-1}}{\alpha_i - \alpha_{i-1}} \qquad (22)$$

Fig. 3 presents an exemplary diagram $\dot{x}$, x_i and x_{sc} as well as x, which results from the analysis of indicator diagram of the engine T359 working when: $n = 1900\text{min}^{-1}$, $g_c = 7.16 \cdot 10^{-5}$ kg/cycle, $Me = 460$ Nm and injection advance angle $\alpha_{ww} = 18$ °CA.

7. Conclusions

Owing to the method of analysing the real indicator diagram for piston self-ignition internal combustion engine put forward in the paper, it is possible to determine self-ignition delay period and the characteristics of the relative amount of heat emitted in combustion. Thus it allows us to estimate the amount of fuel burnt on the basis of kinetic and diffuse mechanism of combustion reaction as well as the duration of these combustion phases in the engine cylinder.

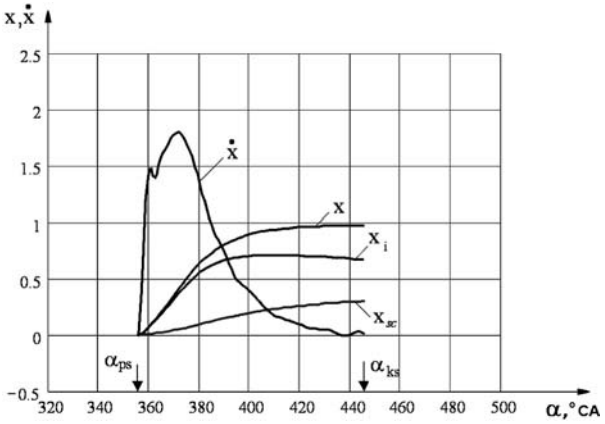

Fig. 3 Relative amounts of heat emitted in combustion and the rate ẋ, at which heat is emitted in engine T359 [3] working when: $n = 1900\ min^{-1}$, $g_c = 7.16 \cdot 10^{-5}$kg/cycle, $p_{pw} = 18.5$ MPa and $\alpha_{ww} = 18$ (CA ahead of TDC. x - relative amount of emitted heat, x_i - heat equivalent to indicated work, x_{sc} - heat transferred out of combustion space walls, respectively. Quantities α_{ps} and $_{ks}$ denote combustion incipience angle and combustion end angle, respectively.

The method worked out by the author could be applied to combustion process identification and also used to control the process course.

References

[1] AMBROZIK, A., SOBOCIŃSKI, R.: *Analysis of Combustion Process in Piston Internal Combustion Engines on the Basis of Indicator Diagram* (in Polish). ZN Transport no. 21, pp. 72–100, Warsaw, 1982.
[2] AMBROZIK A.: *Empirical Dependence Classification for Heat Transfer Coefficient Determination in Piston Internal Combustion Engines* (in Polish). Silniki spalinowe no. 4/19, ed. Zakłady Przemysłu Metalowego H. Cegielskiego, Poznan, 1987.
[3] AMBROZIK, A.: *Evaluation Methods Improvement and Selection of Ways to Perfect the Perspective Indicators of Automotive Diesel Engines Made in Poland* (in Russian). Habilitation Dissertation, Charkow, 1991.
[4] AMBROZIK, A., RAZUMOWSKI, M.: *Model of Calculations for the Working Cycle of Piston Internal Combustion Engines* (in Polish). Journal of KONES Internal Combustion Engines, Warsaw-Poznan, 1995.
[5] AMBROZIK, A., MARCENKO, A. P., PONIEWSKI, M., SZOKOTOW, N.K.: *Exergy Analysis of Piston Internal Combustion Engines* (in Polish). Ed. by the University of Technology, Kielce, 1998, p. 222.
[6] AMBROZIK, A., DANILCZYK, W., KRUCZYŃSKI, S.W.: *Simulation of an indicator diagram of a diesel engine. Polish Academy of Sciences Branch in Lublin.* Commission of Motorization and Power Engineering in Agriculture, vol. III, Lublin, 2003. pp. 12–17.
[7] SEMENOV, N. N.: *Chain Relations* (in Russian). L. Goschimizdat, 1934, p. 555.
[8] QANADILO, H.: *Investigations into and Estimation of Heat Emission Characteristics in Piston,* Self -Ignition Internal Combustion Engines (in Polish). Doctoral thesis. Warsaw, 2002.
[9] RYCHTER, T., TEODORCZYK, A.: *Mathematical Modelling of Piston Engine Working Cycle* (in Polish). PWN, Warsaw, 1990.
[10] SZCZĘSNY, P.: *Numerical Modelling of Heat Emission Process in Internal Combustion Engine* (in Polish). Doctoral thesis, Czestochowa University of Technology, Faculty of Machinery Design, Lublin, 1992.

https://doi.org/10.26552/com.C.2005.1.31-35

Hubert Kuszewski – Kazimierz Lejda – Zygmunt Szlachta *

VISUALISATION RESEARCH INTO FUEL SPRAY PROPAGATION

The results of research into a new construction of a diesel engine multi-hole injector are presented. The injector needle (RSN injector) performs a rotary/swinging movement. During the fuel injection the needle changes the area of atomizing orifices. This design changes the shape of atomized fuel sprays and has impact on their properties. The range of the spray front, the top angle of the spray and the area of the spray projection in a plane perpendicular to the injector axis were analyzed.

1. Introduction

Numerous papers indicate that the present classical systems of fuel injection directly into the combustion chamber, in the most economical directly injected Diesel engines, have reached the limit of development from an ecological point of view. In order to keep the emission of toxic components of exhaust gases within the ranges defined by both the EURO III standard and by the projected EURO IV standard, various modifications to the combustion system become necessary. Initially the fuel injection phase and the distribution of injected material within the combustion chamber should be considered [1, 2, 3, 6, 10]. It is known that injection through a conventional multi-hole nozzle (classical injector), in combination with induced swirl in the air in the chamber fails to ensure that particulates and oxides of nitrogen are not formed. These toxic components are among the most difficult to be subsequently removed from exhaust gases. For a significant advance in this area the mechanism by which the combustible mixture is formed must be radically altered. The overall process involves the following stages: fuel injection/spray formation, evaporation of fuel droplets, admixture with air, reactions immediately before combustion, the combustion process itself.

A fuel spray with a different micro and macro structure might have an important effect on these processes. In order to achieve this it is necessary to use a different type of injector - a new type of construction and modus operation [9]. A design for such a device forms the subject of the paper [4, 5, 7, 8]. The special feature of the spray-nozzle of this injector is the variability of the fuel-spraying holes during injection. The variability of the cross-sections of these holes is achieved by a rotary/swinging movement of a needle (RSN injector). The results of investigations described below show that a spray generated by this design of injector has macro-structural parameters that differ from those of a classical/traditional injector.

2. Results and discussion

The parameters of macrostructure of the stream of sprayed fuel were determined on the basis of measurements carried out using specially constructed equipment, which enabled both a direct observation of the development of the spray during the fuel injection to a chamber of fixed volume [4, 7, 8] and the measurement of the fuel distribution within the spray of droplets.

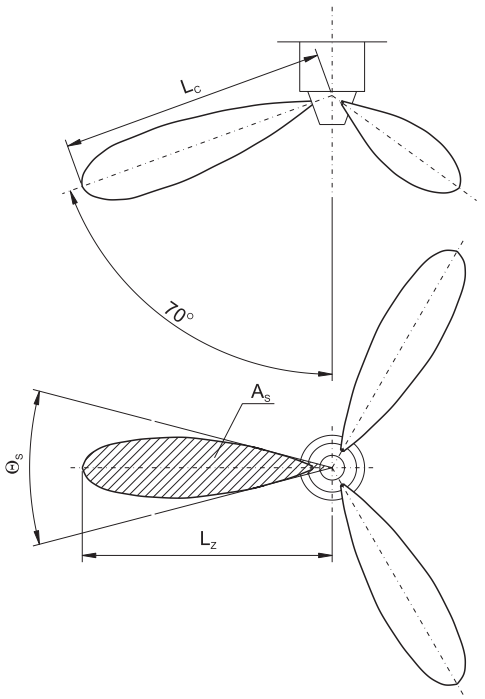

Fig. 1. The method of determining the values of parameters of the fuel spray

* **Hubert Kuszewski[1], Kazimierz Lejda[1], Zygmunt Szlachta[2]**
[1]Rzeszow University of Technology, Faculty of Mechanical Engineering and Aeronautics, Department of Automotive Vehicles and Internal Combustion Engines 8 Powstańców Warszawy Ave., 35-959 Rzeszow, Poland, E-mail: hkuszews@prz.rzeszow.pl (favoured contact), klejda@prz.rzeszow.pl
[2]Cracow University of Technology, Faculty of Mechanical Engineering, Institute of Automotive Vehicle and Internal Combustion Engines, Division of Diesel Engines, 37 Jana Pawła II Ave., 31-864 Cracow, Poland, E-mail: z.szlachta@usk.pk.edu.pl

The visual studies enabled the following to be analyzed: the range of the spray front – L_c, the top angle of the spray – θ_s and the area of the spray projection in a plane perpendicular to the injector axis – A_s. The last criterion of the spray macrostructure estimation was introduced because of the irregular shape of the spray generated by the RSN injector. The method of determination of the values of the analyzed parameters of the spray of injected fuel is depicted in Fig. 1.

A classical injector with a D1LMK 140/M2 pattern sprayer and the new RSN injector denoted "B" were compared. Both sprayers had three outlet holes, the diameter of the holes in the

Basic parameters of practical spray nozzles in visualization research Tab. 1

Symbol	i_r	l_r/d_k	d_i [mm]	d_k [mm]	h_{imax} [mm]	h_{tmax} [mm]	α_{imax} [°]
„B" (with rot.-swing. needle movement)	3	–	0.40	0.60	–	1.09	20

Symbols: i_r – number of spraying holes, l_r/d_k – relation length of the spraying hole to its diameter (in spray nozzle with a rotary-swinging needle the movement section of the spraying hole changes within duration of injection because it is not possible to exactly define this parameter), d_i – diameter of the spraying hole in a needle (only an injector with rotary-swinging needle movement), d_k – diameter of the spraying hole in a spray nozzle holder, h_{imax} – maximum needle stroke (only a classical injector), h_{tmax} – maximum piston stroke (only an injector with rotary-swinging needle movement), α_{imax} – maximum angle of the needle rotation (only an injector with rotary-swinging needle movement)

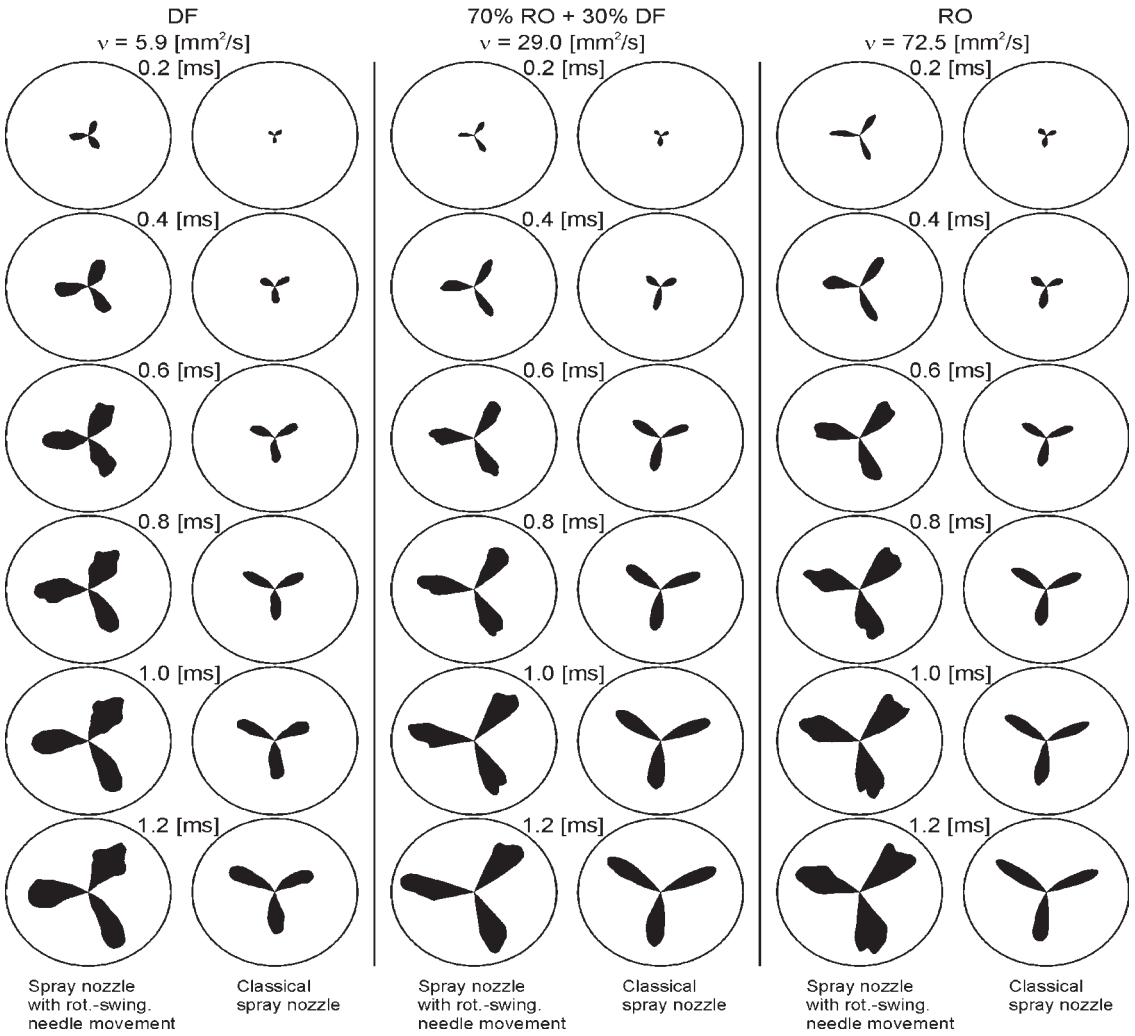

Fig. 2. Pictures of fuel sprays propagation obtained from a three-hole spray nozzle with rotary-swinging needle movement and classical (p_o = 170 [bar], p_b = 20 [bar], q = 130 [mm³/injection], n_p = 600 [rpm], fuel: DF, 70% RO + 30% DF, RO)

classical injector body and the RSN type being equal. The basic parameters of the investigated spray nozzles (classical and "B") are shown in table 1.

In Fig. 2. the example pictures of the fuel sprays propagation achieved in visualization research were shown, which created a basis for their quantitative analysis. The figures illustrate injection of diesel fuel (DF), rape oil (RO) and mixture of these fuels to visualization chambers in identical conditions. From the figures it can be clearly seen that fuel spray generated by a spray nozzle with rotary-swinging needle movement is formed in a different way than fuel spray formed by a classical spray nozzle, which causes differences in the values of an estimation parameters of the macrostructure of fuel spray. In particular it shows that fuel spray formed by a spray nozzle with rotary-swinging needle movement has an irregular form and its surface (in the view on perpendicular surface to the axis of spray nozzle), cone angle and tip penetration in comparison to the classical spray nozzle are mostly evidently larger.

2.1. The range of the spray front

In both injectors the following values were set, being the same for each type: line pressure at the opening of the sprayer p_o = 170 [bar], fuel dose q = 130 [mm^3/injection] and rotary velocity of the camshaft of the injection pump n_p = 600 [rpm]. Fuels of different viscosity (diesel fuel (DF), rape oil (RO), 70/30 RO/DF mixture) were injected into the observation chamber, filled with nitrogen at pressures of 15, 20, and 25 bars.

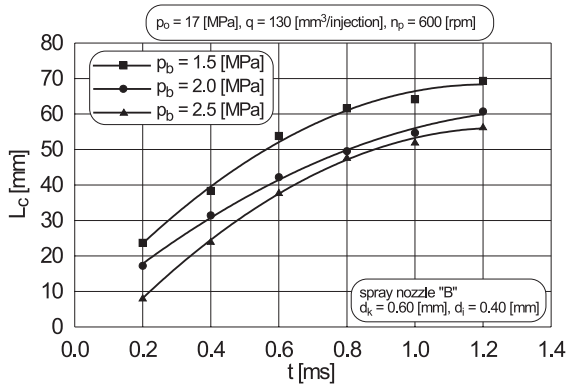

Fig. 3. The range of the diesel fuel spray front formed by the RSN type, at various background pressures in the observation chamber

The range of the spray front for diesel fuel, formed by the RSN sprayer under various values of the background pressure in the observation chamber is presented in Fig. 3. It can be seen that an increase of nitrogen pressure in the observation chamber caused – as was expected – a reduction in the range of the spray front. This phenomenon is characteristic of classical sprayers, and may be ascribed to the effect of the aerodynamic resistance on droplets of variable size. An increase in the background pressure (gas density) causes an increase in aerodynamic resistance, and a reduced dynamic pressure of the gas into which the injection is made, creating adverse conditions for the disintegration of secondary droplets. Therefore, larger droplets with greater penetrative capability are formed (obviously a larger droplet has greater kinetic energy and will, therefore, travel further).

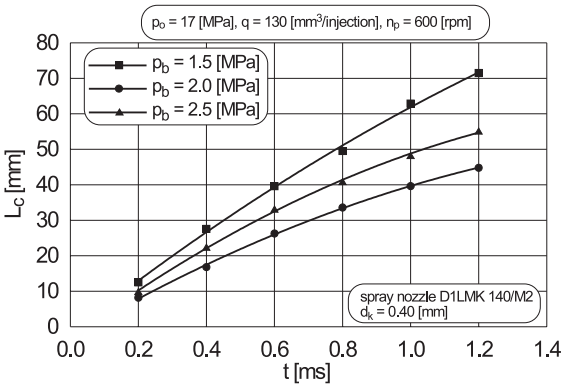

Fig. 4. The range of the diesel fuel spray front formed by the classical injector, at various background pressures in the observation chamber

The greatest range of the front of the diesel fuel spray formed by both the classical injector (Fig. 4) and the RSN injector was observed at p_b = 15 [bar]. However, at p_b = 20 [bar] the range of the front was less than at p_b = 25 [bar]. Most probably this was because of the analyzed (single) injection, at p_b = 25 [bar] the initial velocity of fuel at the sprayer outlet was higher than that at p_b = 20 [bar]. This was caused by the greater difference between the line pressure and that in the observation chamber. Therefore, the greater kinetic energy of the spray at p_b = 25 [bar] had a stronger influence on the movement of the front of the spray than the enhanced aerodynamic resistance of the environment. A comparison of Figs. 3 and 4 shows that generally the range of the front of the spray generated by the RSN sprayer is greater than that of the classical injector.

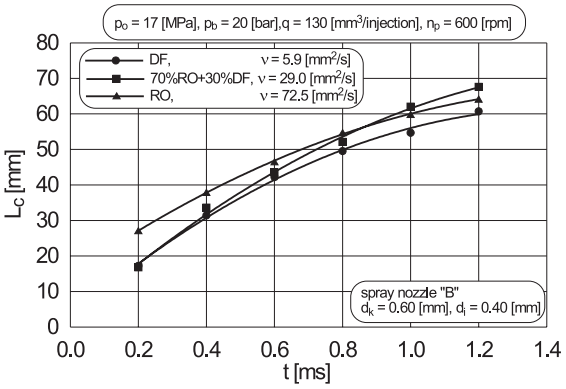

Fig. 5. The range of the front of the spray, formed by the RSN injector for fuels differing in physical properties

As it could be expected, the use of fuels of considerably greater viscosity affected both types of injectors by considerably increas-

ing the injection pressures. This was caused by a reduction in the value of the index of fuel outflow from the sprayer holes. These changes were the main contributor to the increase of the spray front range for fuels of increased viscosity ($RO - \nu = 72.5$ [mm^2/s]; 70/30 $RO/DF - \nu = 29.0$ [mm^2/s]), in relation to diesel fuel ($DF - \nu = 5.9$ [mm^2/s]) - see Figs. 5 and 6. An additional reason for the increase in range of the spray front when using higher viscosity fuels, observed for both types of injectors, was probably the increase in droplet size, due to the conditions conducive to their disintegration being worse.

From a comparison of Figs. 5 and 6 it may be seen that, as in the case of diesel fuel, the spray-range of other fuels was greater for the RSN injector over the whole time of spray development.

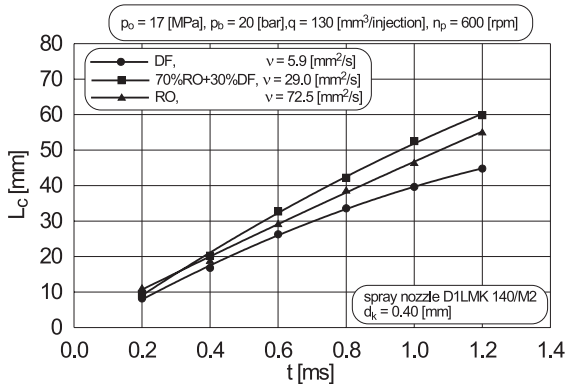

Fig. 6. The range of the front of the spray, formed by the classical injector for fuels differing in physical properties

2.2. The apex angle and surface area of the spray

In Fig. 7 it may be seen that in the case of the RSN sprayer a change in background pressure did not significantly affect the values of the apex angles of the spray over the whole time of its development. However, the spray surface area varied, the greatest area being observed for $p_b = 15$ [bar], i.e. at the background pressure at which the range of the spray was greatest.

Conversely, in the case of the classical injector the effect of pb on the apex angle θ_s was more visible - *cp*. Fig. 8. As it could be expected, the largest apex angles occurred at maximum background pressure. The values of the apex angles of the spray diminished during its development, i.e. the penetration of the spray in a direction perpendicular to its axis was reduced. For mixing this is a negative effect. It may be only partly compensated by the fact that the spray surface area increases with its development. The smallest surface area of the spray was recorded at the intermediate background pressure, $p_b = 20$ [bar], i.e. for a value corresponding to the shortest range of the spray front.

From a comparison of Figs. 7 and 8 it will be seen that the values As achieved by the RSN injector were greater than for the classical injector. It may additionally indicate the better properties of the spray from the RSN injector, due to better air/fuel mixing processes.

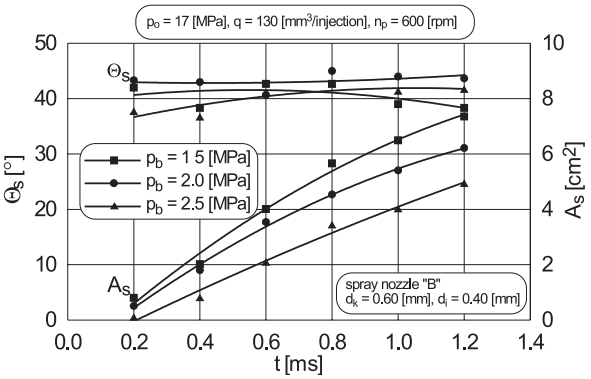

Fig. 7. The apex angle and surface area of the spray formed by the RSN type at various background pressures levels

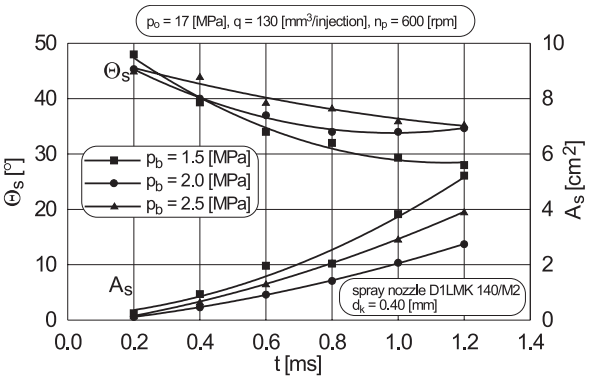

Fig. 8. The apex angle and surface area of the spray formed by the classical injector at various background pressures levels

3. Conclusions

The results of the investigations show that the spray of fuel formed using an RSN-type in a different way than that generated by a classical injector. In particular, the parameters analyzed, i.e. the range of the spray-front, the apex angle of the spray and its surface area, reach greater values for a spray formed by the new RSN type of sprayer. It may positively affect the ecological impact and the performance of engines fitted with injectors of this type.

The variation of the conditions of injection (change of the pressure of the gaseous medium into which fuel is injected, change due to use of fuels of differing viscosity) affects the macrostructure of sprays, generated by each type of injector differently. The best example may be the variance in the apex angle of the spray during spraying RO.

In the case of the classical injector it was found that this angle diminished as the spray developed, while in the case of the RSN injector the opposite tendency was observed.

Nomenclature

Quantity	Unit	Specification
A_s	[cm^2]	surface of view of fuel spray on perpendicular plane to spray nozzle axis
L_c	[mm]	real tip penetration of fuel spray
L_z	[mm]	measured tip penetration of fuel spray
Θ_s	[°]	cone angle of fuel spray
d_k	[mm]	outlet hole diameter in a needle
d_i	[mm]	outlet hole diameter in a spray nozzle body
Q	[mm^3/injection]	fuel dose
T	[ms]	time
n_p	[rpm]	rotational speed of the injection pump camshaft
p_o	[bar]	static opening pressure of injector
p_b	[bar]	ambient gas pressure
p_{wmax}	[bar]	maximum fuel injection pressure
p_{wav}	[bar]	average fuel injection pressure
ν	[mm^2/s]	kinematic viscosity of fuel
DF	–	diesel fuel
RO	–	rape oil

References

[1] DÜRNHOLZ, M., KRÜGER. M.: *Has diesel engine a future as drive of the car?* (in German), 6. Aachener Kolloquium Fahrzeug – und Motorentechnik, Akwizgran 1997.
[2] FRÄNKLE, G.: *Limits of exhaust gas for light duty trucks - Diesel engines* (in German), Symposium Dieselmotorentechnik 98, Technische Akademie Esslingen Esslingen – Ostfildern 1997.
[3] KOLLMANN, K., BARGENDE, M.: *DI diesel engine and DI spark ignition engine - Where the development of motorization is going to?* (in German, Symposium Dieselmotorentechnik 98, Technische Akademie Esslingen Esslingen – Ostfildern 1997.
[4] KUSZEWSKI, H.: *The influence of changing outlet section of injector with a rotary needle on diesel fuel spraying.* (in Polish), Ph.D. Dissertation, Cracow University of Technology, Cracow 2002.
[5] KUSZEWSKI, H., LEJDA, K., SZLACHTA, Z.: *The comparison of fuel sprays formed by classic injector and with rotary-swinging needle movement on the basis of the radial distribution of fuel.* (in Polish) "Motor Transport", Scientific Quarterly of Institute of Motor Transport, Warsaw 2003.
[6] PEAKE, S.: *Vehicle and fuel - Challenges beyond 2000*, Automotive Publishing, London 1997.
[7] SOWA, K., SZLACHTA, Z., ZABŁOCKI, M., KUSZEWSKI, H.: *The test of new environmentally friendly combustion system for high-speed diesel engine with a spray nozzle with changing section of spraying fuel orifices.* (in Polish), Rep. 9 T12 D 016 16, Cracow 2001.
[8] SZLACHTA, Z., KUSZEWSKI, H.: *The influence of changing outlet section of injector with a rotary needle on diesel fuel spraying.* (in Polish), Rep. 5 T12D 026 22, Cracow 2002.
[9] SZYMAŃSKI, J., ZABŁOCKI, M.: *The injector for combustion engine.* (in Polish), Patent Application in Patent Department R.P, No: P-294889, 11. 06. 1992.
[10] ZABŁOCKI, M.: *Injection and burning of fuel in diesel engines.* (in Polish), WKiŁ, Warsaw 1976.

https://doi.org/10.26552/com.C.2005.1.36-40

komunikácie
COMMUNICATIONS

Martin Komlossy – Marián Dzimko – Yoshinori Takeichi – Masao Uemura *

FRICTIONAL BEHAVIOUR OF THIN TIN FILMS WITH A COPPER INTERLAYER

Generally, the purpose of the study is to know the effect of temperature during tin-films deposition on frictional behaviour and lifetime of a tin layer with copper interlayer. In a recent study an experimental approach was performed to investigate the effect of a copper interlayer thickness on frictional behaviour of thin films. In this experiment, copper of 2 μm thickness was deposited between the steel substrate and tin films of 1 μm and 2 μm thicknesses in vacuum environment without and with the heating of the substrate up to 300 °C. The friction tests were performed to determine the friction coefficient and lifetime of lubrication capability.

1. Introduction

Technological use of many tribology products or tribological systems depends on adequate control of friction mechanisms between elements of tribological system consisting of two or more materials. Studies on the surface design, surface engineering, and tribology of coatings and layers have shown that friction and wear of these materials depend significantly on various combinations of materials and environmental conditions.

Micro-tribological phenomena are presently widely investigated. New technologies designed to accomplish the tasks of today and future have also brought about new tribological issues, e.g. efficient drive of machines with micro-tribological joints is limited by power consumption due to friction. The limits of traditional liquid and gaseous lubricants underline the need to use different lubricants for investigation of micro-tribological behaviour of contacting surfaces. In the process of friction and wear thin films, for which the hard substrate keeps up its role, are used in this work. The term thin film refers to a coating of a measurable thickness of up to 2.0 μm. With development of new coating techniques for industrial applications, the significance of thin film lubricants is growing. Such lubrication is commonly used when fluid lubricant could not fulfil its tasks because of high temperature or high vacuum. Other areas of applications which influenced fast innovation of lubricating methods are in the field of aerospace, whole computer media branch, mechatronics and micro machines, where the use of high-tech has become irrevocable. Coatings provide low friction and/or low wear and are often used in a wide range of temperatures, in different environments, including vacuum, usually at low loads and low sliding speeds. The most successful applications enable the reduction of a friction coefficient within a range of two or more order of the magnitude and also lower the wear. [1], [2], [3], [4].

2. Experimental Procedures

2.1 Friction Test Equipment

The equipment used to measure frictional force for a ball slider on a flat surface during experiments under low loads is presented schematically in Fig. 1. The friction test unit was assembled in a vacuum chamber, which was placed on a pneumatic damped table. The vacuum chamber allowed to examine friction behaviour of the tested pairs under different environmental conditions.

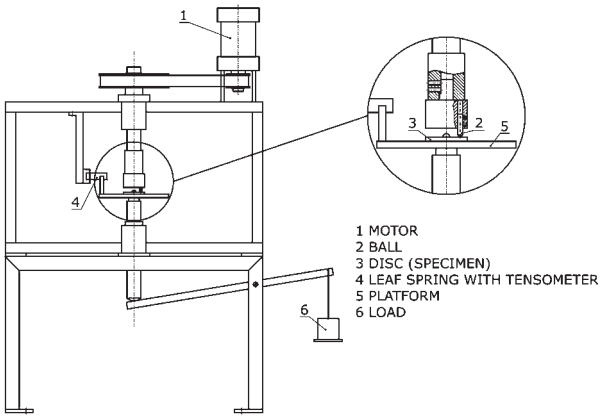

Fig. 1 Friction test apparatus

Friction experiments were carried out in vacuum of 10^{-5} Pa order. The stainless steel ball of a 3 mm diameter was fixed on the tip of the holder. The holder was arranged coaxially in a diameter

* **Martin Komlossy[1], Marián Dzimko[1], Yoshinori Takeichi[2], Masao Uemura[2]**
[1]Faculty of Mechanical Engineering, University of Žilina, Univerzitná 1, SK-010 26 Žilina, E-mail: martin.komlossy@fstroj.utc.sk
[2]Toyohashi University of Technology, Department of Mechanical Engineering, Tempaku-cho, Toyohashi-shi, Aichi, 441 8580, Japan

of 20 mm and the ball rotated on a coated disk specimen with a controlled sliding speed of 8 mm/sec. The load of 100 g applied to the ball resulted in normal force of 1N. The resulted friction forces were measured with a strain gauge placed on a leaf spring. The endurance life friction experiment continued until the tin film broke down. The criterion defining the break down of the film was marked by a sudden or substantial increase in the calculated and measured friction coefficient.

2.2 Temperature Measurement of Substrate

In recent experiments the temperature was measured with a thermocouple attached close to the substrate. There was a hypothesis that the real temperature of the substrate depending on the place of measurement is different from the one showed by the thermocouple. To verify this hypothesis a preliminary testing was undergone. The heater attached to the top of the deposition chamber (Fig. 2) was used for heating. The heater crystal was situated direct above the substrate. The temperature of specimens was measured according to the following procedure:

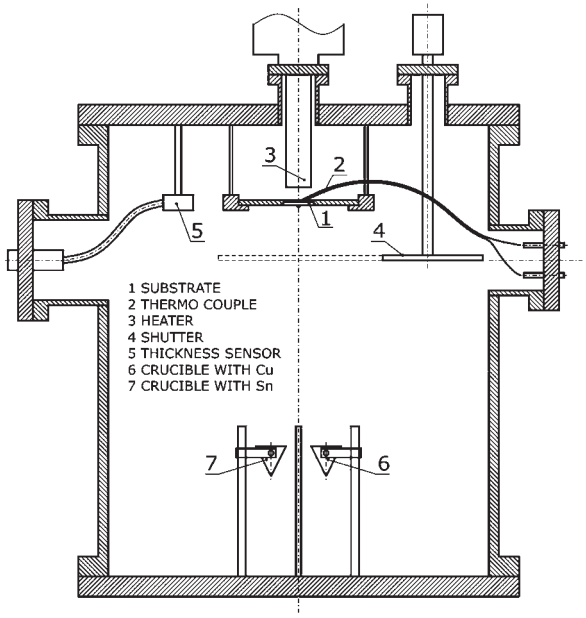

Fig. 2 Film deposition chamber

For the first case

The temperature of the heated specimen side was measured. The specimen substrate was heated continuously up to 300 °C and this temperature remained unchanged for the next 3 hours. Figure 3 shows that the temperature difference measured at two points, i. e. in the margin and in the centre of the substrate, is not significant. So, it can be assumed that there is no remarkable effect on the measurement accuracy of the thin film deposition if the thermocouple is placed in the margin or in the centre of the specimen substrate.

For the second case

The temperature was measured on both sides of the specimen. Two methods for the heating of the specimens were applied.

For the first method, the so-called programmed consistent heating method was chosen. The upper side of the substrate was heated to 100 °C and remained at this temperature for 30 minutes, then the temperature was increased to 200 °C and, again, remained unchanged for the next 30 minutes. Later the temperature was increased to 300 °C and was kept unchanged for 30 minutes (Figure 4).

For the second method, the upper side of the substrate was heated up to 300 °C and kept unchanged for 3 hours (Figure 5). The same procedure was repeated for the temperature of 400 °C (Figure 6).

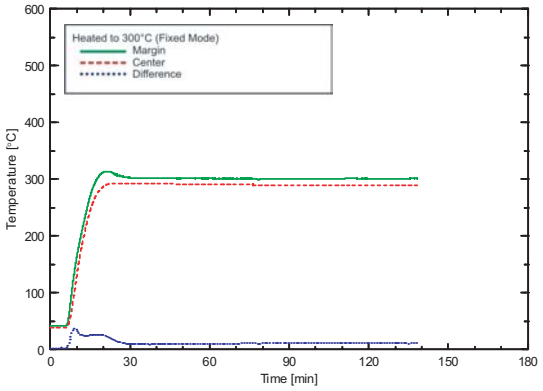

Fig. 3. Temperature in the margin and in the centre of specimen

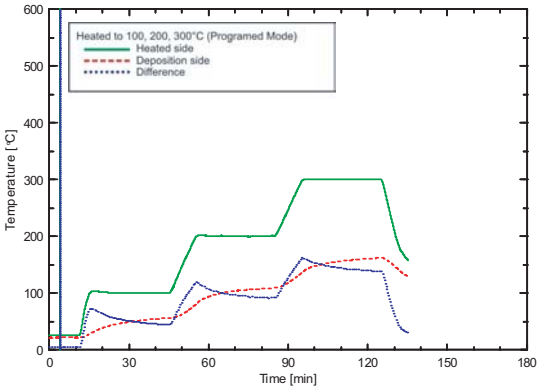

Fig. 4. Programmed consistent heating

For both methods the temperatures on the heated and deposition sides were measured. The results show that the temperature

on the deposition side is nearly by 50% lower when compared to the temperature on the heated side. Accordingly, it can be assumed that, in the case of deposition with heating up to 300 °C measured on the heated side, the real temperature of the substrate on the deposition side will reach the temperature of only 180 °C.

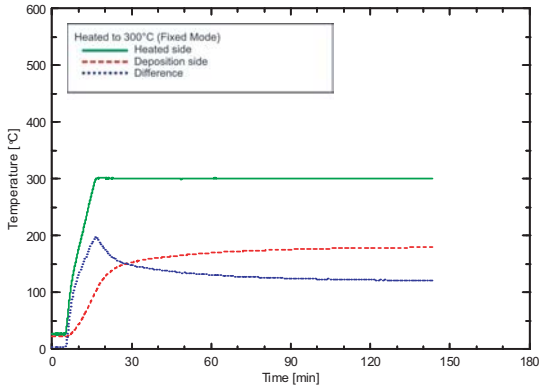

Fig. 5. Heating to 300 °C

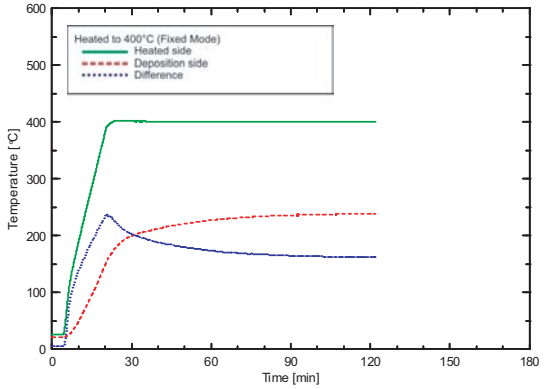

Fig. 6. Heating to 400 °C

2.3 Deposition of Cu and Sn Films for Friction Tests

Before starting the deposition of copper and tin layers for friction tests, the device for thickness monitoring was calibrated. This means that the copper layer on the silicon substrate as well as the tin layer on the silicon substrate were deposited. In cooperation with Kawamura Research Laboratories the Cu and Sn layer thickness was measured with a VK-8500 laser microscope. When the measurement was over the calibration/tooling numbers for Cu and Sn were calculated and set as the thickness reference into the monitor device.

For experiments the thin Sn and Cu films were deposited on a prepared stainless steel substrate by a vacuum deposition method in the evaporating apparatus where the values for vacuum reached 10^{-5} Pa. The deposited metals, i.e. Sn and Cu were evaporated from separate crucibles (Figure 2). The copper layer of 2.0 μm thickness used as an inter-metallic layer was deposited as the first layer to the substrate. After a cooling period of 4 hours the deposition process of the tin layer followed.

There were two different thicknesses of the Sn layer applied: one being 1.0 μm thick and another being 2.0 μm thick. For both film thicknesses the deposition started at a normal room temperature and such specimens are referred to as no-heated. For the specimens referred to as heated, the substrates were heated up to 300 °C, measured on the heated side before the deposition started.

3. Results and discussion

The experimental results aimed at determination of lifetime and friction behaviour of the tested pairs in dependence on the film thickness and based on heated and no-heated substrates before the thin layer deposition are shown in Figs. 7 – 10.

Figure 7 shows two typical results of the test performed with the heated specimen (tin film thickness of 1 (m). The value of the coefficient of friction developed in a very different way. It can be easily seen that for the same experimental conditions the coefficient of friction reached the values within the range of μ = 0.2 to 0.7. Lifetime of the friction pair is also remarkably different and varies from several minutes to tens of hours.

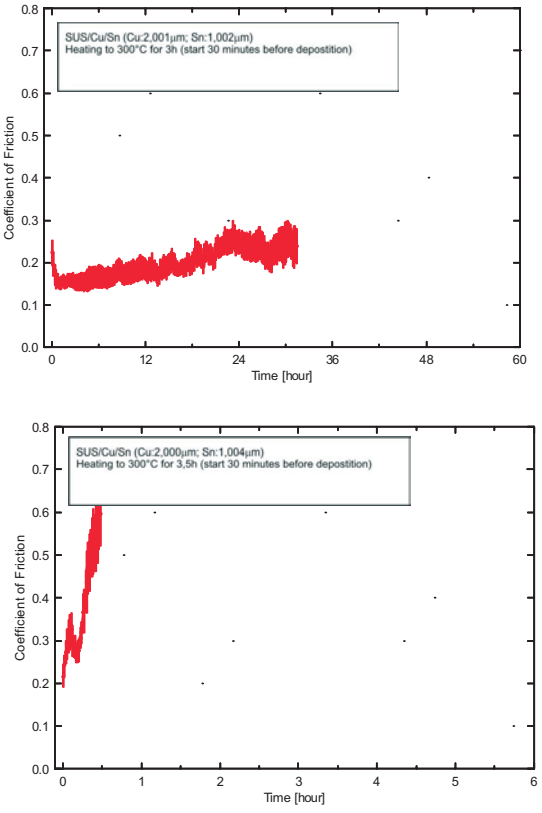

Fig. 7. Friction tests of heated specimens: Cu being 2.0 μm and Sn being 1.0 μm thick

The friction behaviour of the tin film 2 μm thick is plotted in Fig. 8. After the initial phase the friction coefficient slightly decreased to the values μ = 0.12 – 0.15 and remained nearly constant for the whole testing time.

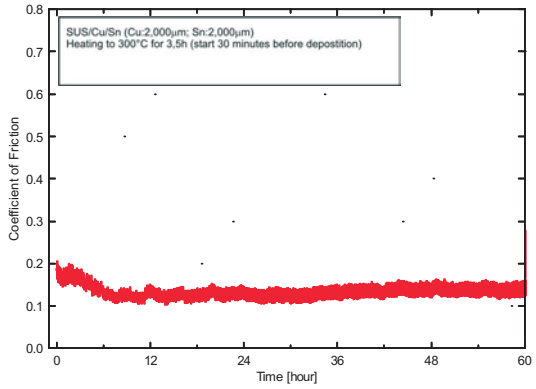

Fig. 8. Friction tests of heated specimens: Cu being 2.0 μm and Sn 2.0 μm thick

The experimental results for friction pairs composed of no-heated specimens of Cu 2.0 μm thick and Sn 1.0 μm or 2.0 μm thick are shown in Figures 9 and 10 respectively. For all the tested pairs there is a remarkable difference in lifetime. The same conclusion is valid for the level of friction μ = 0.1 to 0.3, which was almost unstable with an increasing tendency within 12 hours of testing.

An interesting similarity with Fig. 7 can be seen in Fig. 10, which shows two typical results of the test performed with the no-heated specimen. The values of the friction coefficient do not vary significantly but it can be easily seen that for the same experimental conditions the lifetime of the friction pair is remarkably different.

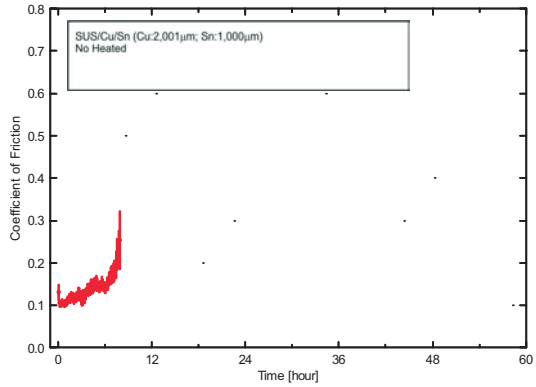

Fig. 9. Friction tests of no-heated specimens: Cu being 2.0 μm and Sn being 1.0 μm thick

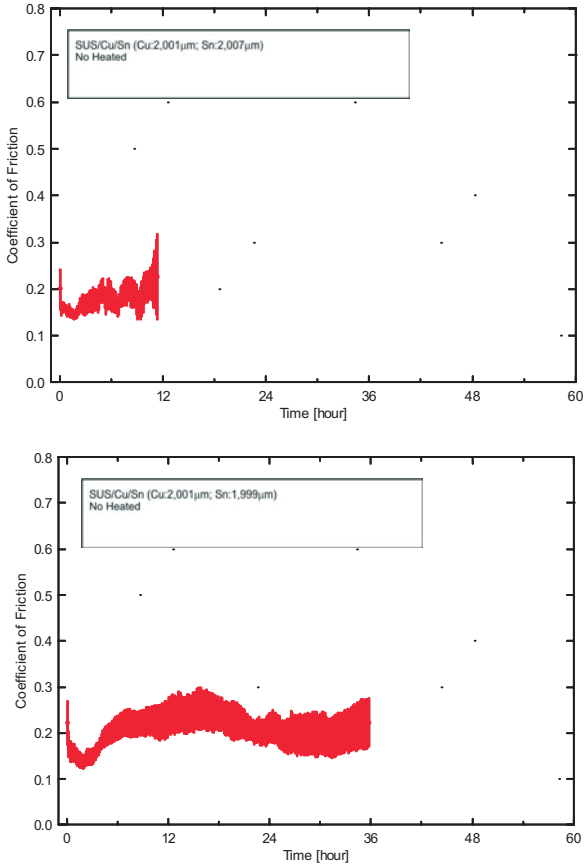

Fig. 10. Friction tests of no-heated specimens: Cu being 2.0 μm and Sn being 2.0 μm thick

4. Conclusions

Frictional properties and their influence on lifetime of friction pairs with thin tin films deposited on a copper interlayer with a constant thickness of 2.0 μm on a stainless steel substrate were investigated. For frictional properties the thinner tin films generally showed higher values for the heated specimens. For the no-heated specimens the values oscillated around μ = 0.2.

However, lifetime grows with an increasing thickness of a Sn layer. Considering also the heating of the substrate, in the case of heated specimens the lifetime is longer than for the no-heated ones.

The difference in lifetime for both types of specimens, i.e. with the heated and no-heated substrate as referred to in Figs. 7 – 10 will need more experimental investigation. Intermetallic compounds between copper and tin (mostly there are two kinds of intermetallic compounds, Cu6Sn5 and CuSn3) emerging during the deposition phase could be responsible for this phenomenon.

References

[1] BHUSHAN, B. AND GUPTA, B. K.: *Materials, coatings, and surface treatments,* Handbook of Tribology, McGraw-Hill, Inc., 1991
[2] URAKAZE, K., DZIMKO, M., UEMURA, M.: *Observation of the friction behaviour between coated and non coated silicon wafers and steel balls under extremely low loads,* In: Proceedings of the international Tribology Conference, Yokohama 1995
[3] DZIMKO, M., URAKAZE, K., HOSOI, N., UEMURA, M.: *Tribological properties of silicon blades coated with thin Pb-Sn films,* Quarterly Journal SCIENCE VISION, July-September 1996, pp. 64 – 70, Pakistan
[4] TAKEICHI, Y., ARIGA, N., LI, C. S., UEMURA, M., DZIMKO, M.: *The thickness effect of copper interlayer on frictional properties of lead-tin film,* Applied Mechanics and Engineering, 1999, vol. 4 pp. 189 – 194.

https://doi.org/10.26552/com.C.2005.1.41-46

Viera Poppeová – Juraj Uríček – Róbert Zahoranský – Tibor Galbavý – Klaus Müller – Swen Schmeisser *

THE DEVELOPMENT OF ROBOT CONTROL, ROBOT SIMULATION AND DIGITAL IMAGE PROCESSING

The automation of manufacturing processes finds its application almost in all spheres of the economy of all industrial developed countries. Its inseparable part is represented by robotisation of manufacturing technologies in production. Nowadays robots and manipulators are quite common building element of automated workplaces, where they safeguard namely manipulation, control and measurement operations, operation and manipulation transport, exchange of tools, removing scraps in production. They are the only real tools for performing operations in dangerous or harmful environment for people (welding, spraying of colour or anticorrosive paint, work with radioactive material, etc.).

Robots are introduced in industrial enterprises at present to allow control of six axes, they are capable to work in learning regime, have sufficient capacity of the control system memory also for a complicated manipulation. They are able to adapt to changing conditions of performance while preserving the required quality based on sensor information about the inner state of the robot as well as about outside robot environment. They have automated exchange of effectors, point or curve movement control (or combined), possibility of connection of their own control system with the host computer, etc.

1. Introduction

Industrial robots are used in a wide range of applications in car industry.

About 50% of robots are used in car production in main industrial countries. Robots are applied in various technologies – welding of car chassis, spraying, and assembling.

Robot applications increase in car industry in all biggest car companies and factories.

For example in *VW factory in Bratislava* some time ago the use of robots in ***model Golf production*** was as follows: *5% in welding, 55% in spraying and 3% in assembling.*

The present situation in ***model Touareg production*** has changed: ***80% in welding, 55% in spraying and 17% in assembling***. There are ***310 robots*** in the welding line for car chassis production.

2. DAAD project "The Development of Robot Control System with Artificial Intelligence Application"

The DAAD project (Deutscher akademischer Austauschdienst) was based on personnel exchange programme between Germany and the Slovak Republic (in the years 2002 – 2003). It was oriented at the robot control system development with application of artificial intelligence. The project participants were: the Section of Robotics at the Faculty of Information and Electronics, the University of Applied Sciences in Mittweida, Germany and the Department of Measurement and Automation at the Faculty of Mechanical Engineering, University of Žilina, Slovakia. At both universities, teachers, PhD. – students and master degree students in last year of study worked on the project.

The main goals of the project:

- Theoretical mastering of robot control systems by applying artificial intelligence methods, mainly digital image processing and sensor systems.
- Development of design alternatives of control system and its optimisation.
- Realisation of the power part control system, owing to mechanical part of robot and drives of its motion axes to design appropriate type of robot control, design of power part particular servo drive, power supply of control units and the central control unit.
- The design of simulation program equipment of robot, computer simulation possibilities – simulation of robot functions, motion and manipulation functions: graphics model of robot (mathematical 3D model, determination of edge visibility, kinematics bindings), the design of simulation algorithms, design of software and verification of correct function.
- The design of implementation of robot into a flexible production system, – the design of robot control with a host computer.

3. The Robot Control System and Simulation Software

The goal of the development was to design software for simulation and control of the SLR 1500 robot (Fig. 1). The SLR 1500 training robot was developed at the University of Žilina in collaboration with a firm IQM Zvolen (Slovakia) to serve for the teaching of robotics at high schools and universities. The training robot

* **Viera Poppeová[1], Juraj Uríček[1], Róbert Zahoranský[1], Tibor Galbavý[1], Klaus Müller[2], Swen Schmeisser[2]**
[1]University of Žilina, Slovakia, E-mail: viera.poppeova@fstroj.utc.sk
[2]University of Applied Sciences Mittweida, Germany

SLR 1500 has an angular design. It has five degrees of freedom, three of them serve to position the end effector in the space and the remaining serve to determine its orientation with respect to the object being manipulated. Kinematics structure of the SLR 1500 robot consists of a rotational waist, two arms and a wrist mechanism. All parts are connected with rotational joints in such way that the arms are not in the same plane but are moved with respect to each other. Such design allows extremely large rotational range of individual arms.

After initialization of the program the model of robot is displayed and may be moved by a mouse with arrows on the control panel. Each arrow presents rotation of the particular arm. The program consists also of functions used for approaching, rotating and shifting of the model robot.

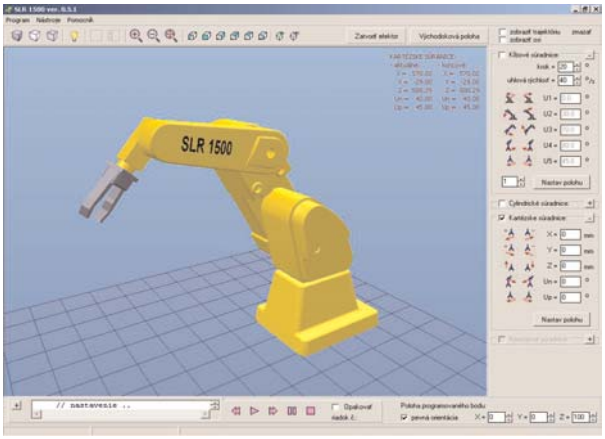

Fig. 1 Robot SLR 1500 Simulation

There are two possibilities how to create the program for the user:

a) *Simulation mode* – movements of particular arms are simulated. The position of the end point is in memory and at the same time a new line of the control program is generated. The program may be modified, i.e. it is possible to erase the line, to insert a new line, change the order. Then it is simulated; it is possible to initialize the program step by step or in cyclic repetition.
b) *Real robot mode* – After switching to this mode, the robot is automatically synchronized and adjusted to the position as shown on the screen. In this mode the task of the control program is to switch on or off the direct engines, located in the arms. Controlling the robot end point is analogical as compared to simulation mode, except the movement of a real robot, the transfer of values from increment sensors (located in arms) to counters, which are on the card PCL 836, is executed. These values are read by the control program and transformed into angles in particular arms by simulation. This feedback and absolute synchronization – real robot – model robot is secured.

The PCL 836 card from Advantech Company is in PC, ISA slot and sends impulses to the power unit, which controls the engines. This unit has its own integrated circuit function. It switches on and off the engines. Further, the card PCL reads counts the impulses from inductive sensors, which are responsible for the robot synchronization and also counts the impulses from incremental sensors used for adjusting the required position of particular arms. The output of program: it is the control program for the SLR 1500 robot, which may be saved on a disk and inserted into memory again later.

In one line of the control program there are the following instructions: line number, instruction MOVE x where x represents number of the point where the robot is to move, duration before gripping the body in ms, effector state, i.e. OPEN or CLOSE, duration after gripping the body in ms.

4. Robot Control in a Collision Situation

In present the industrial robots are able to perform path correction in near trajectory. With suitable sensors they are used for tasks which needed correction of trajectory during the process, according to the immediate situation of environment. By using the sensors for generation copying movement's trajectory, is impossible to exclude automatically collision function by controlling at phase of programming and debugging. In higher-level control systems is necessary to use On-line control, which have big amount especially in Off-line programming.

4.1 Method Description

In this case the parts of the robot have to be defined by geometric formats. An algorithm is calculated by the distance between the formats and checks if the formats interface. If the value of distance between the formats is zero the control system will send an order to stop the movement of the robot arm. Also the control system will report the collision situation. There are a lot of possibilities for describing the parts of the robot arm: In 2D they are point – point, line – point, line – line; in 3D they are ball – ball, ball – flat, flat – flat. Each variant has different needs for hardware and advantages or disadvantages [1].

The ball - ball method: in this example the effector and the barrier are described as a ball. During the robot movement we use mathematics algorithms to count their distance. If the distance is zero, the robot will reject any other movement in the wanted direction. The robot will stop or make movement in the opposite direction. Because of the force of inertia in the robot, the ball does not follow the limit contour, exactly but there is some reserve. Everything is in 3D space and real time.

If we have an object or barrier with a complicated shape, the surface of the ball can have a big distance from the surface of the object. In this example it could be a big disadvantage. Such a big distance is not needed. It makes limits for the robot when they are not needed. The advantage of this method is the small expectation on hardware and work in real time.

The ball - flat method – in this method the effector is described as a ball. The flat describes an object or barrier. We will get better precision when barriers are described this way. During the movement of the robot we count distance of the ball to the flat or flats. The distance has to be bigger than zero, if not, there is a necessity of collision. Again the control system will give the order to stop or to make a movement to the opposite direction. Like in the method before the effector is described with big reserve. It is a disadvantage. Advantage can be a more exact description of the barrier that we still have small hardware requirement and that this method is working in real time.

4.2 Collision 3D Simulation

The collision ball - ball method: in this situation three balls move in 3D space. We use radius condition and mathematics method, which is counting distance between them. If we want to resolve collision successfully we have to know radius of the balls. We have to know where the centres of the balls are, to co-ordinate the system in which the balls move. If we are count correctly, we use a radius condition, we can be sure that the balls are not interfused together, they can just touch with surfaces. One or more balls could define the effector and barrier. For us it is better to have just one for each one. We can follow the centres of the balls with a camera. The camera system reports any changes in barrier co-ordinates and through the mathematics method we know what the changes between the balls are. The action of anti-collision system is counts with new co-ordinates too. We have to choose the point, which is in relationship to centre of ball and we will follow that point by camera. The best way is to choose the point identical to centre of ball. The anti-collision system has to count by inertia of the robot. Because of the simplicity and small financial needs of this method we have chosen it for our application on training robot SLR 1500.

Collision ball - flat method: In this situation we have a collision fixed flat and moving ball. We use the same mathematical method as we did last time and we use a flat condition. We have to know the co-ordinates of the centre and the radius of the ball. We have to know the co-ordinates of the flat and from them we can count the flat equation. If we are to count correctly and we use the radius condition, we can be sure that the ball does not interfuse to flat. The effector is described as a ball and the barrier as a flat. The centre of the ball is again in relationship with the chosen point. On the flat we will choose point too, it is going to define each of the flat. Usually this point is in the middle of the flat. The camera follows this point. The flat position is changed in regard to the point position difference. The anti-collision system reacts in those conditions. This method is reliable and its application is wide.

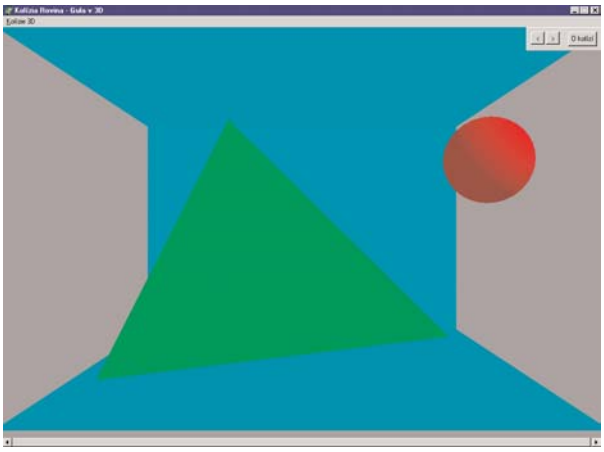

Fig. 3 Collision ball - flat, 3D Simulation

The simulation for 3D collision and the control is very simple and easy to run (Figs. 2 and 3). In 3D simulation these collision combinations are described:

- moving flat to fixed flat,
- general moving flat to a general fixed flat.

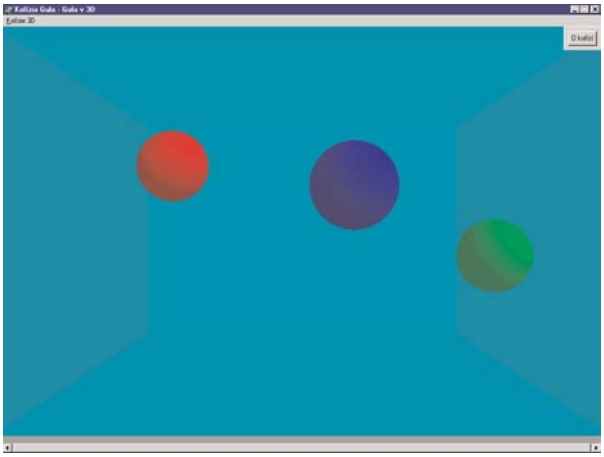

Fig. 2 Collision ball - ball, 3D Simulation

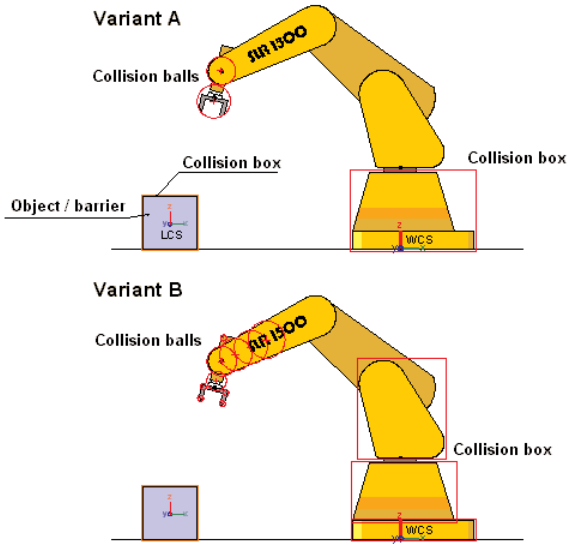

Fig. 4 Possibilities of describing objects by sphere - box method

There are applications for both of them in the robotic system. In these methods we will replace the effector and barrier with the flat or system of flats. The mathematical mechanisms are more complicated in these examples. The need for better hardware is necessary, if we want to get fast reactions in real time. In this case they are reliable and the application could be wide.

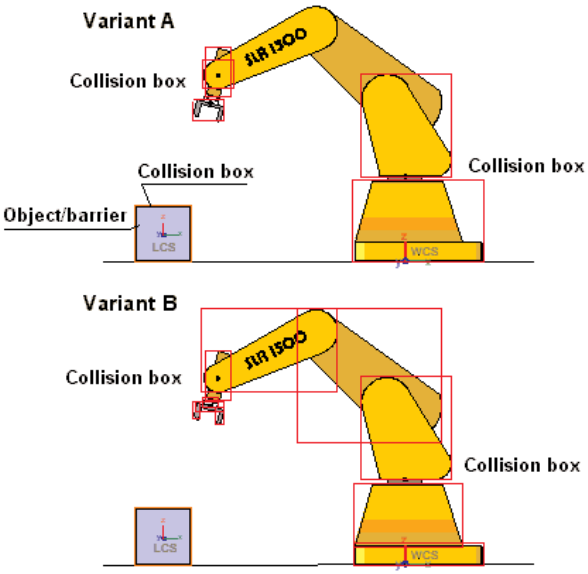

Fig. 5 Possibilities of describing objects by box – box method

5. Digital Analysis of Image

The main task of digital analysis of image is to capture a picture with camera, process it with computer and shows results on an output device, or activate systems of control. It takes a picture of working environment and processes it in these steps: digitalisation, image focusing, filtration and segmentation.

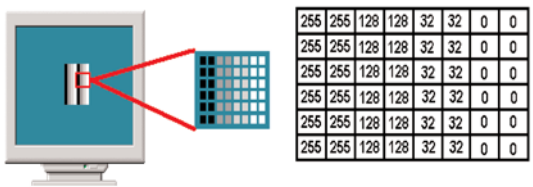

Fig. 6 Presentation of digital image

Digitalisation

The digital image is in the form of function $f(x, y)$, where x and y are co-ordinates in 2D space and functional value corresponds with the intensity of the point. The digital image is recorded in the Matrix – Fig. 6. Digitalization occurs when the linear function $f(x, y)$ is changed to the discreet function $D(x, y)$. Image focusing highlights the difference in intensity.

Filtration

Filtration is the second step in the process. The picture is unclean after digitalization and transit of image data and there is a lot of buzz in it. We can use two ways to filtrate picture: an average value method and median method.

Segmentation

The next step after filtration is segmentation. In this process we separate the profile of the object from the background. There is an optimal value of intensity which represents the limit between the object and the background. In the next step is every place with value under limit repressed by one colour, place with a value under the limit value repressed by other colour. An example of the method is in Fig. 7.

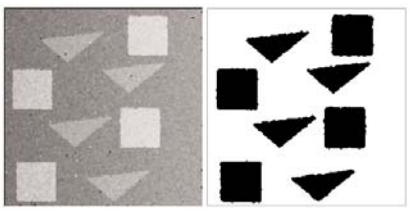

Fig. 7 Segmentation
Image taken by camera *Image after segmentation*

5.1 Description of Computer Subsystem for Digital Analysis of Image

The proposed algorithms and function of the program were tested on the computer system, which was made for the purpose of digital image processing and recognition of objects in image (Fig. 8). The computer system is placed at the Department of Machining and Automation, University of Žilina. Its basic configuration is:

- processor Pentium Celeron 1,2 GHz, memory 128 RAM, hard disk 40 GB,
- graphic card ATI Radeon 7000,
- TV card ATI TV Wonder Bt 878,

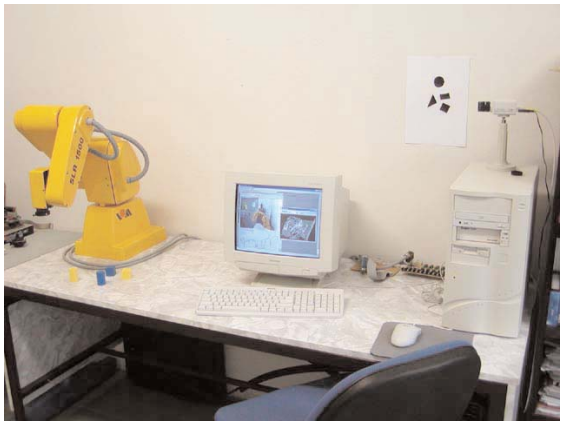

Fig. 8 Workplace with training robot SLR 1500 at University of Žilina

- camera 1/3" CCTV System,
- monitor 15" SVGA,
- keyboard, mouse, network card.

For image processing was used camera 1/3" CCTV System. It is industry camera equipped with CCD sensor. It is resistant against fire and magnetic field. Camera is connected to TV card through coaxial 75-ohm cable with BNC connector.

5.2 Software Image Processing V 3

This original software is used for object recognition. The software scans image and makes a diagnosis (histogram, contour, final function). Now we can see the real shape of the object, we can measure distances and it will tell us how many angles the object has. The project at this time is in the first stage form in which we can work with basic 2D objects (triangles, quadrants).

The picture of the main screen is in Figure 9.

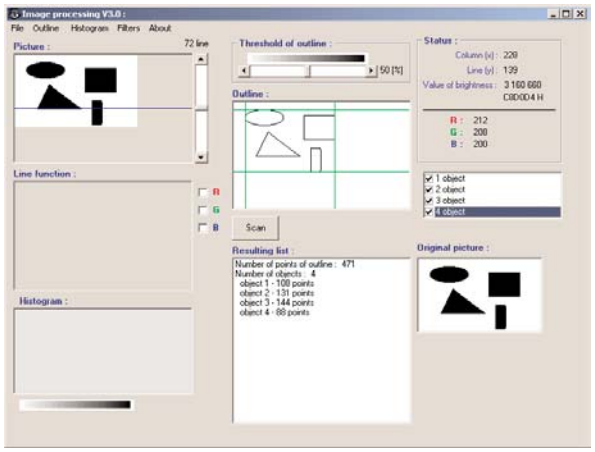

Fig. 9 Picture of main screen

Example of recognized elipse in Fig. 10. There are shown characteristic dimensions of ellipse such as main axis, second axis, middle of ellipse and origin.

6. Conclusion

The robot presents a complicated mechatronical system with several subsystems. The level of adaptability and cognitive ability of processing a perception, thinking and robot decisions making depends, except hardware and sensors, on the level of developed software and control algorithms, from which is control program made.

Sophisticated robotic systems are characterised by the fact that they involve cognitive processes, i.e. processes of perception, "thinking" and decision. Such robotic systems utilise elements of artificial intelligence in their design and performance.

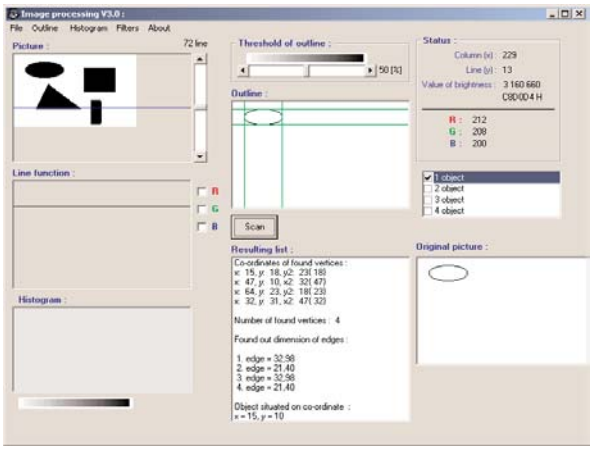

Fig. 10 Recognised ellipse

Development of the robot design will be oriented towards the solution of visualisation problems in the near future:

The ability of shape resolution or the workpiece orientation, interaction of the robot with the environment, computer representation of visualised data, universality of effectors, auto-diagnostics, and communication with the control system in the natural language, etc. Robots with such characteristics become then irreplaceable components of highly productive technologies namely in automated operations.

The present tasks involve designing the appropriate sensor system for adaptive control and design of robot control with application of artificial intelligence - digital image processing, as well as possibility of communication with a host computer and implementation of the robot into a model automated workplace at the department. It is necessary to solve the effector system of the robot.

We can see in Fig. 11 simulation of a car production workplace with robots. Software for complicated simulation is currently developed at Department of Machining and Automation, University of Žilina.

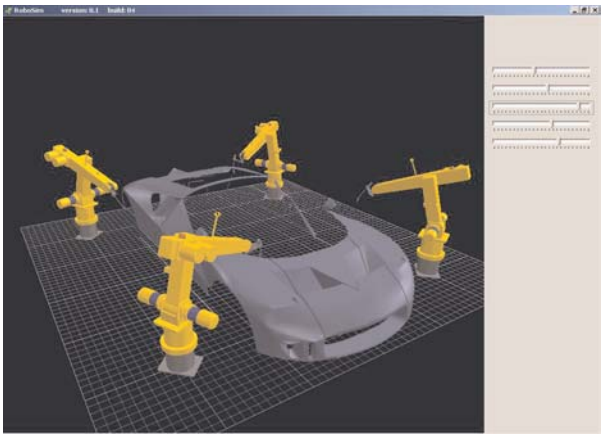

Fig. 11 The robotized workplace simulation

References

[1] MAŘÍK, V., ŠTĚPÁNKOVÁ, O., LAŽANSKÝ, J.: *Artificial Intelligence I and II* (in Czech). Praha, Academia, 1993
[2] POPPEOVÁ, V., URÍČEK, J., ZAHORANSKÝ, R., MŰLLER, K., SCHMEISSER, S.: *Some Results of the Development of SLR 1500 Robot Control System with Artificial Intelligence Application.* In: ISR 2004. Proceedings of 35th International Symposium on Robotics, Paris – Nord Villepinte, France, March 23–26, 2004, s. 35–36
[3] KOLÍBAL, Z., KNOFLÍČEK, R.: *Morphological Analyse of Industrial Robots Building* (in Czech). Vienala., Košice, 2000
[4] MÁDL, J., KAFKA, J., VRABEC, M., DVOŘÁK, R.: *Mechanical Technology* (in Czech). ČVUT Praha, 2000
[5] TOLNAY, M., VLNKA, J., MIHALČAK, P.: *Ultrasonics Effectors for Intensification Manufactoring Processes,* In.: 6th International Conference TMT 2002, Neum, Bosnia and Herzegovina
[6] DEMEČ, P.: *Machine Tools Accuracy and its Mathematical Modelling* (in Slovak). Vienala, Košice, 2001
[7] NOVÁK-MARCINČIN, J., SMRČEK, J.: *Biorobotics* (in Slovak). Elfa, Košice, 1998
[8] HAJDUK, M., BALÁŽ, V., SUKOP, M., ŠIDLOVSKÁ, Ľ.: *WEB Integration of the Robotics Cells*. In: 7th Conference TMT 2003, Barcelona, Spain, 2003
[9] PILC, J., STANČEKOVÁ, D., MIČIETOVÁ, A., SALAJ, J.: *Dedicated machines and Production Links* (in Slovak). EDIS Žilina, 2002
[10] KUMIČÁKOVÁ, D., ČUBOŇOVÁ, N., KURIC, I.: *Importance of Computer Simulation and Animation in Education Area of Manufacturing Technology.* In: Manufacturing technology, Journal for Science, Research and Production, Vol.: 3, June 2003, pp. 40–44.

https://doi.org/10.26552/com.C.2005.1.47-48

Aleksander Nieoczym *

APPLICATION OF A TRANSPORTATION FLUX FOR DETERMINING QUALITATIVE INDICES

A method of using the transportation flux of a manufacturing system for determining its qualitative parameters has been presented. Those subjects were discussed in many papers [1 – 4], however the presented method may be used for a preliminary determination of functionality of manufacturing system parameters when, as a consequence of its modernization a change in equipment of a certain section or a replacement of individual devices was planned. Such actions cause a necessity to determine the system's operating efficiency and reliability after changing parameters as well as the impact of working processes on the product quality. Such actions were conducted as a result of performed research works no. KBN nr 8 T07 D 034 21 [5].

1. Transportation flux

A change in qualitative (final) product parameters can be caused by:

1. A change in nominal data of working equipment. This situation can occur as a consequence of lacking periodical maintenance or a slow wear and tear of the equipment.
2. A supply of a defective workpiece (subassembly) to the working station causing the making of a defective product and under extreme circumstances a damage of a manufacturing tool or a failed action of the working station, e.g. as a result of impossibility to fix the workpiece at the working station. The incoming defected workpieces create a random flow of damage level, whose value, validated as a number of discards, is often estimated in course of production preparation. The damage level value is estimated under specific manufacturing duration time frames and is usually considered as a permissible damage level.
3. A damage of manufacturing tool. If the workpiece was good, we experience a random damage of a tool making impossible to fulfill its basic functions. The product is removed from the working station and the working tool must be replaced.

To conduct a random quality control of a mounted assembly (by sampling) a number of workpieces to be taken for control from among the total number of workpieces in the transportation flux must be determined. This enables determining the process quality by using the basic coefficients, assuming the following initial data:

N – total number of workpieces leaving the working station,
N_D – total number of discarded workpieces
N_K – total number of workpieces subject to control
N_{DK} – total number of workpieces with defects found at the control

The level of discard (defected workpieces):

$$k_D = \frac{N_D}{N} \tag{1}$$

The mean value of discards within a certain time range determined as a results of conducted control processes:

$$k_D = \frac{N_D - N_{DK}}{N - N_K} \tag{2}$$

The coefficient of controlled assemblies:

$$k_K = \frac{N_K}{N} \tag{3}$$

The coefficient of discarded (defected) workpieces:

$$k_U = \frac{N_{DK}}{N_K} \tag{4}$$

The next step is to determine the optimum number of workpieces subject to control in order to determine the share of defected (discarded) products at the whole manufacturing lot. An important precaution is the uniformity and randomness of allocation of defected products among good ones. i.e. a gathering of defected products into clearly visible clusters inside the whole lot is unacceptable. The basic parameter to be determined in this case is k_E – the share of defected products.

N_D – number of defected parts
N_Q – number of good quality parts.

The kE parameter was determined by means of a calculating program created on basis of the Statistic program. After choosing a lot (population) quantity a current share of defected products is determined as a ratio of actually known number of defected products to the number of controlled ones. An accuracy of analysis can be supplemented by indicating the initial (inaccurate calculation) and final (accurate calculation) point of stabilization. This is the point at the diagram (Fig. 1) determining such a number of controlled products after which the curve of quantity of defected products is stabilized. To find the versatile point of stabilization

* **Aleksander Nieoczym**
Technical University of Lublin, ul. Nadbystrzycka 36, 20-618 Lublin, Poland, E-mail: a.nieoczym@pollub.pl

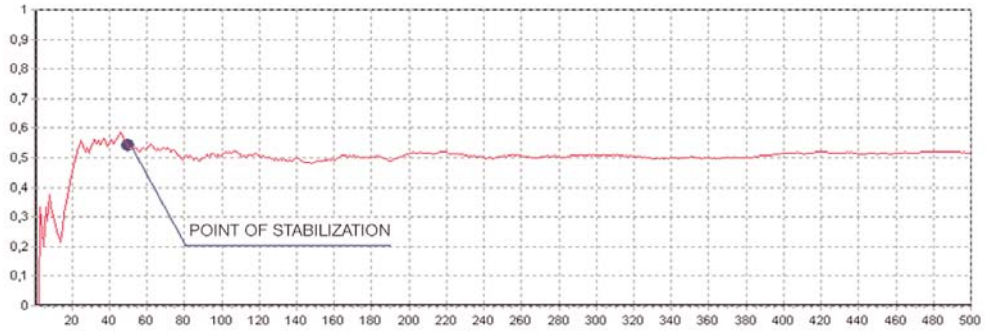

for a certain size of the lot, the program analyses several sets of equal size (the number of defected parts at each set is a random value), whereas the point of stabilization is an arithmetic mean of all points of tested sets of equal size.

2. Process monitoring at the working station

Sensors are used to control the manufacturing processes. The sensors are placed not only at the working station, where the main process is conducted but also at devices being components of tooling e.g. supplying or fixing devices. In many cases they are flexible working stations able to process workpieces of various geometric forms and various numbers of treatment cycles. Therefore, not in each case it is needed to acquire data from all measurement sensors. At every case the number of active sensors, i.e. the number of process parameters and variables to be read out. The S parameters (states) are determined and divided into subsets S_n containing qualitatively identical parameters corresponding to treatment operations at working stations. The S parameters correspond also with L_m parameters aligned by quality and measured at the tooling. The S states are e.g. process speed, process time, the L parameters are e.g. position of supplying device's arm, speed of supplying workpieces into a working station.

To conduct the general control of work, it is enough to read out parameters of randomly selected S_n or L_m subsets. This enables determining the place of arising of irregularities within the group of parts read out by one of S or L subsets. In case of full control all S and L states are used. Let T stand for the quantity of measured parameters:

$$T = (S_n \lceil L_m), \quad n = (1 \ldots N), \quad m = (1 \ldots M) \tag{5}$$

Two extreme cases can be obtained, if $n = 1$ and m = M, then $T = M + 1$, i.e. the control gets parametric. If only the work readiness is controlled, only one signal S_n $(n + 1)$ is obtained, but to find the irregularities, all $m = M$ parameters must be tested. The second extreme case is analogous. At constant L_m all S_n $(n = N)$ parameters are read out. Having assumed: $n = m = N$, in the first case the area of investigation is: $A = n_m = N$, the number of measured parameters: $T = n + m = 1 + N$. For the second case: $A = N^2$.

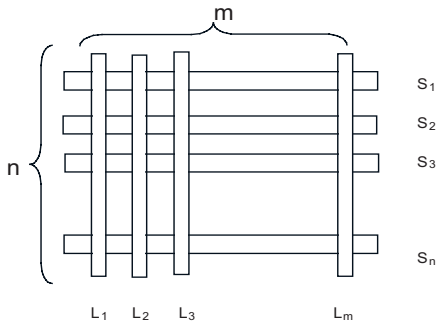

Fig. 2. Graphic presentation of relationship between parameters of the working process states and parameters of tooling [6].

S1 ... Sn - parameters, states corresponding to a certain process operation at the working station, L1 ... Lm - parameters measured at the tooling, A = mn = N - the whole area of investigation.

References

[1] CHRYSSOLOURIS, G.: *Manufacturing systems,* Theory and practice, Springer - Verlang, New York 1992.
[2] DASZCZIENKO, A., BIEŁOUSOW, A.: *Design of automated line* (in Russian). High School, Moscow, 1986.
[3] DRUŻININ, G.: *About evaluation reliability technological systems with loading devices* (in Russian). Standardization and Quality, n10, pp 8 – 12, 1994.
[4] KUMAR, V., WANG, S.: *Reliability enhancement by time and space redundancy in multistage interconnection networks,* IEEE Tranis. Reliab., vol 40, n 4, pp. 461 – 473, 1991
[5] NIEOCZYM, A.: *Problems designing hierarchical organized assembly systems* (in Polish). LTN, Lublin, 2002.
[6] *Fundamental problems of reliability in theory and practice* (in Russian). Moscow, 1975.

https://doi.org/10.26552/com.C.2005.1.49-53

František Brumerčík – Roman Kocúr – Milan Pažičan – Michal Lukáč *

DIFFERENTIAL HYDRO-MECHANICAL TRANSMISSIONS WITH HYDROSTATIC UNITS

At present, hydromechanical transmissions are used especially in agricultural and defence vehicles. These transmissions have potential to be used also in other vehicles, for example commercial cars and buses. Differential hydromechanical transmission generation needs to achieve comparable parameters in comparison with the competition to prove maximum of drive comfort, safety, reliability and efficiency.

Keywords: *transmission, power split, epicyclical gears, hydrostatic unit, continuously variable transmission – CVT, drive comfort, safety*

1. Introduction

Vehicle producers and transmission developers use the principles of continuously variable transmission without power flow break. The most known producers developed differential transmissions with hydrostatic units placed in parallel power flow branch. Agricultural tractors, defence vehicles and special crawlers are equipped with this type of transmission. The new innovative solutions are listed below.

2. Deutz-fahr Agrotron

The demands to a modern infinitely variable transmission are clear – high tractive force with low hydrostatic involvement, low maintenance costs and user convenience. The Agrotron TTV transmission, developed in DEUTZ-FAHR and ZF collaboration, has entered new dimensions in stepless transmission technology: Practical operating convenience, high efficiency and exemplary economy are the main characteristics of this transmission.

High mechanical efficiency

A hitherto unsurpassed efficiency for a stepless transmission is possible due to the use of state-of-the-art technology. In each of the four working ranges the maximum driving power is mechanically transferred. The hydrostatic share is reduced to a minimum, ensuring maximum efficiency without hydraulic losses, at lower speeds during fieldwork.

Intelligent transmission design

The stepless, performance-graded transmission of the Agrotron TTV comprises four main components – planetary transmission, the hydrostatic unit, the shuttle clutches and the electronic control unit. The high degree of efficiency is ensured due to the direct power flow from engine to the, planetary transmission, shuttle transmission, PTO and axle.

Fig. 1: Agrotron TTV gearbox cross section and detail of the power split point

Variability from 0 to 50 km/h

The transmission comprises four planetary trains. The entire speed range is practically divided into the four working ranges by the planetary trains. The speed is steplessly varied within each working range by a hydrostatic unit. This gives you the possibility of infinitely variable travel speeds from 0 – 50 km.h^{-1}, using the combination of the planetary trains and the hydrostatic unit. The planetary trains are inter-connected by maintenance-free long life multi-plate clutches.

Coordination

The hydrostatic variable displacement pump is directly driven, via the main shaft, from the engine. The variable displacement pump determines the oil flow rate and therefore, the speed of the

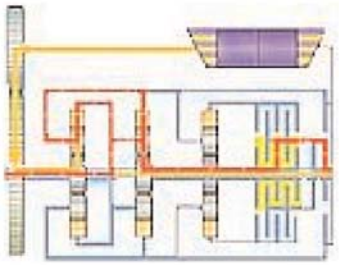

Fig. 2: Power flow through Agrotron TTV gearbox

* **František Brumerčík, Roman Kocúr, Milan Pažičan, Michal Lukáč**
Department of Design and Machine Elements, Faculty of Mechanical Engineering, University of Zilina, Slovakia
E-mail: frantisek.brumercik@fstroj.utc.sk, roman.kocur@fstroj.utc.sk, milan.pazican@fstroj.utc.sk, michal.lukac@fstroj.utc.sk

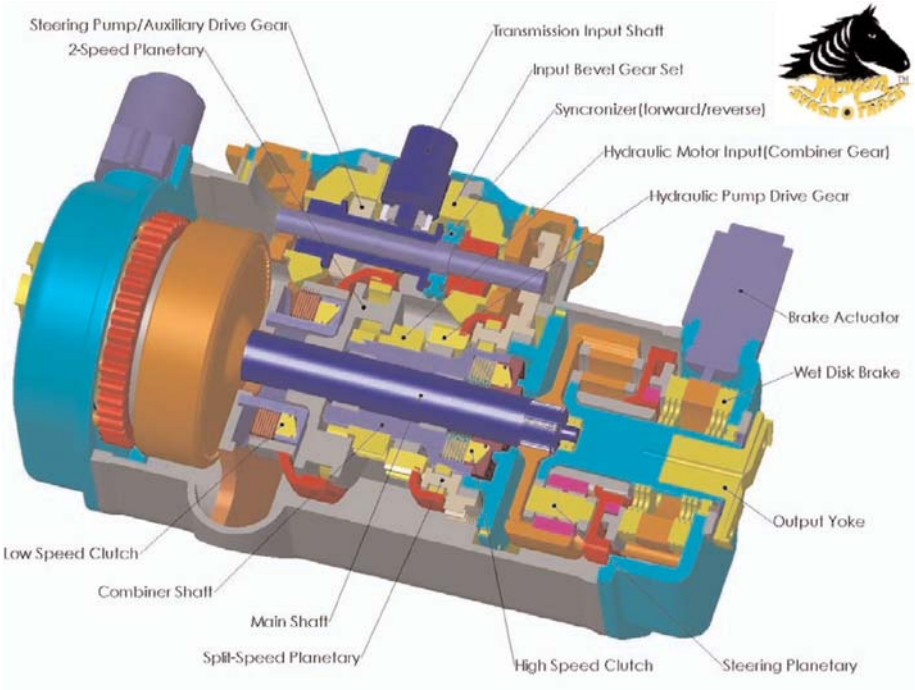

Fig. 3: Silvatech CVT cross section

fixed output motor. The less oil pumped the lower the speed of the fixed output motor and therefore the lower the hydrostatic power share.

3. Silvatech defence

Silvatech Continuously Variable Transmission was developed especially for defence vehicles, but it can be used also in other applications.

Applications and features

Silvatech CVT can be used in vocational trucks, cement mixers, refuse trucks, agriculture, defence, forestry, mining, buses, construction. It provides:

- faster acceleration
- reliable on board diagnostics
- driving without shifting means greater working comfort and valuable contribution to safety
- low heat load
- the vehicle could be stopped without operating the brake, even on slopes or inclines
- reduced emissions
- each speed is continuously variable
- automatic operation with heavy loads in the optimum power zone is easily possible
- the ideal operating condition of the entire system is automatically assured for every situation

The compact design and advanced drive system is ideal for military applications.

SILVATECH'S power pack offers a user features that allows for optimum performance resulting in improved vehicle mobility with smoother, immediate, and more efficient vehicle response.

Silvatech has been producing reliable, rugged mobile application drive systems with 80% less moving parts than conventional drive trains for the past decade. Any operational trouble, should it arise, is quickly diagnosed and repaired, by local technicians, usually in the field.

4. Torvec-IVT

Torvec's breakthrough Infinitely Variable Transmission (IVT™) combines the Company's innovative and patented hydraulic pump technology with patented gearing and valving resulting in a technological marvel. The transmission reaches efficiencies in ranges where others aren't even measured, and also cuts down on noxious emissions.

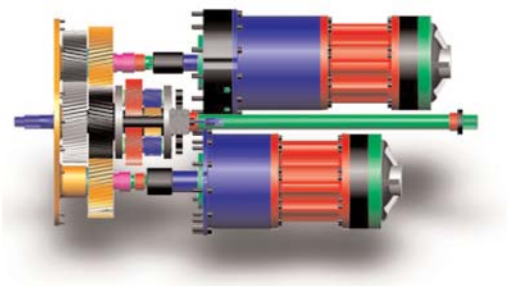

Fig. 5: Torvec-IVT scheme

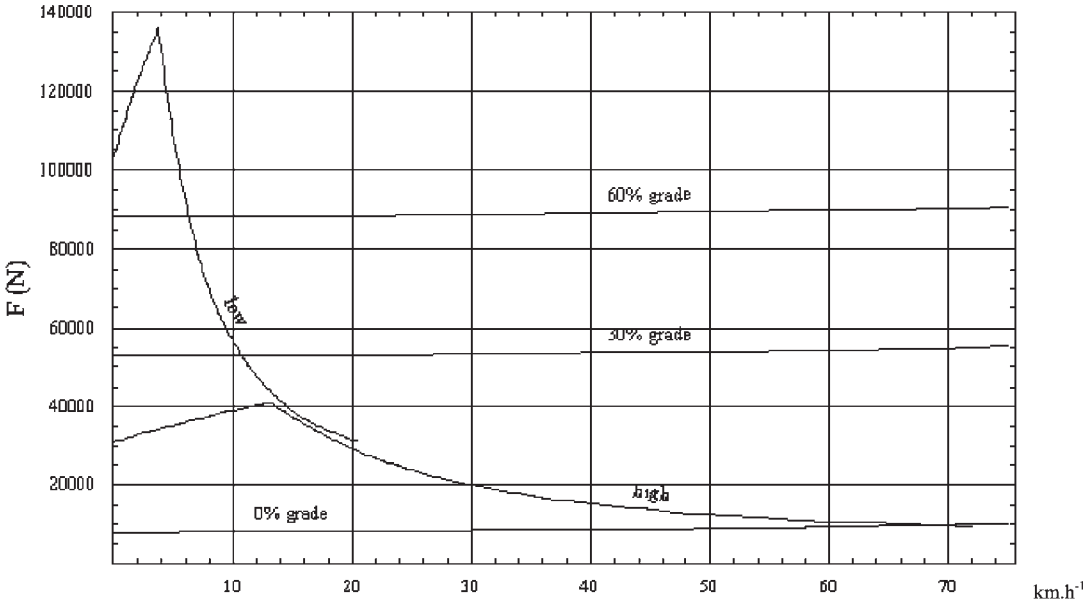

Fig.. 4: Performance diagram of vehicle equipped with Silvatech CVT

The configuration shown here is designed for high-torque diesel applications. The Torvec IVT™ design was an offshoot of our already proven tracked vehicle steering mechanism. The transmission can bolt into existing drive trains with no redesign of the automobile. There is no economic penalty in choosing the IVT™ to replace existing automotive transmissions.

The IVT™ is designed for reliability and durability. There are over 70% fewer parts to fail, all key wear parts operate in hydraulic fluid containment, and there is minimal metal on metal contact. Safety is also inherent in the design. The IVT™ is equally as safe as a conventional transmission, there are very few functions to control and the transmission eliminates vehicle creep (forward movement) at idle while in Drive.

Based upon these results and automotive industry requests, Torvec is currently installing an even less expensive version of the IVT™ using only its patented pump and motor, in a gasoline powered GM Tahoe SUV. Torvec believes that this installation will demonstrate that its IVT™ technology is commercially ready for production and utilization in the full spectrum of gasoline and diesel powered vehicles.

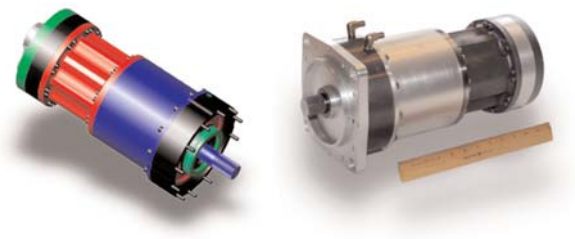

Fig. 6: Torvec's 200 cm^3 displacement pump – CAD model and a prototype

Hydraulic pump / motor

Torvec has redefined the science of hydraulics. The result is the Torvec Hydraulic Pump and Motor – the major breakthrough behind the IVT™.

These pumps and motors have a place of their own in the industrial pump market. Current hydraulics suffer from critical problems:

- Rotating piston group
- Inefficient valving
- Hydraulic whine
- Heavy housings

Existing pumps need to be large and heavy in order to deliver the desired power. The size and weight prove detrimental in automotive design, as valuable space and weight are eaten up by the hardware.

Torvec innovation led to the design of their own Hydraulic Pump. Torvec has eliminated the rotating piston group (the cylinders are stationary), making the pump tremendously powerful and easy to manufacture.Torvec's patented valving has been integrated to increase efficiency and reduce noise (hydraulic whine).

The challenge was to deliver the necessary power while reducing the size and weight of the pump, using parts that can be manufactured at high volume and low cost. The design solution resulted in a pump with extremely high power density (horsepower to weight ratio), at less than half of the industry standard weight for a comparable hydraulic pump. For example, most 200 cm^3 displacement pumps range from 90.7 – 122.5 kg, while Torvec's displacement pump weighs approximately 34 kg.

5. Steyr CVT

Hydrostatic unit

A hydrostatic fixed displacement motor, which is directly pressurised with the oil flow conveyed by the pump, is mounted back to back onto a variable hydrostatic pump. Through electro-hydraulic adjustment of the inclined plate (55 cm^3 capacity, 430 bar maximum pressure) in the hydrostatic pump both the speed as well as the rotational direction of the hydrostatic motor can be changed.

Figure 8 shows three clearly defined modes in the compound planetary gear. The internal gear depicted in red supplies the mechanical portion of the power transmission, is directly driven by the engine and thus always rotates in the same direction according to the engine speed.

The sun gear shown in green is driven by the hydrostatic motor and transmits the hydrostatic power.

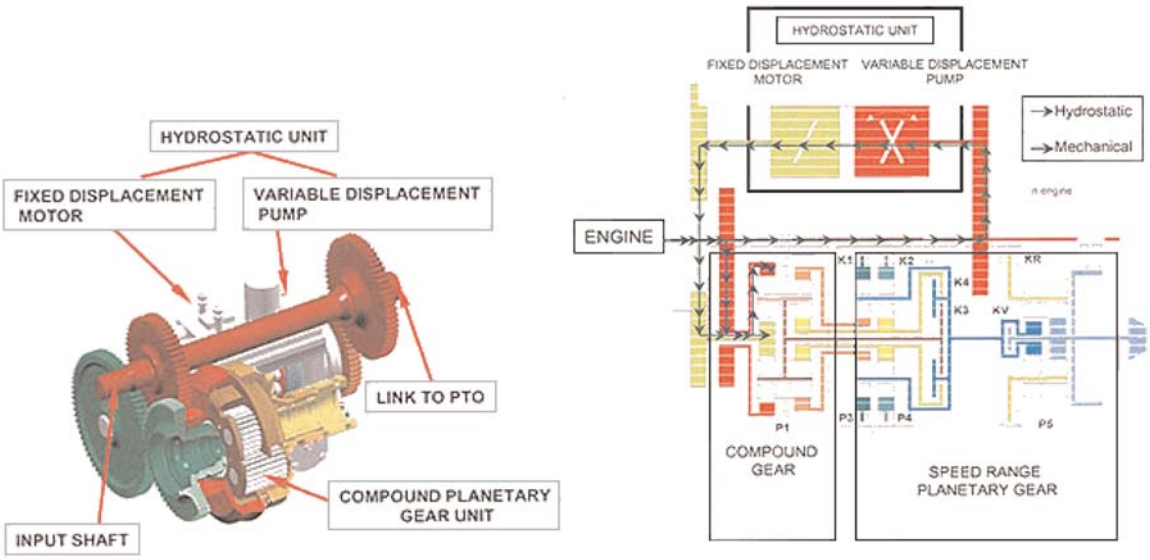

Fig. 7: Steyr CVT gearbox – parts and power split figuration

Compound planetary gear

This unit consists of a 5-shaft planetary gear with two input shafts and three output shafts in which the actual superposition of the mechanical and hydrostatic power takes place.

Mechanical 4-range transmission

Planetary units in which 4 speed ranges are attained are connected to the compound planetary gear. The changeover between the individual speed ranges is carried out through overlap closing of special claw clutches at synchronous speeds without tractive force interruption. A planetary unit with direct link in forward travel and reversal of rotational direction in reverse travel is connected to the above.

Transmission and vehicle electronics

Special electronics enable control and regulation of transmission as well as interplay between the individual components. The mechanical power at the internal gear and the hydrostatic power at the sun gear of the compound planetary gear together provide the appropriate output in the respective speed ranges.

Through the superposition of the two input speeds (mechanical and hydrostatic) it is possible to achieve variable output speeds at a constant engine speed. In this way the travelling speed of 0 to 50 km/h can be achieved forwards and backwards with continuously variable control and without tractive force interruption.

The speed and rotational direction of the sun gear can be varied by adjusting the inclined plate at the hydrostatic pump from the maximum speed in the opposite direction (mode 1), via stop (mode 2) to synchronous operation (mode 3) with the internal gear.

The respective output, which is now transmitted to the mechanical 4-range gear, results from the sum of sun gear and internal gear.

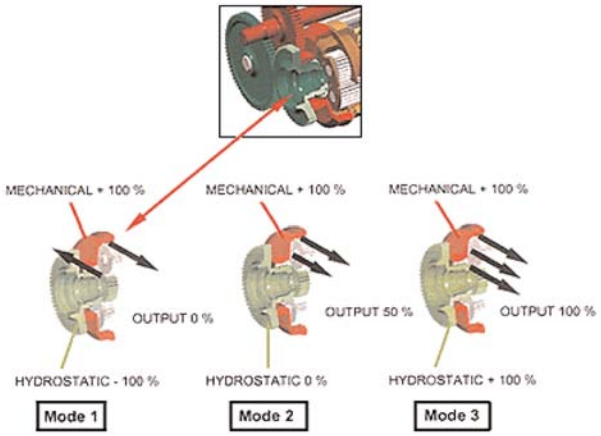

Fig. 8: Three speed modes of Steyr CVT

6. Fendt-Vario-Gearbox

The engine output is directed to a planetary drive via a torsional vibration damper. Power is directed to the hydrostatic branch via the ring gear, and to the mechanical branch via the sun wheel. Both power trains are subsequently reunited at a collecting shaft with direct connection to the rear axle.

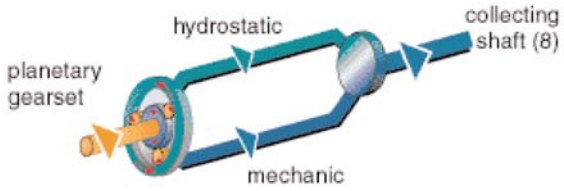

Fig. 9: Power split in Fendt-Vario gearbox

Hydraulic drive unit

The hydraulic branch consists of a top-efficiency variable pump, which drives two adjustable hydraulic motors on a common shaft. Pump and hydraulic motors are controlled in unison and have a particularly wide swing angle of 45°, which creates max. efficiency – a big advantage.

Mechanical drive unit

In the mechanical branch, which consists of planetary gears and range control, the residual torque is transferred via geared wheels to the collecting shaft where the two drive trains are combined.

Power splitting

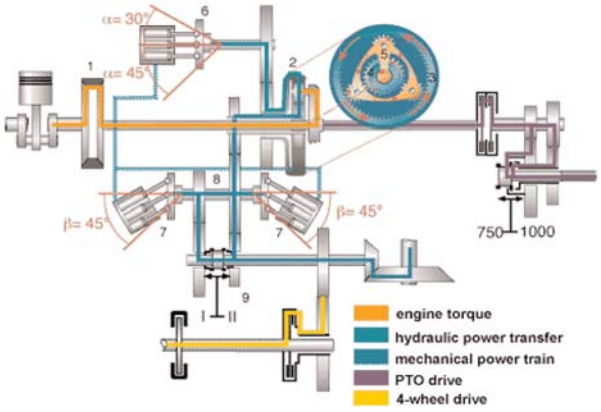

Fig. 10: Layout of Fendt-Vario with the power split representation: 1 torsional vibration damper, 2 planetary gear set, ring gear, 4 sun wheel, 5 planet carrier, 6 hydraulic motor, 7 hydraulic pump (400/700 Vario with own hydraulic motor), 8 collecting shaft, 9 travel range selector

7. Conclusion

The above named and listed solutions of hydromechanical transmissions with hydrostatic units show the potential of this transmission type. There are many useful properties that improve vehicle drive comfort (driveability), safety and fuel consumption. The result is that these transmission concepts designed with accent to required specific parameters achievement can also be used in other vehicles, not only in agricultural, defence and special ones. That is one of the main ideas in development of differential hydromechanical transmission with power split and hydrostatic units assigned for buses.

References

[1] http:/www.deutz-fahr.de
[2] http://www.silvatechgroup.com
[3] http:/www.torvec.com
[4] http://www.bonhillmarketing.co.uk/cvt.htm
[5] http:/www.fendt.com
[6] MÁLIK, L., KUČERA, Ľ.: *Mechanic, hydraulic and hydromechanical transmissions* (in Slovak), EDIS – publisher of ŽU, Žilina, 1999.
[7] MÁLIK, L., ŠOŠKA, M.: *Hydrostatic-mechanic power transmission* (in Slovak). EDIS – publisher of ŽU, Žilina, 2002.
[8] MIKLUSAK, J: *Stress analysis of gear box size A*, Final report, 05/2004-AUT
[9] LOOMAN, J.: *Gearboxes. Basics, designs, vehicle applications* (in German). Springer – publishing, Berlin, Heidelberg, 1996.
[10] PODHORSKÝ, J., HRČEK, S.: *New approaches and technologies in machine elements design* (in Slovak). In: 45-th international machine elements and mechanisms departments conference, september 2004, Blansko, Czech Republic. ISBN 80-214-2702-7
[11] United States Patent Nr. 5186692, *Hydromechanical orbital transmission*
[12] United States Patent Nr. 5513553, *Hydraulic machine with gear-mounted swash-plate*
[13] PODHORSKÝ, J.: *Expert system for design support*, G.E.P. Miskolc, 1994
[14] PODHORSKÝ, J.: *Information in design process and its processing* (in Slovak), 1-st scientific PhD-student conferrence, Košice, 1995
[15] MIKLUŠÁK, J.: *Use of modern computation methods by spur gearing analysis* (in Slovak), 45-th international machine elements and mechanisms departments conference, Blansko 2004

Prof. Ing. Dr.h.c. Miroslav Steiner, DrSc. - Celebtates his 75th Birthday

Professor Steiner was born on November 20, 1929 in Prague. After having been apprenticed, he continued studying at an engineering high school, graduated from the Prague Technical University in 1953 and in 1958 was awarded the scientific degree of Candidate of Science (PhD degree) in the Research Institute of Transport in Prague. In 2003 he was awarded the honorary degree of Dr. h. c. at the University of Żilina.

Professor Steiner has contributed greatly to the building and development of scientific areas focusing on safety of transport systems, dynamics of road vehicles – relations to the route, complex solutions to transport systems. He gradually dealt with conceptual tasks resulting from the development of transport and automobile industry where he could make use of his knowledge gathered during his study stays in France.

He founded and directed state-wide research programs of road traffic safety and in this area he contributed to the building of the first international test laboratory of restrain systems in the former East European countries. Professor Steiner also initiated the establishment of the branch "implementation of mathematical methods in road transport". He was a co-founder of the joint research workplace of the Czecho-Slovak Academy of Sciences and Federal Ministry of Transport aimed at basic research in the area of safety and reliability of transportation systems.

In the area of interaction between means of transport and the route he elaborated a theory of their mutual interaction from the point of view of vertical dynamic forces, methods of measurement and evaluation of impacts. He designed methods of determination of dynamic impulse factors destination, designed and verified methods and instruments for evaluation of road surface quality.

He spread his knowledge and experience from construction and operation of vehicles as a university teacher at the Czech Technical University – Faculty of Transport, at the University of Žilina and at the University of Pardubice, where he has been working up to this day. He lectured also at various universities abroad, e.g. in De Kalb in the US., in Tokyo, Vienna, Hamburg, Dresden, and Budapest.

During the last five years he actively participated in congresses and conferences (Beograd, Budapest) and was awarded various diplomas and recognitions. His publication activity is wide and numerous.

We all would like to wish Professor Steiner every success, sound health and a lot of vigour and optimism for the years to come.

COMMUNICATIONS – Scientific Letters of the University of Žilina
Writer's Guidelines

1. Submissions for publication must be unpublished and not be a multiple submission.
2. Manuscripts written **in English language** must include abstract also written in English. The submission should not exceed 7 pages (format A4, Times Roman size 12). The **abstract** should not exceed 10 lines.
3. Submissions should be sent: **by e-mail** (as attachment in system Microsoft WORD) to one of the following addresses: *holesa@nic.utc.sk* or *vrablova@nic.utc.sk* or *polednak@fsi.utc.sk* **with a hard copy** (to be assessed by the editorial board) **or on a 3.5″ diskette** with a hard copy to the following address: Zilinska univerzita, OVaV, Moyzesova 20, SK-10 26 Zilina, Slovakia.
4. Abbreviations, which are not common, must be used in full when mentioned for the first time.
5. Figures, graphs and diagrams, if not processed by Microsoft WORD, must be sent in electronic form (as GIF, JPG, TIFF, BMP files) or drawn in contrast on white paper, one copy enclosed. Photographs for publication must be either contrastive or on a slide.
6. References are to be marked either in the text or as footnotes numbered respectively. Numbers must be in square brackets. The list of references should follow the paper (according to **ISO 690**).
7. The author's exact **mailing address of the organisation where the author works, full names, e-mail address or fax or telephone number,** must be enclosed.
8. The editorial board will assess the submission in its following session. In the case that the article is accepted for future volumes, the board submits the manuscript to the editors for review and language correction. After reviewing and incorporating the editor's remarks, the final draft (before printing) will be sent to authors for final review and adjustment.
9. The deadlines for submissions are as follows: September 30, December 31, March 31 and June 30.
10. Topics for the year 2005: 2/2005 – Transport – technologies, management and economics, 3/2005 – Security engineering.

POKYNY PRE AUTOROV PRÍSPEVKOV DO ČASOPISU KOMUNIKÁCIE – vedecké listy Žilinskej univerzity

1. Redakcia prijíma iba príspevky doteraz nepublikované alebo inde nezaslané na uverejnenie.
2. Rukopis musí byť **v jazyku anglickom**. Príspevok by nemal prekročiť 7 strán (formát A4, písmo Times Roman 12 bodové). K článku dodá autor **resumé** v rozsahu maximálne 10 riadkov (v anglickom jazyku).
3. Príspevok prosíme poslať: **e-mailom**, ako prílohu spracovanú v aplikácii Microsoft WORD, na adresu: *holesa@nic.utc.sk* alebo *polednak@fsi.utc.sk* príp. *vrablova@nic.utc.sk* (alebo doručiť na diskete 3,5″) **a jeden výtlačok** článku na adresu Žilinská univerzita, OVaV, Moyzesova 20, 010 26 Žilina.
4. Skratky, ktoré nie sú bežné, je nutné pri ich prvom použití rozpísať v plnom znení.
5. Obrázky, grafy a schémy, pokiaľ nie sú spracované v Microsoft WORD, je potrebné doručiť buď v digitálnej forme (ako GIF, JPG, TIFF, BMP súbory), prípadne nakresliť kontrastne na bielom papieri a predložiť v jednom exemplári. Pri požiadavke na uverejnenie fotografie priložiť ako podklad kontrastnú fotografiu alebo diapozitív.
6. Odvolania na literatúru sa označujú v texte alebo v poznámkach pod čiarou príslušným poradovým číslom v hranatej zátvorke. **Zoznam použitej literatúry** je uvedený za príspevkom. Citovanie literatúry musí byť **podľa STN 01 0197 (ISO 690)** „Bibliografické odkazy".
7. K rukopisu treba pripojiť **plné meno a priezvisko autora a adresu inštitúcie v ktorej pracuje, e-mail adresu** alebo číslo telefónu event. faxu.
8. Príspevok posúdi redakčná rada na svojom najbližšom zasadnutí a v prípade jeho zaradenia do niektorého z budúcich čísiel podrobí rukopis recenziám a jazykovej korektúre. Pred tlačou bude poslaný autorovi na definitívnu kontrolu.
9. Termíny na dodanie príspevkov do čísiel v roku sú: 30. september, 31. december, 31. marec a 30. jún.
10. Nosné témy v roku 2005: 2/2005 – Doprava – technológie, riadenie a ekonomika, 3/2005 – Bezpečnostné inžinierstvo.

komunikácie
COMMUNICATIONS

VEDECKÉ LISTY ŽILINSKEJ UNIVERZITY
SCIENTIFIC LETTERS OF THE UNIVERSITY OF ŽILINA
7. ROČNÍK – VOLUME 7

Adresa redakcie:
Address of the editorial office:
Žilinská univerzita
Oddelenie pre vedu a výskum
Office for Science and Research
Univerzitná 1, Slovakia
SK 010 26 Žilina
E-mail: komunikacie@nic.utc.sk, polednak@fsi.utc.sk,

Každý článok bol oponovaný dvoma oponentmi.
Each paper was reviewed by two reviewers.

Časopis je excerpovaný v Compendexe
Journal is excerpted in Compendex

Vydáva Žilinská univerzita
v EDIS – vydavateľstve ŽU
J. M. Hurbana 15, 010 26 Žilina
pod registračným číslom 1989/98
ISSN 1335-4205

It is published by the University of Žilina in
EDIS - Publishing Institution of Žilina University
Registered No: 1989/98
ISSN 1335-4205

Objednávky na predplatné prijíma redakcia
Vychádza štvrťročne
Ročné predplatné na rok 2005 je 500,– Sk

Order forms should be returned to the editorial office
Published quarterly
The subscription rate for year 2005 is 500 SKK

Jednotlivé čísla časopisu sú uverejnené tiež na:
http://www.utc.sk/komunikacie
Single issues of the journal can be found on:
http://www.utc.sk/komunikacie